3-2004

Experimental and Computational Analysis of Modes in a Partially Constrained Plate

Robert M. Vandawaker

EXPERIMENTAL AND COMPUTATIONAL ANALYSIS OF MODES IN A PARTIALLY CONSTRAINED PLATE

THESIS

Robert M. Vandawaker, Captain, USAF

AFIT/GAE/ENY/04-M15

DEPARTMENT OF THE AIR FORCE
AIR UNIVERSITY

AIR FORCE INSTITUTE OF TECHNOLOGY

Wright-Patterson Air Force Base, Ohio

The views expressed in this thesis are those of the author and do not reflect the official policy or position of the United States Air Force, Department of Defense, or the U.S. Government.

AFIT/GAE/ENY/04-M15

EXPERIMENTAL AND COMPUTATIONAL ANALYSIS OF MODES IN A PARTIALLY CONSTRAINED PLATE

THESIS

Presented to the Faculty

Department of Aeronautics and Astronautics

Graduate School of Engineering and Management

Air Force Institute of Technology

Air University

Air Education and Training Command

In Partial Fulfillment of the Requirements for the

Degree of Master of Science in Aeronautical Engineering

Robert M. Vandawaker, BS

Captain, USAF

March 2004

AFIT/GAE/ENY/04-M15

EXPERIMENTAL AND COMPUTATIONAL ANALYSIS OF MODES IN A PARTIALLY CONSTRAINED PLATE

Robert M. Vandawaker, BS

Captain, USAF

Approved:

___//signed//_____	_____
Dr. Anthony N. Palazotto (Chairman)	Date
___//signed//_____	_____
Major Richard G. Cobb Ph.D. (Member)	Date
___//signed//_____	_____
Dr. Marina B. Ruggles-Wrenn (Member)	Date

Abstract

The need for aircraft, both military and civilian, to serve longer and cost less to operate is ever present. Numerous directives and policies are changing the way maintenance and service life are incorporated into every day decisions. The ability to potentially extend service life and reduce operating and maintenance costs are key factors in many choices with aircraft programs. The field of structural health monitoring (SHM) attempts to reduce labor and cost by allowing technicians to monitor selected properties of an aircraft's structure to detect impending failure. This research examines methods to detect damage to a thermal protection system (TPS) tile using representative aluminum plates. Plates are subjected to modal analysis in single and joined conditions in an attempt to provide the capability of sensing damage to a tile on the surface of a vehicle while the sensors remain on the superstructure of the airframe. Jointly, the development of a means to model the system using finite element techniques is explored. It is found that the finite element modeling technique produces correlating modal frequencies within a 7.19% worst case average when compared to the physical tests. This leads to the ability to compare mode shapes and frequencies to detect damage in a system.

Acknowledgments

I would like to express my sincere appreciation to my faculty advisor, Dr. Anthony Palazotto, for his guidance and support throughout the course of this thesis effort. I would also like to thank Maj Richard Cobb, Mr. Mark Haney and Mr. Mark Derriso for their assistance in this research effort.

Robert M. Vandawaker

Table of Contents

Page

Page

Page

List of Figures

Page

Page

Page

Page

List of Tables

Page

EXPERIMENTAL AND COMPUTATIONAL ANALYSIS OF MODES IN A PARTIALLY CONSTRAINED PLATE

I. Introduction

The art of modeling important dynamic phenomena is the basis for modal analysis. The earliest known investigation into modal analysis dates back approximately 6700 years to the Babylonians. The Babylonians developed the calendar, based on harmonic analysis, which was used in Egypt to predict the flooding of the Nile (12). This research provides the backbone of modern modal analysis.

Today a major focus of modal analysis is the field of structural health monitoring (SHM). SHM arose to offset the cost and time intensiveness of inspecting structures, whether they are bridges, aircraft or automobiles. Health monitoring has many forms, from civil applications in bridges to medical to advanced technology aircraft sensors. These are but a few of the rapidly developing field of structural health monitoring.

Whether it is known as structural health monitoring, integrated vehicle health management or one of numerous other acronyms the main goals are to detect failure, predict lifecycle and reduce total cost. SHM takes root in the quest for longer life cycles, reduced operating costs and the quest to prevent accidents. The ability to take control of these parameters is of growing concern to the United States Air Force. Presently, numerous aircraft in the USAF inventory are near or beyond their initial projected lifecycle (13). The Deputy Under Secretary of Defense for Logistics and Material Readiness has signed a memorandum to establish condition based maintenance (CBM).

"CBM is a set of maintenance processes and capabilities derived, in large part, from real-time assessment of weapon system condition obtained from embedded sensors and/or external tests and measurements using portable equipment" (13). At the forefront of developing this process is the Air Force Research Laboratory Air Vehicle Directorate (AFRL/VA) and its Integrated Vehicle Health Management (IVHM) programs. Figures 1 and 2 depict the proposed system architecture for the IVHM process. Additionally, Department of Defense Instruction 5000.2 states:

> 3.9.2.4 The DoD Components shall initiate system modifications, as necessary, to improve performance and reduce ownership costs.
>
> 3.9.2.4.1 PMs shall optimize operational readiness through affordable, integrated, embedded diagnostics and prognostics, and embedded training and testing; serialized item management; automatic identification technology (AIT); and iterative technology refreshment.

Advanced age poses many problems in keeping these vehicles in the air. Lengthy maintenance and inspection routines are the norm for aircraft of high flight time because the aircraft are operating beyond their expected life cycle. The inspections do prove vital in cases where known defects exist and inspection is the only means of verification. However, time intensive and laborious examination may not always be necessary. Health monitoring is a tool that is of great use in these cases.

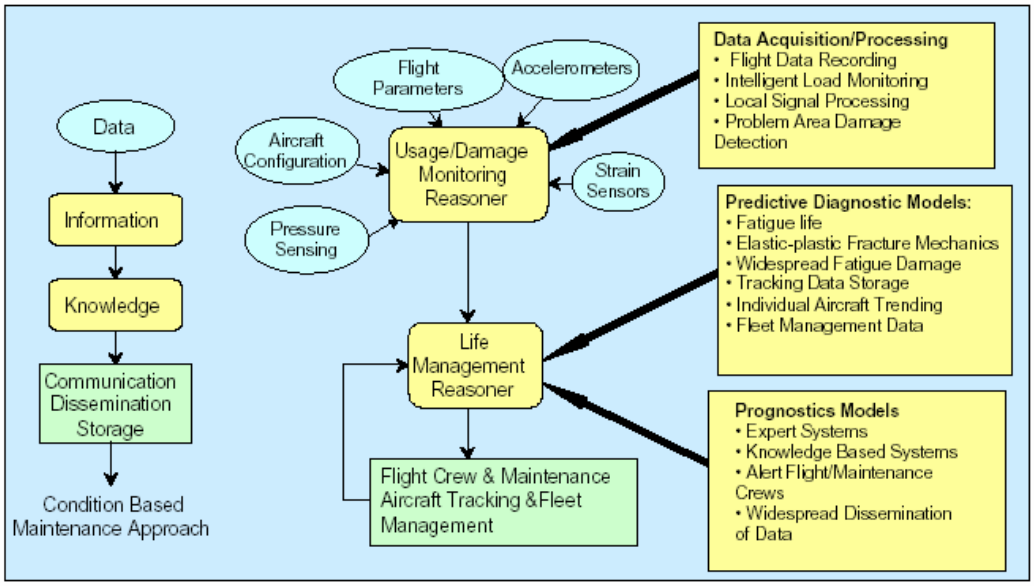

Figure 1.1. IVHM System Architecture Concept (13)

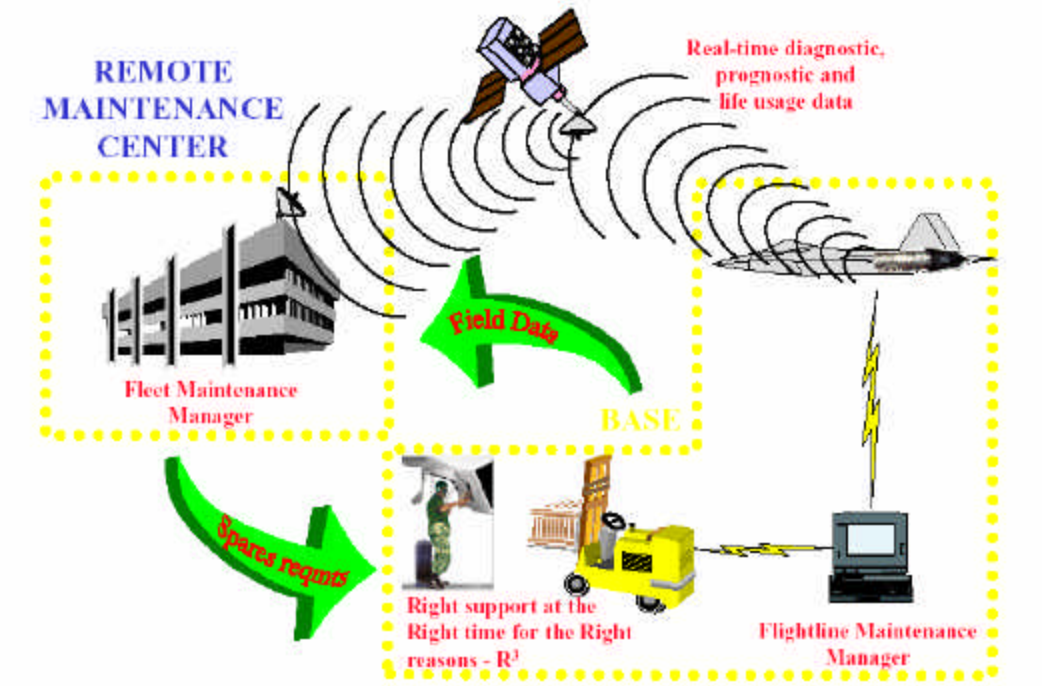

Figure 1.2. IVHM Process (13)

Health Monitoring Motivation

The field of health monitoring is a derivative of the broader nondestructive investigation (NDI). NDI is used in many fields for a broad range of applications. These processes include visual inspection, x-ray analysis, magna flux and vibration signature to name a few (24). These tests are difficult or impossible to accomplish while the structure is in operation, with the exception of vibration analysis. These processes are often laborious and costly to perform at specified intervals over the life of a bridge or vehicle. This leads to health monitoring to provide a real time or near real time picture of the structural condition of a system.

One need only perform a simple literature search to reveal the vast number of individuals and companies dedicated to the task of health monitoring and management. The reason for this is that the development of management and monitoring techniques to predict and warn of failures is becoming of greater importance to industry. Health monitoring has the ability to reduce costs, both labor and material, by accurately predicting when and/or where a part will fail. As the cost of maintenance rises, the need for businesses to trim other expenses is of greater importance. One of the best ways to reduce expenses and maintenance time, provided the technology is at acceptable standards for the intended use, is health monitoring (31, 34).

The past has shown that unnecessary inspection and premature replacement of parts is costly and labor intensive. Aircraft and various other mechanical systems have parts replaced at predetermined times to insure they do not fail in operation (38). The loads and conditions seen throughout these lifecycles are not always consistent. For

example, two aircraft engines are to have their compressor blades replaced at a set number of hours of operations. Engine 1 is subjected to numerous take offs, high speed maneuvers and other high stress environments over the life time and engine 2 is used on constant low speed, fixed altitude missions seeing much less fatigue. At the end of the predetermined cycle both engines must be refurbished with new blades, inspection shows that the blades from engine 1 are more fatigued that those of engine 2. The blades of engine 2 show little to no signs of wear, but they still must be replaced, enter health monitoring. With SHM the frequency, stress or other pertinent information about the blade can be examined with out replacing the blade. This data is then compared to a baseline from blades that have been tested to failure. When the threshold is reached, perhaps many hundred hours after scheduled replacement, the blades can now be replaced. Averaged across an entire fleet of aircraft, the labor saved and delayed cost expenditure has great potential (31).

Tools and Techniques

A seemingly endless variety of analysis techniques exist for a wide range of available data measurements. Some common types of measurements used in analysis are strain, stress, acceleration and frequency to name a few. Various combinations of the aforementioned techniques are also used such as the measurement of acceleration being used to find the frequencies of the system. The type of data to collect is not set in stone as there are many techniques available for the type of data chosen to collect. The data type being collected is determined by several factors including cost, ease of collection,

ease of use and weight among others. It is up to the designer to choose the best measurement for the application and to find the proper sensor package.

The joint development of techniques to perform structural health monitoring and electronics suites designed to match is critical. The type of analysis dictates the sensor package that is utilized. Various sensors exist on the market and the development of new sensors is ongoing. From simple accelerometers fixed to key points on a structure to integral piezoelectric layers in composite panels, there is a sensor to fit most needs. The key to making sensor packages more useful is making them lighter and more easily integrated into the structure. If each sensor requires an elaborate wiring relay in order to work then extra weight is added to the system, which may have large drawbacks. To this end, new lightweight integrated wireless networks are being developed for just this purpose (12).

The types and amount of post processing on the data collected from the structures sensors varies depending on the analysis technique. The designer of the system must determine what the best data measurement and analysis technique is optimum for his or her given system. For some it may be comparing a shift in resonant frequency as a part begins to fail. Other designers might dictate that strain in a system is the best indicator of impending failure. Still more might insist on using both strain and frequency analysis to accurately predict failure. As with sensor packages and data collection, processing techniques are an evolving field.

How does one go about knowing where to look for strain, displacement or damage characteristics in a system? Cobb and Liebst (8) proposed a method of placing

sensors and identifying structural damage from minimal sensor information using first-order partial eigenstructure sensitivity to changes in the structure (8). Experience is one way to develop sensor locations based on what may happen in a system. Without *a priori* knowledge of a system, it is difficult to predict effects of damage to the system. It is very time consuming to guess at sensor locations and relocate them based on observed outcomes. Such an ad hoc method is susceptible to error if the data is misinterpreted or experimental variance is present. Thus the use of finite element analysis (FEA) to determine initial placement of sensors becomes important.

FEA involves solving lengthy equations with numerous matrices and outputs that become more difficult to track as the system gets larger. This offers great advantage when solving a complex system of substructures. Wide varieties of programs exist to perform FEA, from dedicated software packages like ABAQUS and NASTRAN to analysis add-ons for MATLAB or FORTRAN programs. It is user preference as to what program or package best fits the needs of the analysis.

Research Objective

The focus area of this research is the detection of damage in the bolted system used in joining two sets of vertically joined plates. These plates represent the superstructure and thermal protection tile system of future space systems, see Figure 1.3 below.

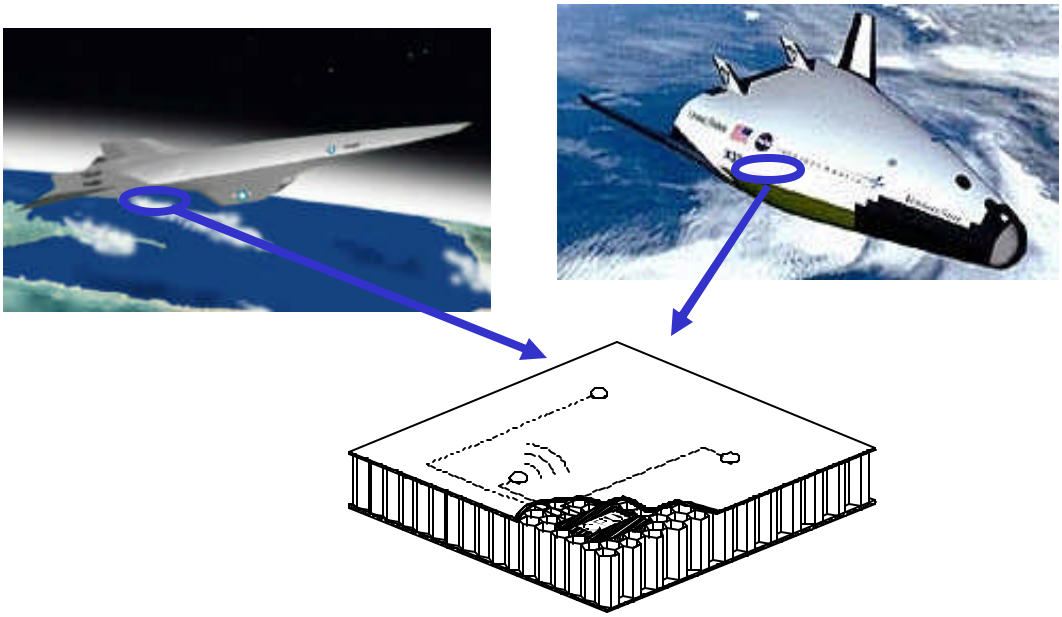

Figure 1.3. Thermal Protection System (TPS) Applications (14)

The research performed falls into three categories. First, the development of accurate finite element models to predict the performance of the systems being examined. Secondly, testing of a physical model is conducted and compared to the FEA solution for validation and sensor optimization. Lastly, the development and identification of analysis techniques to determine system damage detection. These three areas each have their own subsections which are examined in great detail in later sections. The major thrust is to incorporate frequency comparisons between undamaged and damaged specimens.

The ability to detect damage in a structure using a limited number of sensors is the end goal of this research. The investigation entails examining inputs from sensors mounted on the superstructure of an aircraft. In this experiment the superstructure is represented by a large aluminum plate. Three cases are run with increasing complexity in

the structure. The cases considered are a 12 in by 12 in plate, 12 in by 24 in plate and two joined plates with the top plate 12 in by 24 in and the bottom plate 12 in by 28 in. Damage to the plate systems is characterized by the removal of a bolt from the system. Removing the bolts individually from the plates results in a corresponding change in the system, allowing detection of the "damage." The details of this investigation are laid forth in the subsequent sections.

II. Background

Chapter Overview

Structural health monitoring in the field of aerospace is the concentration of this research, but the application is valid beyond flight dynamics. Structural dynamics is a broad topic relating to bridges, buildings and vehicles to name a few. This chapter provides the theoretical background for structural dynamics and SHM.

Structural Dynamics Perspective

In a world of high performance computers and analysis programs it is sometimes difficult to see the big picture of a mechanical system. Countless hours are generally spent designing and testing a structure on a computer before it ever exists in reality. This can lead to problems if the designer accepts the computational results at face value. A key in computer processing is the knowledge that the data output can only be as good as the data input into the system. If the designer does not take the time to study the performance data of the system, i.e. stress, strain, modal factor and numerous others, the final output may ultimately fail. Regardless of the design or use of a particular structure or system it is important to be familiar with the theory and equations behind the design. Each part of a design team knows which part of the system is most important, theirs. Taking this into account they each have desires for design and testing. Regardless of what each system or structure is designed to do there are some fundamental truths. The system will react to outside or perhaps internal influences, not always positively. Also, as most systems age or are fatigued they tend to change and perhaps weaken. This can

lead to failure if left unchecked. This is why testing and intense analysis is critical in a fielded system. If certain risks are accepted, such as limited life of system parts or predicted failure a system may be put in place to monitor these parameters so failure does not occur. The following sections will discuss the equations and methods behind modal responses and analysis.

Fundamental Equations

A host of equations and theory lay behind the model development, data collection and data analysis a system. In an attempt to provide a basic background some of these equations are explored here. The derivation of these equations is in most cases lengthy and will not be discussed in detail, but is available in references (9, 28).

The fundamental equation behind modal analysis of structures to find natural frequencies and modes is as follows:

$$\mathbf{M}\{\ddot{q}(t)\}+\mathbf{C}\{\dot{q}(t)\}+\mathbf{K}\{q(t)\}=\{Q(t)\} \tag{2.1}$$

where q(t) are generalized degrees of freedom and Q(t) are the applied forces. The matrices **M**, **C** and **K** are the mass, damping and stiffness respectively. For an undamped or lightly damped system the matrix **C** can be ignored and Equation (2.1) becomes:

$$\mathbf{M}\{\ddot{q}(t)\}+\mathbf{K}\{q(t)\}=\{Q(t)\} \tag{2.2}$$

Free vibration is the general case when the applied force is equal to zero and is given by:

$$\mathbf{M}\{\ddot{q}(t)\}+\mathbf{K}\{q(t)\}=\{0\} \tag{2.3}$$

Solving this equation for the natural frequencies, w, and eigenvectors, $\{q\}$, is accomplished by solving:

$$\left(\mathbf{K} - w_i^2 \mathbf{M}\right)\{q\}_i = \{0\} \tag{2.4}$$

resulting in a number of w_i and $\{q\}_i$. The subscripts, i, represent the modes of the given system. There are a multitude of methods to solve Equation (2.4) depending on the complexity of the problem and the preference of the solver. These methods can be found in (9, 28) and provide a range of solution techniques.

Frequency Response Function

A vast majority of analysis techniques and data observation are in the form of the frequency response function (FRF). The FRF is defined as follows:

$$FRF(w) = \frac{X(w)}{F(w)} = \frac{1}{1 - \left(\frac{w}{w_n}\right)^2 + 2x\left(\frac{w}{w_n}\right)} \tag{2.5}$$

where X(w) and F(w) are the Fast Fourier Transforms (FFT) of the response of the system and excitation force respectively (7, 18). The remaining variables are the damping of the system, ξ, and ω and ω_n which are the driving frequency and natural frequency. Basically, the FRF is a ratio of structural response to an applied load. Expressed as a transfer function, the FRF is expressed:

$$H(iw) = \mathrm{F}\left\{h(t)\right\} = \int_{-\infty}^{\infty} h(t) e^{-i w t} dt \tag{2.6}$$

where $\mathcal{F}$ is the Fourier Transform and *h(t)* is the impulse response function of the system. The impulse response of a system is the response of a system with zero initial conditions.

$$S_{xy}(w) = S_{xx}(w) \int_{-\infty}^{\infty} h(x)\, e^{-i w x}\, dx \tag{2.7}$$

S_{xy} is the auto spectral density and S_{xx} is the cross spectral density. The spectral densities are the relationships between the inputs and outputs to and from a system using frequency and time histories. From Equation (2.6) it is seen that (2.7) is equivalent to (2.8).

$$S_{xy}(w) = S_{xx}(w)H(w) \tag{2.8}$$

Furthermore the FRF can be expressed:

$$H(w) = \frac{S_{xy}(w)}{S_{xx}(w)} \tag{2.9}$$

$$H(w_k) = \frac{S_{xy_k}}{S_{xx_k}} \tag{2.10}$$

For the discrete case, provided the number of averages is large enough, $H(w)$ can be approximated using the average values of the signals as seen in (2.10). The subscript, k, represents the number of averages taken for the signal. Additionally, the FRF solution has real and imaginary parts corresponding to the phase and magnitude of the response.

Coherence

Another means to analyze a system is the measure of linearity between the input and output of the system which is coherence, γ^2. The following equations establish the relationship.

$$H_1(w) = \frac{S_{xy}(w)}{S_{xx}(w)} \tag{2.11}$$

$$H_2(w) = \frac{S_{yy}(w)}{S_{yx}(w)} \tag{2.12}$$

$$g^2 = \frac{H_1(w)}{H_2(w)} = \frac{|S_{xy}|^2}{S_{xx}S_{yy}} \tag{2.13}$$

$$g^2 \leq 1 \tag{2.14}$$

The transfer functions $H_1(w)$ and $H_2(w)$ are derived in the same manner as (2.6)-(2.9) and neglect input or output noise. Provided there is no averaging $H_1(w)$ and $H_2(w)$ are identical. $H_1(w)$ and $H_2(w)$ are estimators of the FRF, where $H_1(w)$ minimizes error in the response signal and $H_2(w)$ minimizes input noise error (18). Also, S_{xx} and S_{xy} are as defined previously. Most testing produces noise, whether it be on the input or output side, which leads to averaging of the signal in the hopes of eliminating or reducing the effect of the noise on the FRF. The coherence of a system is a good means to verify the quality of the FRF. Coherence ideally would be 1 for a linear system. In practice the coherence varies across the frequency spectrum, typically dropping at resonance and antiresonance. Antiresonance is a frequency at which the frequency response goes to zero for a particular degree of freedom (17). As a precursory analysis tool, the coherence can provide insight into the validity of the test (7, 18). Figure 2.1 shows the process of producing frequency response and coherence functions. It begins with the input signal from a generator and response signal from a sensor and follows through all of the computational techniques that are described in the preceding sections. The end result is coherence and frequency response function outputs.

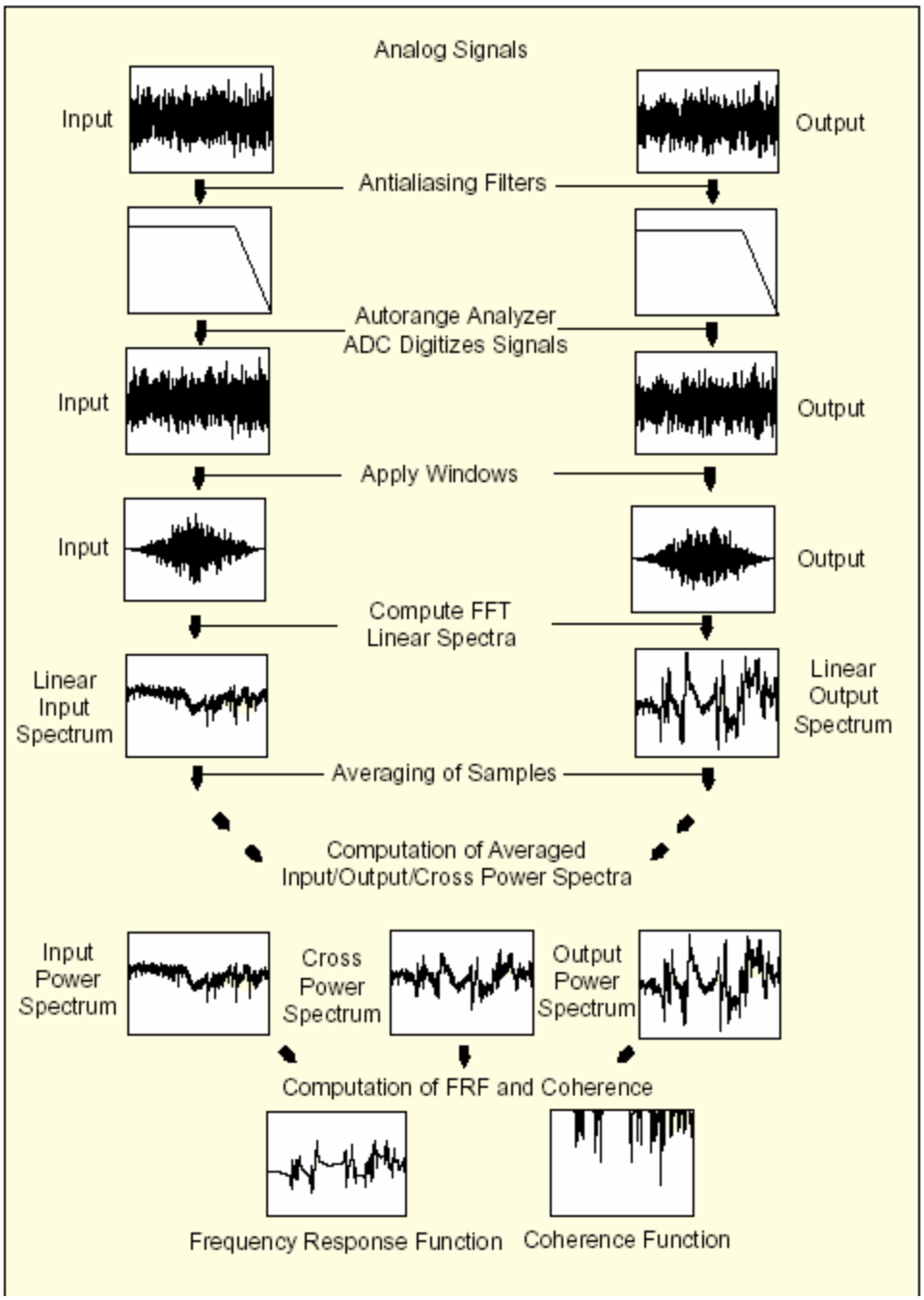

Figure 2.1. Frequency Response Analysis Process (4)

The first step in Figure 2.1 is to collection of input and output signals. These signals pass through antialiasing filters, which prevent frequencies greater than half the sample rate from popping up in the signal by utilizing a low pass filter with a sharp cut-off (18).

Windows are then applied to these signals to minimize the leakage, power from neighboring frequencies adding to adjacent frequencies (18). After this, the system is averaged as it is collected and techniques detailed for the frequency response and coherence are applied to provide the FRFs and coherence for the data.

Analysis Techniques

How does one go about performing analysis on a system? There are a multitude of analysis techniques and processes ranging from basic manual calculations to laser testing and high performance computing methods. Several of these methods are examined below, but this is by no means a complete analysis of the types of tests that are available to characterize systems. Health monitoring is a rapidly evolving field with new techniques and equipment under constant development.

Modal analysis

To truly understand the approach of SHM, a background in modal analysis is important. Modal analysis is a process where dynamic response of a structure is used to characterize resonant frequency, mode shapes and damping of the system. The analysis is generally performed using a shaker or instrumented hammer to excite the structure. Accelerometers are placed at predetermined locations on the system to record the response of the structure. The output from the accelerometers is often fed into software to calculate the frequency response function (FRF) and other relevant data to the test. Provided enough accelerometers are placed on the system, modes shapes are discernable from the responses (10, 36, 18). Loading accelerometers onto a structure can have its

drawbacks. Accelerometers add weight to a system; this can affect the natural frequencies if too much weight is placed in one location. Light weight sensors on a heavy structure have little effect on the frequencies or mode shapes of the system. This is essential for accurate measurement of the response of the system.

FRF Optimization

The widespread use of modal analysis and historical examples of tests make it a top contender for many SHM processes. In 1996, Lim et al introduced a method of health monitoring using a modal parameter algorithm. This method was tested on a 12-bay truss and uses force transducers, displacement sensors and accelerometers to collect modal data from the structure. These data are processed to determine the frequency response functions of the system. The FRF data are used to identify modes individually in the truss using an algorithm designed to locate the damage on the structure (26). Numerous other experiments and methods have been proposed and demonstrated on a wide range of civil structures and a variety of vehicle types.

The type of structures examined is far ranging. Simple laboratory experiments and validation of processing techniques are generally performed on basic structures. These structures include cantilever beams of varying dimensions and plates in numerous configurations. The cantilever beam model is preferred for is simplicity and the vast amount of knowledge published about the characteristics of beams. One such example is the examination of a cantilever beam by Bartkowicz, et al in 1996. Their beam was excited and an array of accelerometers used to send data to a computer for processing of the modal data. They also induced damage to the beam by removing material from

several sections to characterize the beam's modal parameters under this condition. Computer software was then used to find the FRFs of the system and compare the natural frequencies to identify damaged states (5).

The frequency response function optimization (FRFO) technique introduced by Schulz et al in 1996 is another method to characterize a system. This method uses accelerometers located at optimum positions to collect modal data. The optimum sensor location is found though finite element modeling, which is refined to match the real world system. The structure is then excited and the response of the structure measured to be processed and monitored. FRFO uses receptance data, displacement/force, as a parametric identification tool to compare damaged to undamaged FRFs. This technique does not perform extensive modal or eigenstructure analysis and is only suggested for small or medium systems due to computational burden (33).

Laser Vibrometry

The use of laser vibrometry allows a system to be examined without attaching sensors. Eliminating sensors from the system can give a more accurate depiction of the fielded characteristics by eliminating the weight associated with attached sensors. Laser vibrometry works by shooting a laser beam at a structure and using the reflected beam from the structure to calculate minute differences in the acceleration, velocity or displacement. The structure must be first excited by the method chosen by the tester. The data from these tests are compiled by a computer and analyzed with one of many computer programs designed for modal analysis (35). A major disadvantage to using laser vibrometry is the fact that the laser needs to remain still during the testing of the

system. Since the relative time the beam takes to travel and return to the sensor is what is measured, if the laser is also moving with some random motion it becomes impossible to decipher the structure's true modal response.

Energy Methods

The use of strain present in a system to determine physical characteristics is another way to quantify a structure. One technique utilizing an energy method is the Statistical Energy Analysis (SEA). The SEA process involves regarding a system as a series of interconnected subsystems with the average of the subsystem energies representing the entire system. The energy balance in each subsystem is a function of excitation power, power lost to damping and energy flowing to other subsystems (40). Mace and Wester, along with Mace and Rosenberg, studied the energy flow between two edge-coupled plates. Their research focused on ensemble averaging of the energy flow between the plates and the effect of irregularities on the subsystems.

Other investigations have been performed into the energy distribution of the classical example of the cantilever beam. Yang et al investigated the balance of energy in a cantilever beam subject to cracks under constant loading situations. These studies involved modeling the strain energy variations through the cracked beam. The model was used to find the equivalent bending stiffness and equivalent depth of the crack in the beam. Once the strain energy is modeled the vibration for the beam is then studied. These data are used to find the natural frequencies of the beam (41).

The use of energy methods to determine damage in a structure has advantages in that that strength of materials is generally known. If there is little other knowledge about the

structure prior to sensors being installed the levels of strain and/or stress in a given member can be a good indicator of impending failure. If a catastrophic failure is eminent or too much strain is present in a particular location, it is possible to take action to prevent the failure.

Acoustic Emission

Acoustic emission (AE) testing is an ultrasonic technique of nondestructive testing (NDT).

> "Ultrasonic nondestructive testing introduces high frequency sound waves into a test object to obtain information about the object without altering or damaging it in any way. Two basic quantities are measured in ultrasonic testing; they are time of flight or the amount of time for the sound to travel through the sample and amplitude of received signal. Based on velocity and round trip time of flight through the material the material thickness can be calculated…
>
> The most common methods of ultrasonic examination utilize either longitudinal waves or shear waves. Other forms of sound propagation exist, including surface waves and Lamb waves.
>
> • The longitudinal wave is a compressional wave in which the particle motion is in the same direction as the propagation of the wave.
> • The shear wave is a wave motion in which the particle motion is perpendicular to the direction of the propagation.
> • Surface (Rayleigh) waves have an elliptical particle motion and travel across the surface of a material. Their velocity is approximately 90% of the shear wave velocity of the material and their depth of penetration is approximately equal to one wavelength.
> • Plate (Lamb) waves have a complex vibration occurring in materials where thickness is less than the wavelength of ultrasound introduced into it." (29)

In their study of acoustic emissions in thin plates, Prosser, Gorman and Humes (31) explored the propagation of waves and dynamic response of thin aluminum and composite plates. Their studies included low and high speed impacts to show AE signals

could discern frequency shifts and modal components. They conclude that AE is feasible for detecting and locating damage in air and spacecraft.

Another way to examine AE is the propagation of Lamb waves. Giurgiutiu and others (20-23) use embedded piezoelectric wafer active sensors (PWAS) to track wave propagation through structures. The PWAS are used as both actuator and sensor in the systems to both excite waves and detect their movement. The PWAS system has been used to detect cracks in beams, plates and aircraft structures. A pulse-echo method is used to detect damage. This means a wave is generated by the piezoelectric active sensor and the time it takes to return to the sensor is used to locate and identify damage. This technology has produced numerous papers and investigations.

Finite Element Analysis

The use of finite element analysis (FEA) to explore structures is becoming an important tool for engineers. FEA can help to pinpoint areas of interest in a structure to monitor for failure or modal characteristics. FEA is also a tool to test structural changes before time and money are committed to make changes in a system. The use of high-speed computers and analysis software is vital in the examination of complex structures. Considering finite element techniques when examining a model is often the first step in testing a structure. In many experiments and analyses FE is the only testing performed on a system. Accuracy of a model comes into play when trying to match a model to a system.

What exactly is a finite element model? Depending on the analysis method, manual or computer, it may be many matrices on a piece of paper or a picture on a

computer screen. Regardless of the complexity of the model or how it appears on a computer screen, all FE models come down to mass, stiffness and damping matrices, **M**, **K** and **C**. Depending on the intricacy of the structure, the structure's shape and the solver's preference a variety of solution methods can be employed to solve the problem. They all solve the same equation, (2.1), just in different techniques as previously mentioned. This research uses ABAQUS to solve finite element models. The chosen solution method for ABAQUS is the Lanczos method, discussed in the Results section and in references 1 and 9.

Once a model's physical properties are decided, the constraints and boundary conditions are decided. The final step is to mesh the model with the designer's choice of mesh properties. The mesh can have a host of sizes and shapes depending on the complexity of the model and accuracy desired. The types of mesh are discussed in the Experimental Set-up section of this thesis. With meshing done the analysis is performed and a solution is calculated. Depending on the software used, it may be numerical or in graphical format. It is then up to the engineer to interpret the results and decide if the FE model needs to be tuned.

Model tuning is the process of modifying the finite element model to more closely represent the physical structure. There are a host of methods available in published works explaining how to tune a finite element model. One method is to adjust the mass or stiffness matrices of the structure to obtain results more closely resembling the physical system (6). Mesh refinement and redistribution can affect the modal parameters as well. Boundary conditions can also be adjusted to obtain the desired results. The

bottom line is to accurately depict the physical model the finite element model is representing.

Processing and Damage Detection

After the data are collected from the sensors it is up to processing techniques to determine the condition of the system. Some processing techniques have been discussed above, but they bear reemphasis. Many techniques use FRF data from the structure to characterize the system in pristine and damaged states. These data can be utilized in many ways, from the Modal Assurance Criteria (MAC) or one of its derivatives to pattern recognition (3). The MAC compares the eigenvectors of the system to determine if it matches a base system. This bases system can be a finite element model or another state of the system. This technique is discussed further in Section 3.

Pattern recognition relies on gathering data about the undamaged state and using it as a baseline for future analysis. This baseline is stored in the diagnostic computer that records the output of sensors on a structure and is continuously compared to the different states of the system. Provided the detection algorithm designed properly, the location of damage on the structure can also be determined.

Some processing techniques are performed "real-time" or near "real-time" by a computer on the structure. This on board processing can provide the operator with indicators that the structure is about to fail, thus needing to be shut down. Still others require that the system output be downloaded to a processing station after the data are collected and/or the vehicle is done with its mission. Often it is the complexity of the calculations or the necessity of human interpretation of the data that requires detached

processing stations. Space requirements and weight may be other limiting factors as to the remote processing of data.

The combination of some or all of the listed and unreferenced collection and processing techniques can yield the ability to accurately detect damage in a structure. Enduring rigorous or even light duty causes structures to weaken over time and perhaps catastrophically fail. Some failures give little warning and real-time analysis of the structure can provide an added measure of safety. Safety, as mentioned previously, is one of the driving factors for structural health monitoring.

III. Experimental Set-up

Chapter Overview

This section deals with the setup of the experiment and the actual testing of the models. These tests and analysis are performed using a combination of the techniques discussed in the Background section. Additionally, the choices made for the models and techniques used in this research are discussed.

Material Selection

The selection of materials for an experiment varies widely and is generally up to the engineer's discretion. The actual material used for the Thermal Protection System (TPS) tiles is a carbon fiber composite. Due to the cost and lead time required to obtain an actual TPS tile, it was decided that aluminum would be used instead. A review of materials led to the selection of 2024-T3 aluminum for the plates. The main factors in selecting 2024-T3 were machinability, cost, and availability. Table 3.1 shows the material properties of the aluminum. Also, the material chosen for the stand-offs is 2024-T3. Finally, the bolts chosen for the tests were ¼-20 UNC, grade 5, zinc plated steel. The next section will discuss the uses and experimental set-up for the aforementioned materials.

Table 3.1. Selected Material Properties of 2024-T3 (37)

Modulus of Elasticity	10.6 Msi
Density	0.100 lb/in^3
Poisson's Ratio	0.32

Test Article Configuration

The methods of this examination are an attempt to approximate the structure and installation of the TPS tiles. Figures 3.1-3.3 show the configurations of the plates for the tests conducted. All plates are 0.190" thick. Figure 3.1 shows a 12" x 12" plate, plate 1, which is used to compare results to a test conducted by AFRL/VA (14). Plate 1 has four bolts fixing it to the test table.

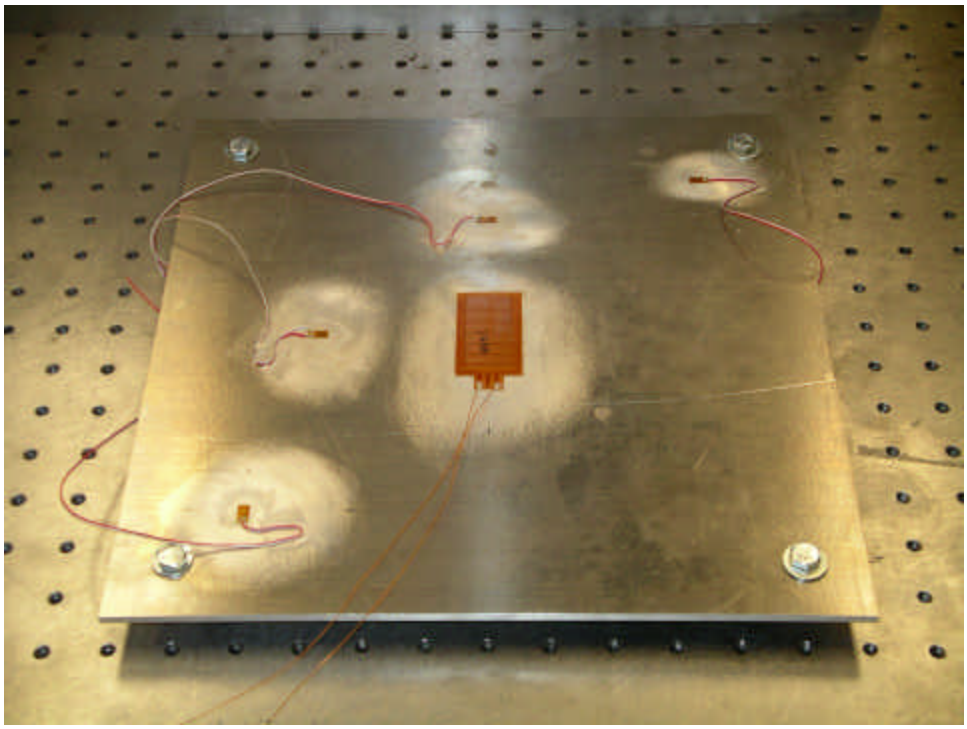

Figure 3.1. 12" x 12" Plate Configuration

The second set of tests run is on a larger 12" x 24" plate. This single plate has 3 rows of bolts at 3 bolts per row affixing it to the table. This size is chosen as it is half the size of the original TPS panel, which is symmetric.

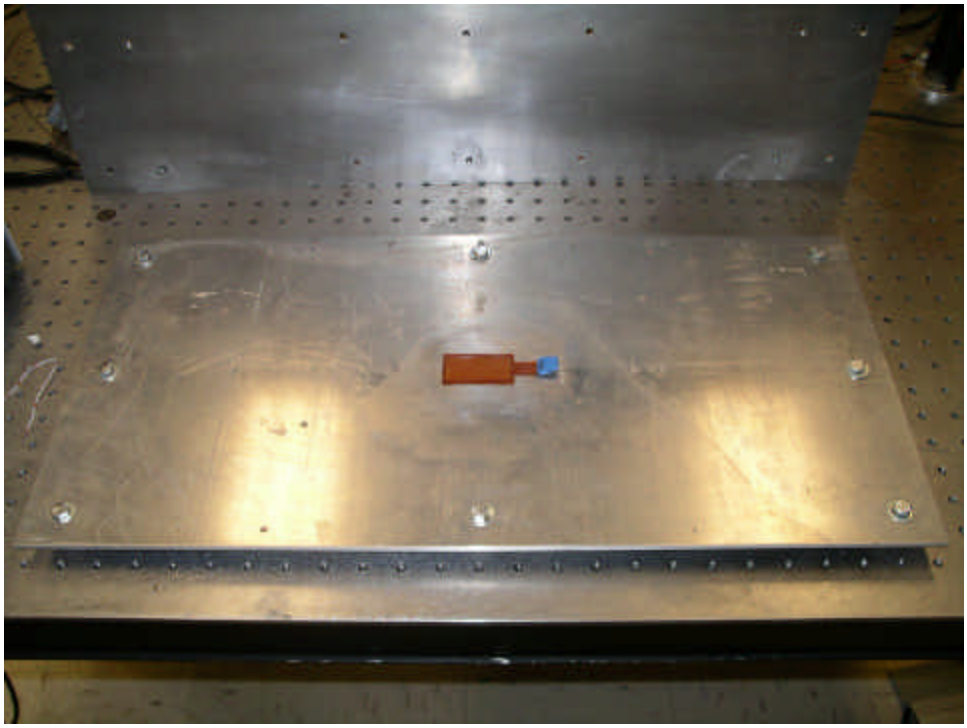

Figure 3.2. 12” x 24” Plate Configuration

Seen below, Figure 3.3 shows the experimental set-up for testing the joined plate configuration. This arrangement has a 12” x 24” plate joined to a 12”x 28” plate. The TPS tile is represented by the upper 12” x 24” plate with the lower plate representing the superstructure of the aircraft. As with the previous analyses the plate are joined together and to the table.

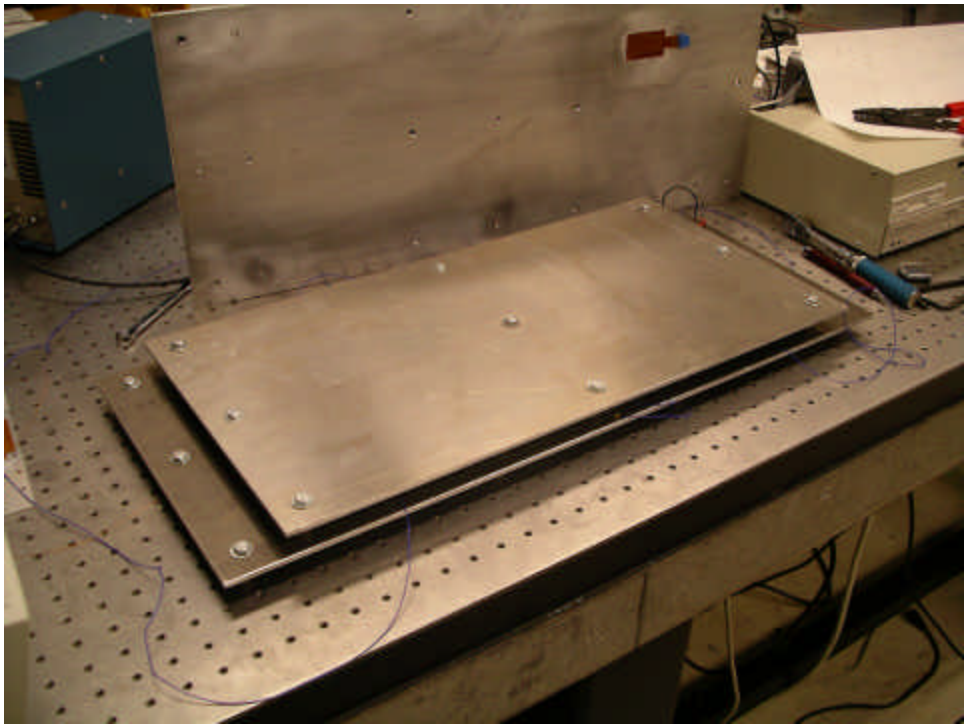

Figure 3.3. Joined Plate Configuration

Figure 3.4 shows the configuration with a bolt and spacer removed as well as a view of the bolt and spacer connection. The bolt and spacer removal condition is repeated in the physical tests as necessary to simulate damage at specified locations in the plate systems.

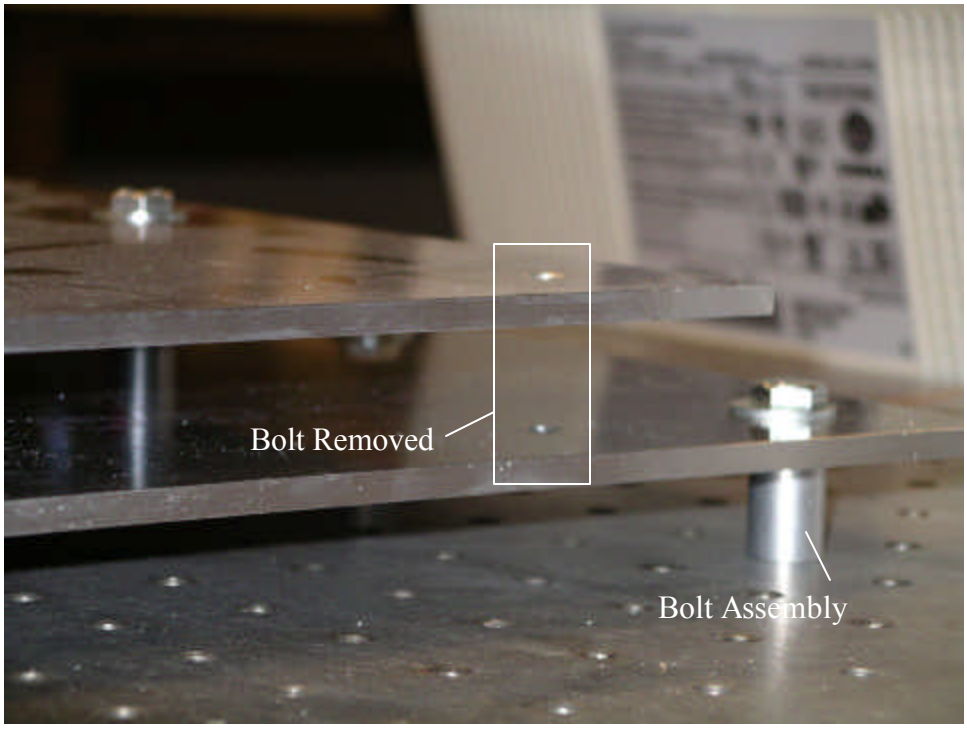

Figure 3.4. Bolt and Spacer Conditions

Finite Element Model

The approach of this research being twofold, physical testing and model comparison, necessitates the development of an accurate model. Prior to any physical testing of the articles, finite element models were created. These models are used to analyze the systems prior to physical testing and to provide initial placement for sensors. With the material specifications determined and the sizes of the plates established the next step is to analyze the systems. The finite element program selected for this research is ABAQUS. (1) The ABAQUS/CAE program was utilized for its graphical user interface which allows the user to visualize the structures as they are being designed. The ABAQUS/CAE software also allows the user to graphically picture the structural response of the plates as they undergo deformations. This ability proved invaluable in

selecting locations for initial sensor placement. Although the fundamental equation for vibrations was mentioned previously, it is worth reiterating. Equation (3.1) is the equation solved by ABAQUS during its modal analysis routine.

$$\left(w^2 * \mathbf{M}_{M\,N} + \mathbf{K}_{M\,N}\right) f_N = 0 \tag{3.1}$$

In this equation w are the natural frequencies, **M** and **K** are the mass and stiffness matrices respectively, and the vector f represents the eigenvectors. The subscripts M and N are the dimensions of the matrices, where M is the number of rows and N is the number of columns. The solution methods remain as before.

Case 1

The first case examined is the 12" x 12" plate configuration. This case is examined to validate results from a previous test run by AFRL/VA. Initially the bolts were modeled as deformable bodies, but after preliminary physical testing of the model it was observed that modeling the bolts as rigid bodies was a better approach. This phenomenon is discussed further in the Results chapter. The nodes around the bolt holes in the plate are constrained from rotating or translating in any direction, thus negating the need to model the spacer or bolt in the system. This method was also discovered during initial testing of the physical model and is discussed in the Results chapter. Further development of the FE model includes constraining the base of the bolt in the three displacement and three rotational degrees of freedom. With the constraining

accomplished the next step is to mesh the structure. Since the bolts are rigid bodies, they do not need to be meshed as they cannot deform.

The number of elements affects the quality of the resonance frequencies from the solution to Equation (3.1). A mesh convergence study was carried out to verify that the solution converged. The results study can be found in Table 4.1.

The test conditions analyzed in the FE model are done with all bolts fastening the plate rigidly to the table. The next case is to remove the bolt, which in the computer model is done by removing the bolt and the constraint at that point. This leaves one corner of the plate with no connection between the plate and the test table. Only one condition is examined as the plate is symmetric about all axes. The results of these tests will be discussed in the following chapter. With the results of case 1 established, the 12" x 24" plate is the next hurdle.

Case 2

Furthering the investigation leads to the next step, a more complex problem. The problem becomes more difficult as a result of having a larger system with more connections to rigid parts. Also, the part is no longer a square and thus not possessing the same symmetric properties. The same techniques used in the model development in case 1 carry through to case 2.

The analysis conditions of case 2 are similar in that bolts are removed to replicate damage to the system. The difference between the cases is that more bolts are removed from the system in case 2 due to different physical dimensions. In these tests bolts 1, 2 and 4 are removed from the plate at different times to simulate damage. Refer to Figure

3.2 for bolt numbering schemes. In short the bolt numbering scheme begins with number 1 in the upper left quadrant, if viewed from the longest side of the plate, with numbers increasing toward the base of the plate. This process begins again in the center of the plate and on the right side. Therefore this testing process removes 1 bolt from a corner, 1 from the center of the short side of the plate and 1 bolt from the long side of the plate. Once this analysis is complete case 3 is the next step.

Case 3

The modeling continues with inclusion of a second plate to represent the superstructure of the aircraft, seen in Figure 3.3. This set-up consists of a 12" x 24" plate bolted to a 12" x 28" which is in turn fixed to the test table. The numbering pattern for this set-up is the same as in case 2. In this analysis, bolts 1, 2, 4, 5, 10, 11 and 13 and their constraints are removed individually.

Sensor Placement Selection

Once all of the finite element analysis is completed by the computer it is time for human decisions to be made. These decisions revolve around selecting the optimal placement for accelerometers on the structures. The best locations are those where the plate moves the greatest, thus allowing a large range of motion. The worst positions to place sensors are at the node points that remain stationary during modes. These points tend to undergo constant acceleration due to the transition from acceleration in one direction and then another. This leads to what appears to as noise in the response as the

sensor is constantly in motion. The proper selection of sensor locations is crucial to adequately measuring the system response. (39)

In order to properly select nodes on which to place the accelerometers analysis of all modes collected is important. To appropriately choose locations, video files are created by ABAQUS of the motion of the plate for each mode. Upon viewing each mode, the locations with maximum motion that are not located on nodes that do not move are recorded. From these sites the best are chosen for sensor placement. These placements provide the initial testing locations for the physical plates.

Physical Model Testing

To ensure the accuracy of the finite element results, physical testing of the modeled plates is necessary. Once these data are collected, they are then used to determine if the structure is damaged. Detection of damage in the systems will then qualify the analysis technique. Modal analysis of the previously mentioned systems is conducted as described in the following sections.

Test Article Preparation

The key to any good test program is proper preparation and equipment selection. Prior to any physical testing of the plate, they must first be manufactured. This is done by drilling and tapping holes in the plates as required by drawings. The only remaining manufacturing task is to cut the spacers to length and drill clearance holes through them. With the machining complete the sensor package is now attached and the piezoelectric actuators are bonded to the plates.

The piezoelectric patches are chosen as the means to excite the structures. The actuator patch chosen for these tests is the Active Control eXperts (ACX) qp10ni strain actuator. This patch utilizes voltage from a signal generator which is converted to strain by the patch to induce movement in the structure. The qp10ni strain actuator has 2 modes, a longitudinal and a transverse strain, depending on the pin to which the voltage is applied. The pin configuration chosen for the tests conducted in this series of tests applies a longitudinal strain. Longitudinal strain takes advantage of the d31 effect, which means as the voltage is applied the patch increases in length while decreasing in width (2). This length change induces a strain in the structure eliciting a response. The patches are bonded to the structure per manufacturer recommendations using supplied 2 part epoxy (2).

Electronics and Software Set-up

Software configuration and equipment set-up is another key to simplifying testing and providing uniformity. This research uses the Data Physics Corporation's SignalCalc® 620 version 3.0.439 dynamic signal analyzer software to perform data collection and initial processing. This software in conjunction with the Agilent Technologies E8408A VXI Mainframe is used to gather and process data from the plates. SignalCalc® is used to set-up the test parameters, control the excitation signal and record and process the response data. For all tests 4096 data points are collected to provide data resolution. Also each test is run for 200 exponential averages with 50% overlap in the recorded signal to reduce noise in the data and to speed processing (7, 18). For all plates a 2V input signal is used. A Hanning window is applied to that data (7). For the 12" x

12” plate a chirp signal ranging from 1Hz to 1000Hz is used. For the 12” x 24” plate and the joined plates a 1Hz to 1250Hz chirp signal is used. The increase frequency range for the larger plates is to capture higher end modes. A chirp signal is a sine wave with linearly increasing frequency which looks like:

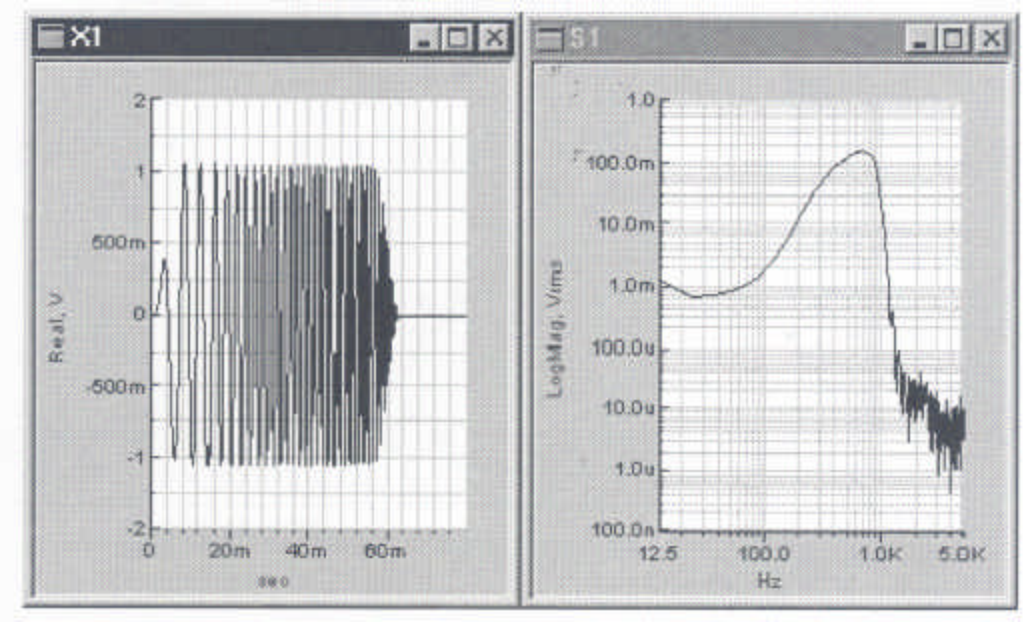

Figure 3.5. Time History and Spectrom of a Chirp signal (11)

This signal is processed though the Agilent E8408A and then sent to the ACX EL-1224 power amplifier and finally on to the piezoelectric actuator. Once the piezoactuator transfers strain to the structure, the PCB Piezotronics 352C22 accelerometers are excited and send their signal through PCB 482A16 Signal Conditioners and the Agilent mainframe to the SignalCalc® 620 software. Figure 3.6 shows the above process.

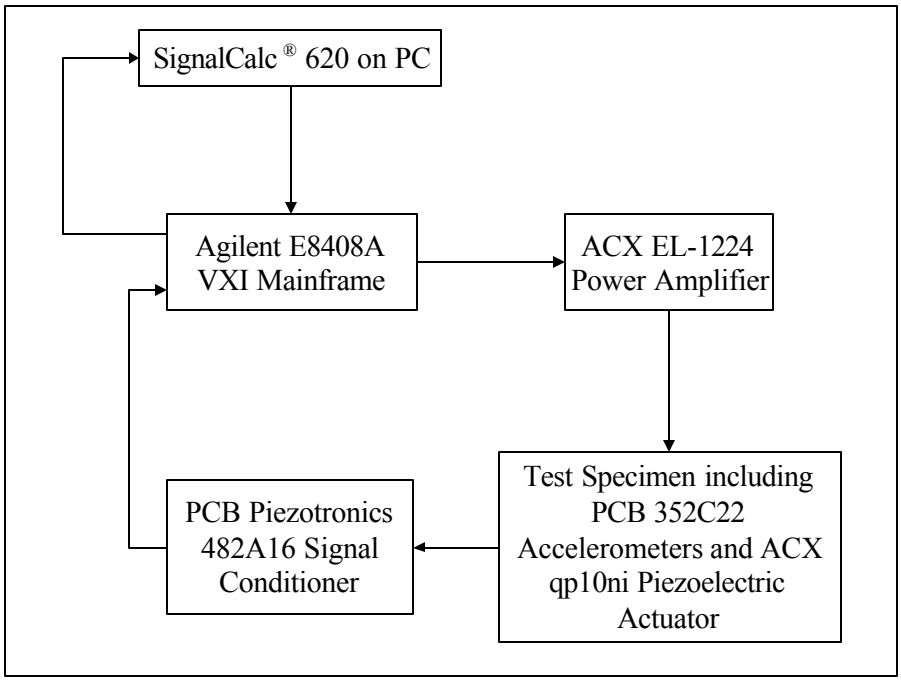

Figure 3.6. Test Equipment Layout and Data Flow

Accelerometer selection and placement as well as piezoelectric actuator effects are key issues to deal with prior to testing. In order to reduce mass loading on the structure being tested it is necessary to use lightweight accelerometers (39). The accelerometers used in this research weigh .017 oz, which when compared to the weight of large aluminum plates in miniscule (30). Another factor in testing is the means of attaching the accelerometers to the test articles. Since this research uses several plates and adjustable sensor placement, it is necessary to be able to move and remove the sensors as needed. To this end wax is used to secure the accelerometers per manufacturer specifications (30).

Piezoelectric actuation also has effects on the plate during the testing. Proulx and Cheng researched the effects of piezoactuation on plates and found that modal coupling

can become a problem at higher frequencies (32). With the actuation and measurement considerations accounted for testing and processing can now commence. With the results of the finite element analysis in hand, the accelerometers are placed according to optimal data collection points.

Test Procedure

With the aforementioned considerations taken into account the physical testing of the plates can now commence. First, all sensor and actuator leads are attached to their respective amplifiers, conditioners and analyzers. Second, prior to each test all bolts are loosened and tightened to 50 in-lbs of torque with a calibrated torque wrench. This is done to ensure that the bolt and spacer systems behave as rigid connections. As stated previously, the bolt and spacer are removed to simulate damaged in the system. The structures are attached to a Newport Corporation optical table, which is very rigid so it will not flex with the plate motion. Also, the optical table provides vibration isolation and damping since it is floating on a cushion of compressed air. Last, the SignalCalc® 620 software is configured to capture the data and calculate the frequency response and coherence of the data. The data collected is then recorded to a MATLAB® file for exportation and post-processing.

Post Processing

Initial processing of the accelerometer data is performed by SignalCalc® 620, to include FRF and coherence data as well as formatting the data for MATLAB®. Once in MATLAB® the data is further analyzed. The data are first processed to determine

resonant frequencies. From there the eigenvectors of the system are formed by creating a vector of the displacements from each test. Once all eigenvectors are determined, they are normalized by dividing by the largest nodal deflection in the vector. These normalized eigenvectors are then compared to those from the FE solution, which are normalized to the same node. The MATLAB processing was completed through a program developed by the author.

Physical and Finite Element Comparison

The method by which they are compared is the Modal Assurance Criterion (MAC). The MAC is used to compare the eigenvectors of a system to those of another system, in this case physical to finite element. The equation is as follows:

$$MAC = \frac{(f)_{FEA} \cdot (f)_{EXP}^{T}}{\left[(f)_{FEA} \cdot (f)_{FEA}^{T}\right] * \left[(f)_{EXP} \cdot (f)_{EXP}^{T}\right]} \tag{3.2}$$

where f represents the eigenvectors of the finite element and experimental tests (17). The eigenvectors are found using the method described for Equation (4.1). When the eigenvectors have a large imaginary portion after normalization, they are disregarded. This relates to the discussion in Chapter 4 about noise in the system. When the imaginary part of the eigenvector, the phase contribution, is large, there is a large difference in the response of the system due to the noise. This is discussed further in Chapter 4. The output of this equation is a scalar number corresponding to the percentage that the two vectors agree. The MATLAB® analysis performs the MAC calculation and compares each physical mode of the plate to each finite element solution.

This produces a matrix of the scalar results which shows how each physical mode compares to its corresponding FE mode. The higher the scalar number in each comparison the greater degree of agreement exists between the FE solution and the actual experimental results. (3) The results of these tests are found in the Results chapter of this research.

Once the MAC matrix is formed using the above technique it is further processed to draw out the pertinent data. This is done by first identifying all MAC data with mode shape correlation of 70% and above (3, 17). Once the modes of interest are identified the rows and columns of the matrix that don't have a correlation of over 70% in them are deleted. Further analysis of the matrix is performed to remove correlations that occur at large differences in modal frequencies. A large difference is described as that which is over 30%. These steps generally leave a matrix with modal comparisons of interest along the diagonal of the matrix. If there are other selected MAC quantities that qualify for the comparison criteria the MAC and percent difference in the frequencies are then compared to determine which data are kept. This process is repeated for each process of simulating damage and the comparisons are repeated.

The initial MAC comparison between the finite element and physical models is the baseline used to determine which modes can be found with a high degree of certainty. Once determined, the frequencies of the undamaged case are used as a baseline for future testing. A shift in frequency is an indicator of a change in the system. It is this shift that is used as a qualifier to look for damage in the system. If there is a shift in frequency then the mode shape of the shifted frequency is compared to the baseline case. This is

also the basis for determining where the damage lies on the structure. Once these results are obtained, they are processed in the same manner as the previous step. The results for the MAC for the physical tests are then checked to see if the modes which have good correlation for between the damaged and undamaged cases also have correlation between the physical and finite element results. This means checking the MAC from the initial step. If there are modes that appear in the FEA versus experimental and in the undamaged experimental versus damaged experimental then the mode shapes are obtained from ABAQUS® for comparison. The mode shapes of the damaged finite element tests are then compared to those of the undamaged FE solution. Figure 3.7 shows the process.

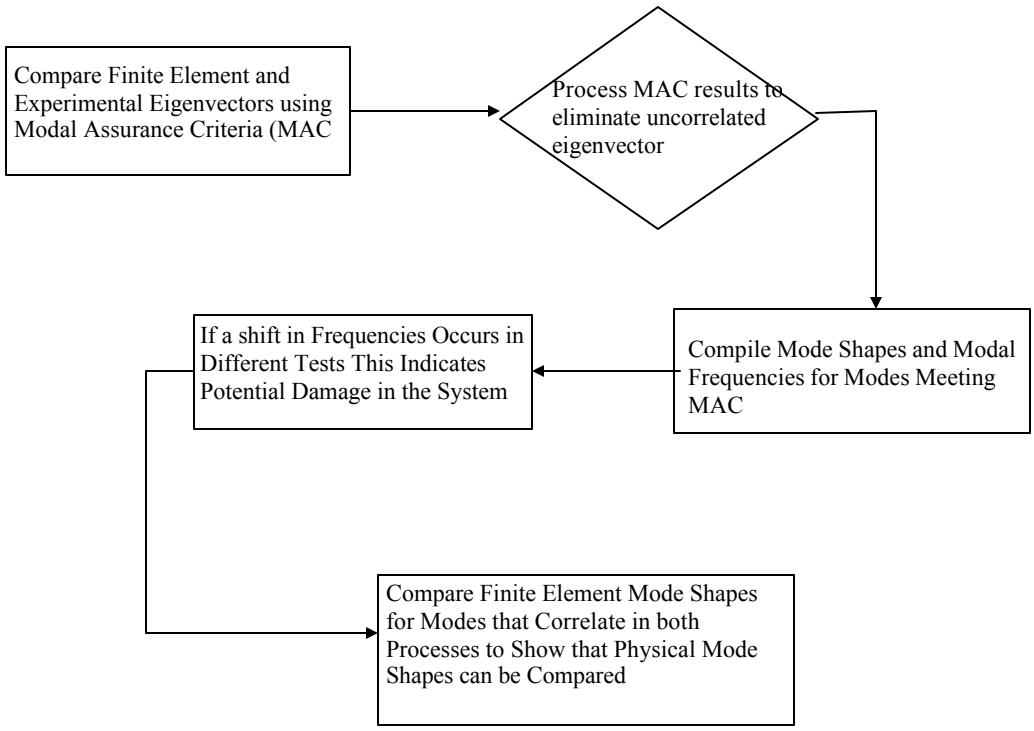

Figure 3.7. Data Analysis Technique, Post Collection

Assumptions

In any experimental analysis certain assumptions are made before the testing begins. In this research several assumptions are made:

- Plate are symmetric
- Material properties do not vary throughout plates
- Damping is negligible and can be ignored
- Plates behave linearly.

The validity of these assumptions is discussed in later chapters. With these assumptions in hand the testing is begun.

This concludes the set-up and testing for this experiment, the next step is the analysis and discussion of the results.

IV. Analysis and Results

Chapter Overview

The preceding sections of this research have dealt with the theory, set-up and background of the investigation. This section presents the results of the many facets of the research and explains the meaning behind the data collected. The data presentation and correlation is done using graphs and tables. As there are many nodes for each plate set-up and numerous frequencies and mode shapes only a few of the graphs and tables are presented in this section. The remainder of the visual data is found in Appendices as noted in the following sections.

Model Validation and Comparison

Validation of the finite element model has several facets:

- A convergence study is conducted to determine if the FE solution converges to a specific solution set.
- Examination and comparison of the mode shapes to the experimental investigations.
- Comparison and verification of modal frequencies to provide basis for comparison to the physical data.

The results are broken down into the individual cases studied.

Case 1

The first case examined is the 12" x 12" plate bolted to the optical table. This plate is modeled in ABAQUS CAE® and a convergence study conducted. This is the first

step in modeling the structure to determine if the solution given by the program is accurate. The results of this study are found in Table 4.1.

Table 4.1. 12" x 12" Mesh Convergence Study

	Global Mesh Size in Inches					
	0.1	**0.15**	**0.2**	**0.25**	**0.3**	**0.5**
	Natural Frequency (Hz)					
Mode	***Percent Difference in Frequency***					
1	238.77	240.17	241.5	245.29	249.81	258.75
		-0.59%	*-0.55%*	*-1.57%*	*-1.84%*	*-3.58%*
2	406.76	411.23	419.18	435.16	462.45	502.3
		-1.10%	*-1.93%*	*-3.81%*	*-6.27%*	*-8.62%*
3	406.79	411.33	419.28	435.25	463.35	635.65
		-1.12%	*-1.93%*	*-3.81%*	*-6.46%*	*-37.19%*
4	431.39	434.61	438.47	447.78	463.64	639.15
		-0.75%	*-0.89%*	*-2.12%*	*-3.54%*	*-37.85%*
5	706.99	717.81	741	783.96	875.09	1046.7
		-1.53%	*-3.23%*	*-5.80%*	*-11.62%*	*-19.61%*
6	919.06	923.38	929.09	943.83	968.79	1051.7
		-0.47%	*-0.62%*	*-1.59%*	*-2.64%*	*-8.56%*
7	919.11	923.69	929.65	944.06	969.87	1368
		-0.50%	*-0.65%*	*-1.55%*	*-2.73%*	*-41.05%*
8	955.89	962.45	973.58	996.19	1032.8	1389.8
		-0.69%	*-1.16%*	*-2.32%*	*-3.68%*	*-34.57%*
9	1210.4	1222.3	1241	1282.8	1356.2	1735.5
		-0.98%	*-1.53%*	*-3.37%*	*-5.72%*	*-27.97%*
10	1325.1	1341.4	1373.9	1438.5	1569.2	1830.7
		-1.23%	*-2.42%*	*-4.70%*	*-9.09%*	*-16.66%*

The finite element frequencies found for each mode are shown in Table 4.1. Below the frequencies are the percent difference between the coarse frequency and the next more refined mesh size. It is seen in Table 4.1 that the frequencies do, in fact, converge towards a unique solution. With these results in hand, a mesh size of 0.1" is used for all

12” x 12” plate finite element examinations. In all models five elements are used through the thickness of the plate. This mesh size results in a model with 73285 elements. Each of these elements has 6 degrees of freedom, 3 translational and 3 rotational.

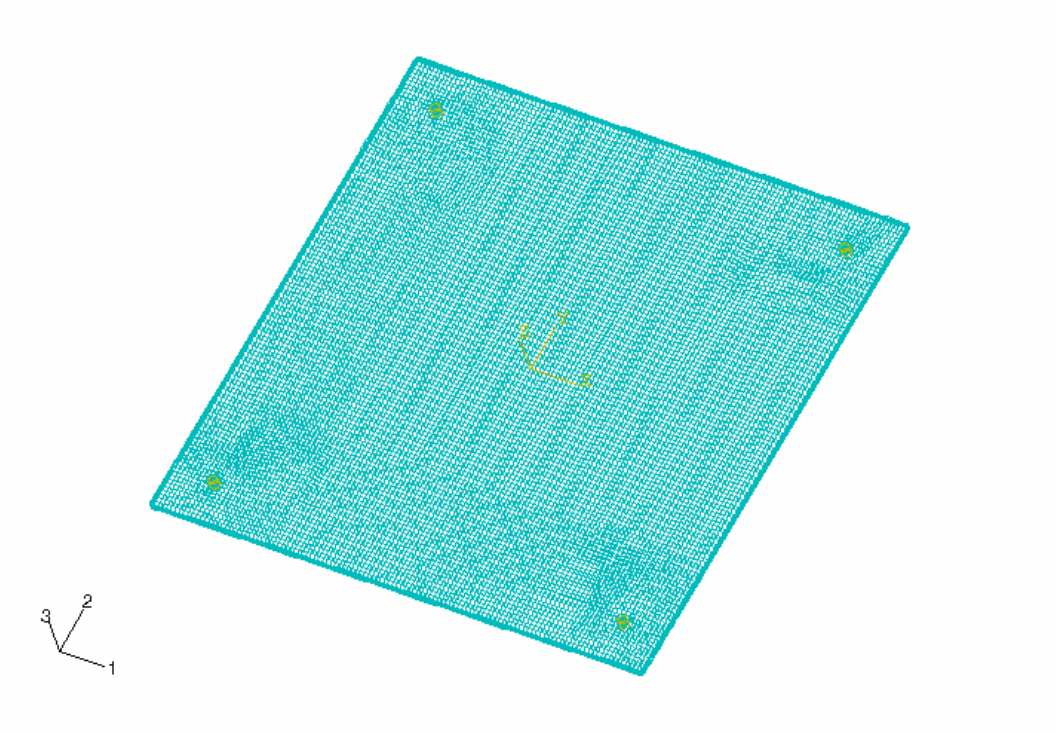

Figure 4.1. Mesh for 12” x 12” Plate

Figure 4.1 displays the mesh for the 12” x 12”. The very dense mesh size is noted along with the swept nature of the elements around the bolt holes. Closer examination of the bolt holes reveals the interior surface of the holes whose nodes are constrained from rotation or translation (see Figure 4.2). The global axis system is also located in the lower left corner of the figure.

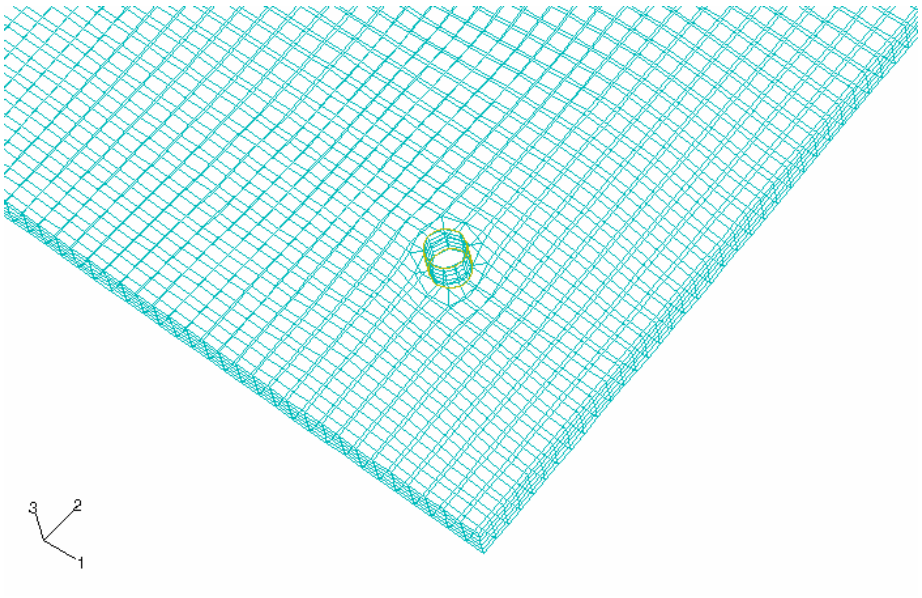

Figure 4.2. Close up of Mesh Region Near Bolt Hole

The FE solution is compared to the results found from physically testing the structure. Figure 4.3 shows the location of the accelerometers on the structure.

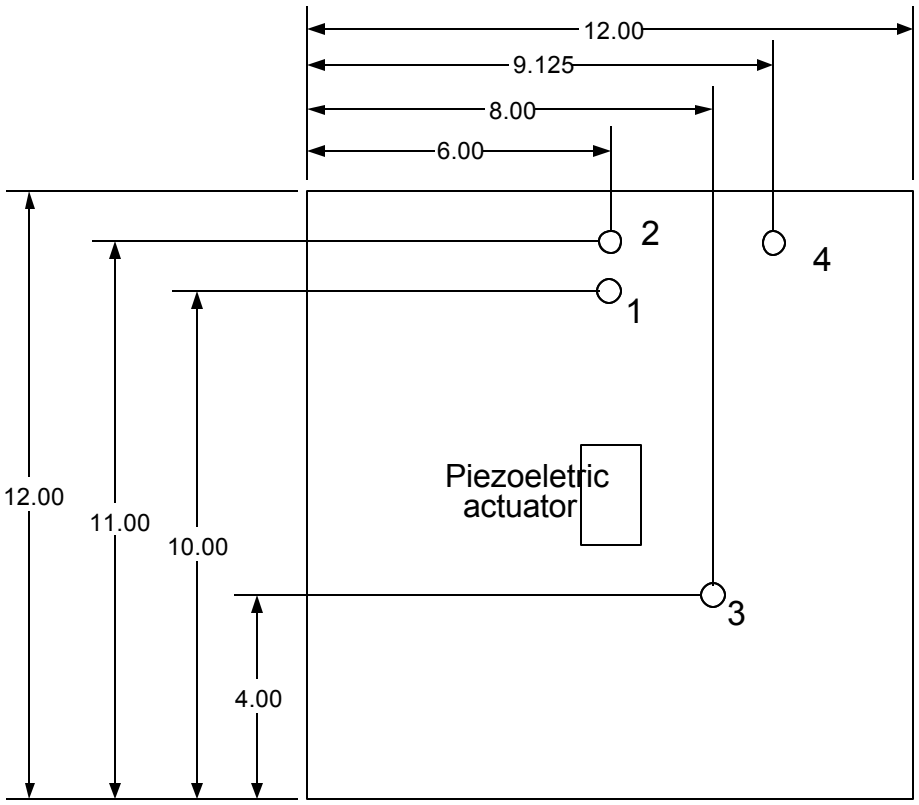

Figure 4.3. Schematic of 12" x 12" System (Sensors labeled 1-4)

The locations of these sensors derive from an attempt to correlate the results with data from a series of tests conducted by AFRL/VASM (14). There is a slight difference in the plate configuration in that the bolts in this research are 1 inch from the edges and in the AFRL/VASM study the bolts are 0.5 inches from the edges. With this difference in mind the plate studied in this research is anticipated to be slightly stiffer due to the bolts being placed closer together. This is in fact the case as the frequencies found by AFRL were slightly lower than those found in the case 1 tests (14).

Figure 4.4 shows the physical response of the plate under excitation.

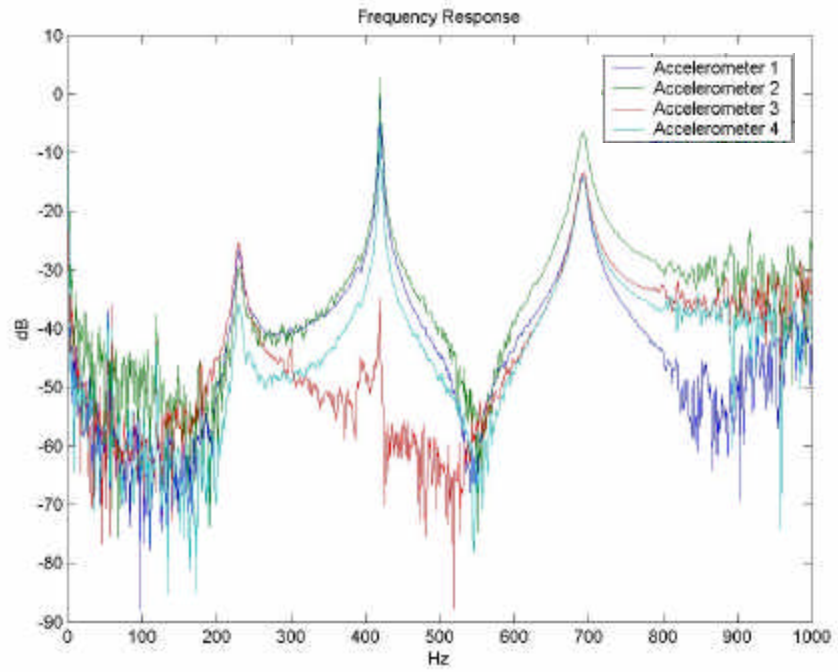
Frequency Response
Accelerometer 1
Accelerometer 2
Accelerometer 3
Accelerometer 4
dB
Hz
10
0
-10
-20
-30
-40
-50
-60
-70
-80
-90
0
100
200
300
400
500
600
700
800
900
1000

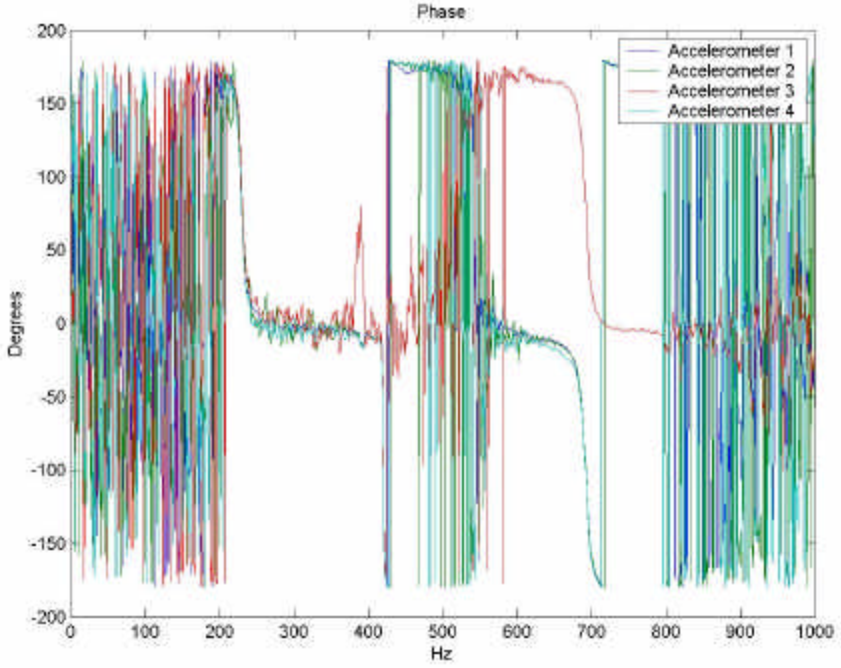
Phase
Accelerometer 1
Accelerometer 2
Accelerometer 3
Accelerometer 4
Degrees
Hz
200
150
100
50
0
-50
-100
-150
-200
0
100
200
300
400
500
600
700
800
900
1000

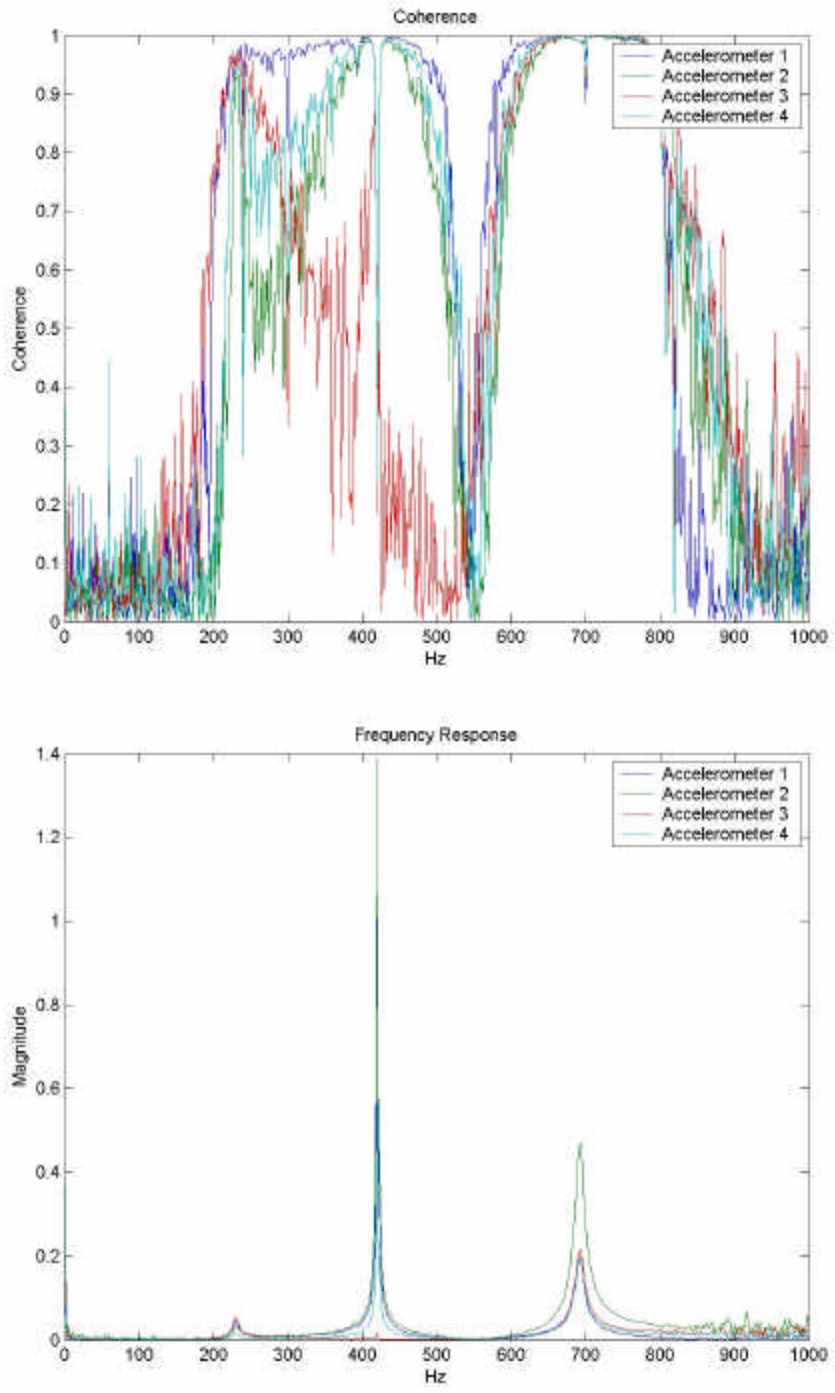

Figure 4.4. Magnitude, Phase and Coherence of 12x12 All bolts

This data shows well defined peaks representing modes of the system. This data is processed to pick the peaks and their associated frequencies. The eigenvectors for the physical response is found by taking the magnitude and phase data from Figure 4.4. This is done by multiplying the magnitude of the response by the cosine of the phase to produce a real part and by the sine of the phase to produce an imaginary part as in Equation (4.1). These eigenvectors are then normalized and used in Equation (3.2) to find the MAC.

$$f = magnitude * (\cos(q) + i \sin(q)) \tag{4.1}$$

where f are the eigenvectors and q is the phase angle. Figure 4.4 shows the frequency response in straight magnitude and logarithmic magnitude. The peaks in the straight magnitude graph correlate to the large peaks in the log scale magnitude. It is also seen that antiresonance in the log scale goes to zero in the straight magnitude scale, as discussed in Chapter 2. Observing the magnitude graph in Figure 4.4 also shows very little damping in the system. This is noticed by the width of the modal peaks, which is very narrow, thus little damping is present validating the assumption where damping is neglected (7). It is observed in the data in Figure 4.4 that there is noise in the low and high frequency bands. This phenomenon is discussed later in this Chapter. Figure 4.5 shows the Modal Assurance Criteria for the 12" x 12" plate undamaged configuration in graphical form.

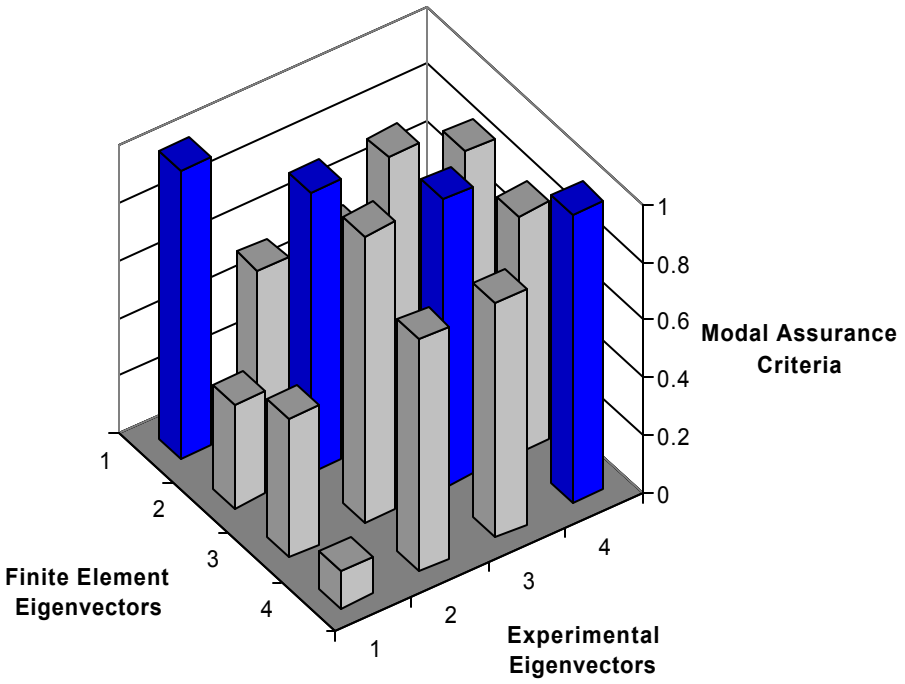

Figure 4.5. MAC for Undamaged Plate

It is observed from viewing Figure 4.5 that the diagonal entries, darker columns, in the figure are the highest values. This is due to the fact that the mode shapes have the strongest agreement at these locations. Alternatively, it means that mode 1 from the finite element solution agrees best with the first mode of the experimental data. Figure 4.5 shows the relationship between the finite element and experimental eigenvectors as discussed in Chapter 3. What this means is that the eigenvectors formed by the 4 sensors responses match well with the equivalent nodal response from the FE model. It is also seen that there is a large amount of correlation in the other modes of the plate as well. This is attributed to the symmetry of the plate. Table 4.2 shows the frequencies associated with the MAC agreements.

Table 4.2 MAC Correlated Frequencies

Mode	FEA Frequency (Hz)		EXP Frequency (Hz)		Percent Difference
1	230		238.77		-3.81%
2	391.25		406.76		-3.96%
3	420		431.39		-2.71%
4	692.5		706.99		-2.09%

Each of the MAC correlations from Figure 4.5 have corresponding frequencies for the FE and experimental tests. In this research, only the diagonal entries in the MAC, which are dark in the figures, are of concern. When compared, these values should be close to ensure that the model accurately represents the physical system. Examining Table 4.2 shows a small difference in the resonant frequencies found in the finite element and physical tests. The average difference is 3.15% for the modes that correlate. The finite element mode shapes and their accompanying frequencies for the undamaged case are found in Figures 4.6 through 4.9.

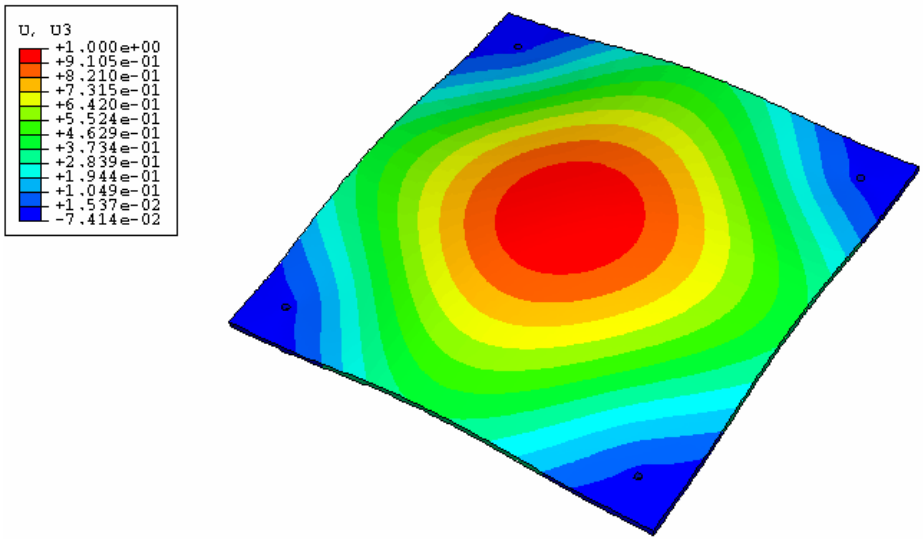

Figure 4.6. First MAC Matching Mode 238.77 Hz

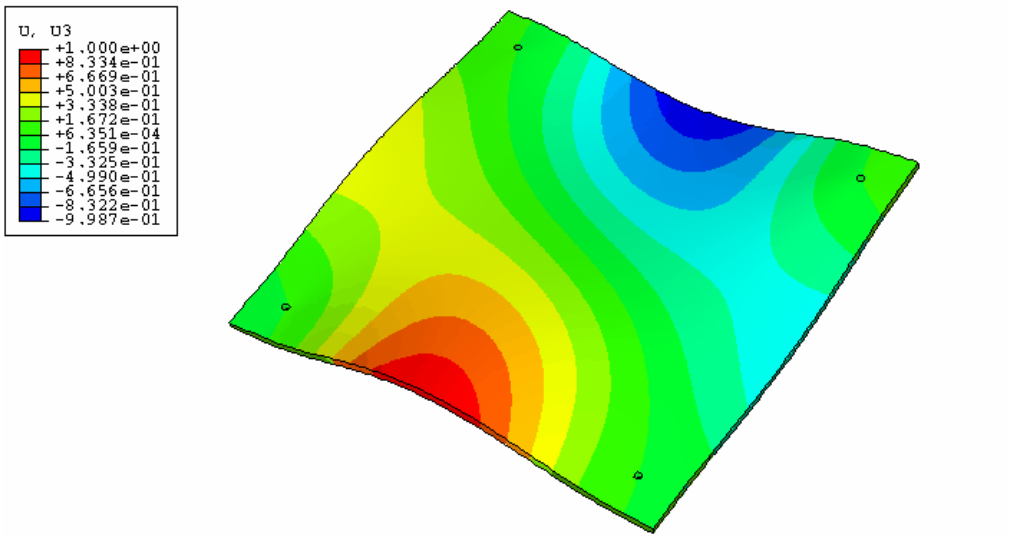

Figure 4.7. Second MAC Matching Mode 406.76 Hz

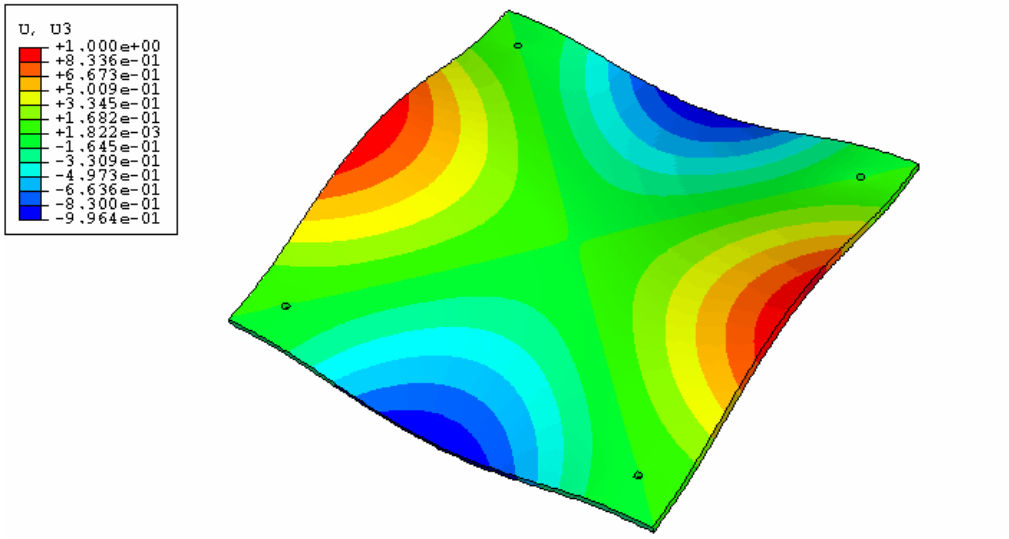

Figure 4.8. Third MAC matching Mode 431.39 Hz

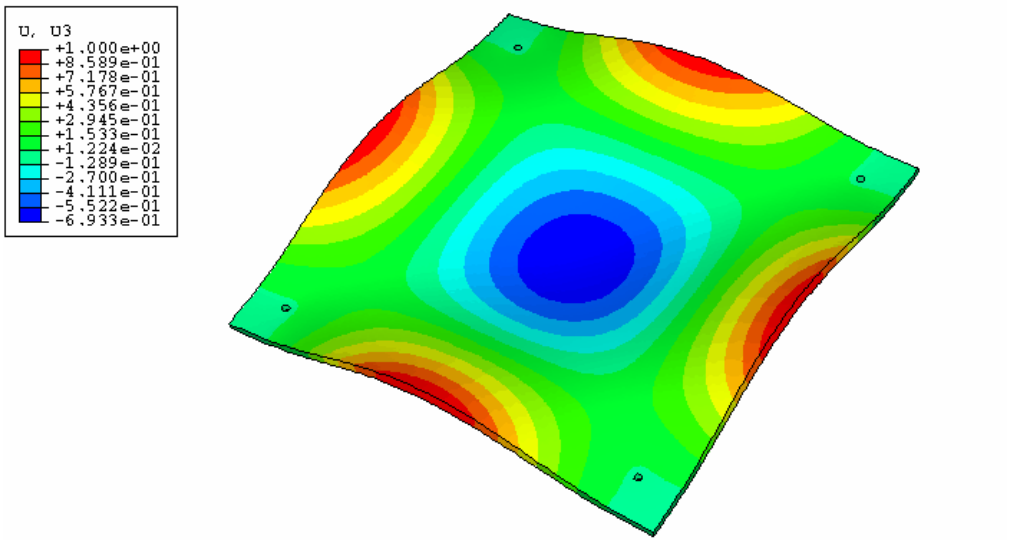

Figure 4.9. Fourth MAC Matching Mode 706.99 Hz

As mentioned in Chapter 3, a study of the effects of bolt torque on the physical system response was also conducted. Table 4.3 shows the results of the torque study.

Table 4.3 12" x 12" Plate Bolt Torque Study

All Bolts	Frequency (Hz)						
Mode	5 in-lb	10 in-lb	20 in-lb	40 in-lb	Over Torqued		FEA
1	212.5	213.75	226.25	228.75	230		238.77
2	367.5	370	383.75	388.75	391.25		406.76
3	385	391.25	410	416.25	420		431.39
4	678.75	681.25	687.5	691.25	692.5		706.99
Percent Difference Between Torques							
Mode	5-10	10-20	20-40	40-Over Torque			
1	0.58%	5.52%	1.09%	0.54%			
2	0.68%	3.58%	1.29%	0.64%			
3	1.60%	4.57%	1.50%	0.89%			
4	0.37%	0.91%	0.54%	0.18%			

Bolt 3	Frequency (Hz)						
Mode	5 in-lb	10 in-lb	20 in-lb	40 in-lb	Over Torqued		FEA
1	83.75	83.75	85	85	85		91.36
2	227.5	236.25	241.25	243.75	245		256.6
3	282.5	295	305	308.75	311.25		337.73
4	363.75	383.75	396.25	400	405		418.06
5	421.25	432.5	437.5	440	442.5		458.17
6	485	611.25	673.75	703.75	706.25		730.5
Percent Difference Between Torques							
Mode	5-10	10-20	20-40	40-Over Torque			
1	0.00%	1.47%	0.00%	0.00%			
2	3.70%	2.07%	1.03%	0.51%			
3	4.24%	3.28%	1.21%	0.80%			
4	5.21%	3.15%	0.94%	1.23%			
5	2.60%	1.14%	0.57%	0.56%			
6	20.65%	9.28%	4.26%	0.35%			

Experimental torque testing is conducted on the bolts to determine the effect of varied amounts of torque on the systems resonant frequencies. These tests begin with the complete removal of all bolts from the system and replacing them in the system and applying a set amount of torque with an Armstrong 64-031 torque wrench. The torques range from 5 to 40 in-lb and include a case where the bolts are tightened greatly beyond the measurable range of the torque wrench. It is observed in Table 4.3 that as the torque on the bolts is increased, the frequencies shift as the system becomes stiffer, approaching the rigid body results that arise from the MAC results between the finite element solution and the physical tests. These tests are the basis of modeling the bolts as rigid members in the FE model. This assumption produces frequencies within a 3.15% average of physical tests. The next set of data is for the damaged case.

The damaged case examined for the 12” x 12” plate involves removing bolt 3 from the plate, see Figure 4.10.

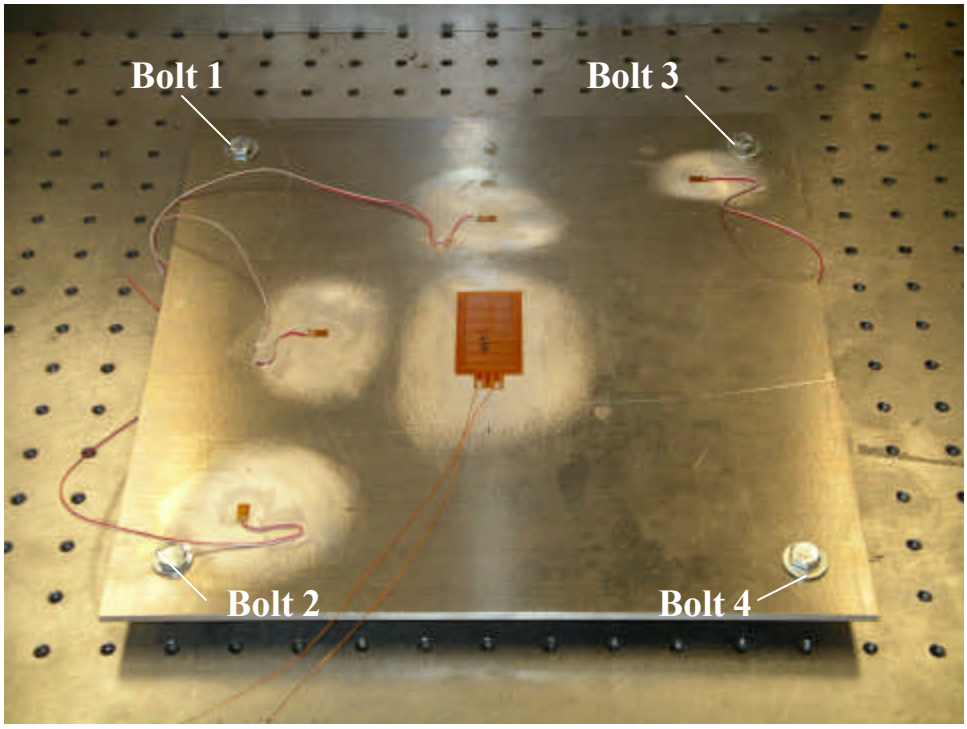

Figure 4.10. 12” x 12” Plate Configuration.

Similar to the undamaged case, the frequencies are found for the damaged modes and compared to the FE solutions. The frequency response and coherence of the damaged physical tests are found in Figure 4.11. These are again analyzed in the same manner as for the undamaged case.

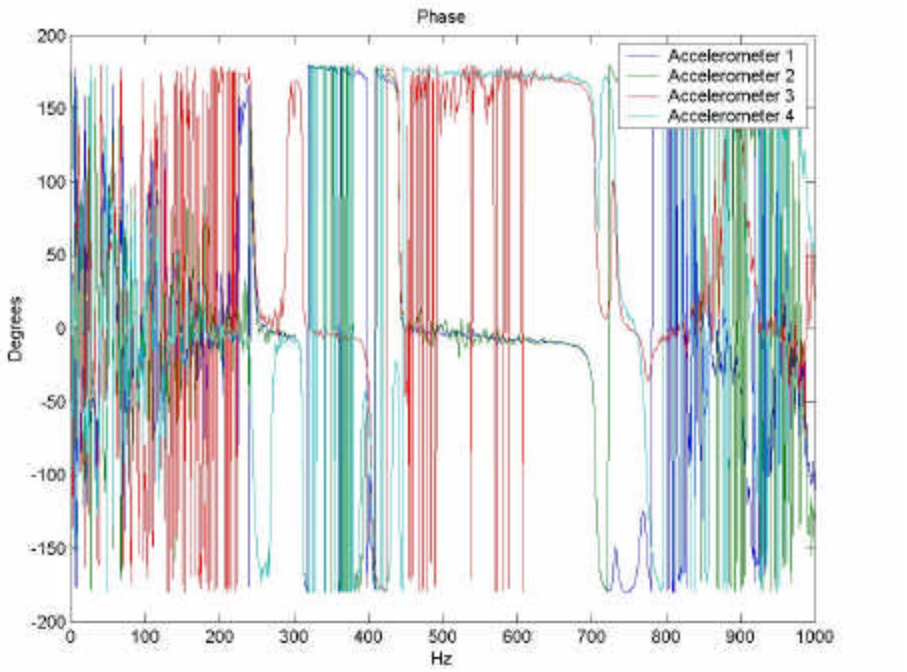
Phase
Accelerometer 1
Accelerometer 2
Accelerometer 3
Accelerometer 4
Degrees
Hz
200
150
100
50
0
-50
-100
-150
-200
0
100
200
300
400
500
600
700
800
900
1000

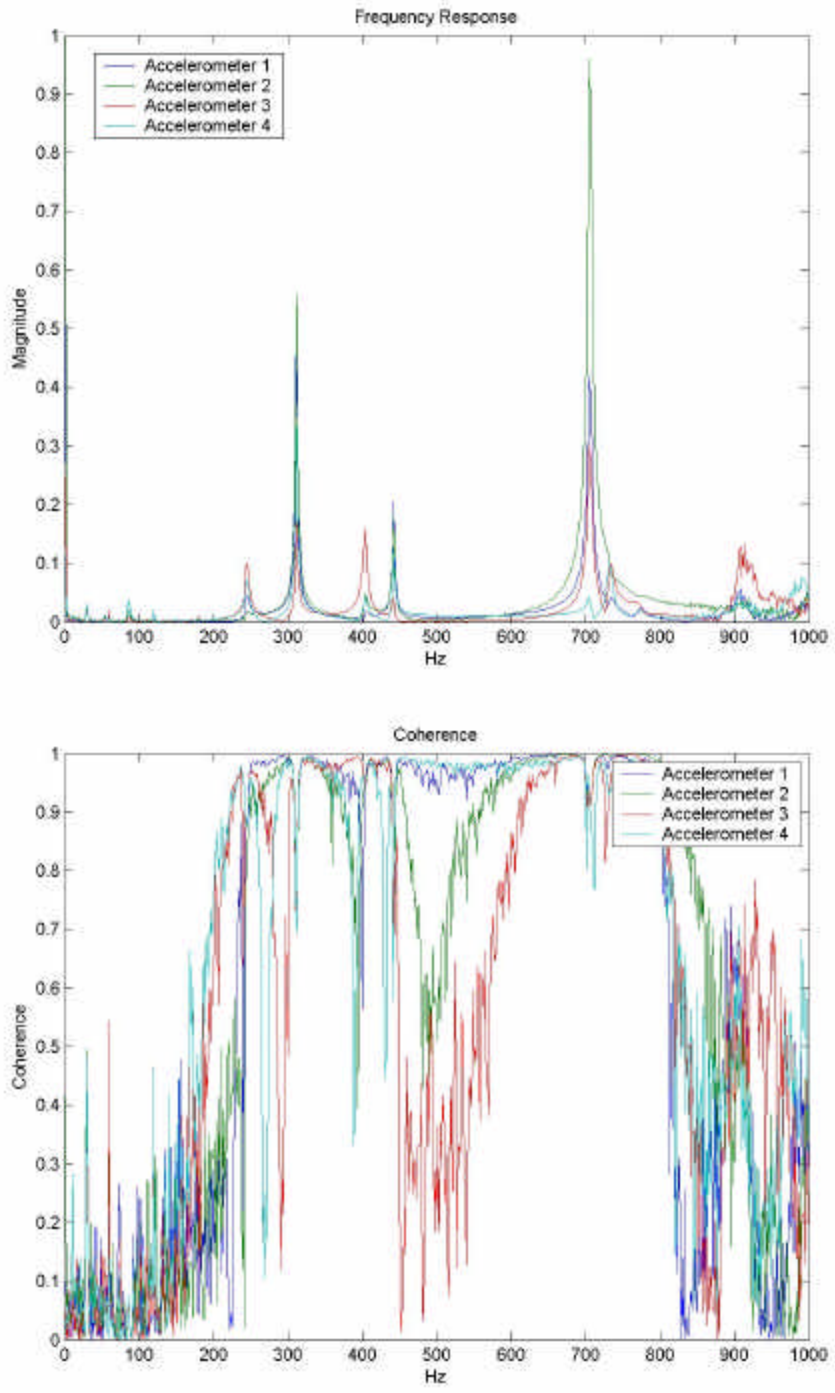

Figure 4.11. Bolt 3 Removed Frequency Response and Coherence

It is clear that there are numerous resonant peaks in the response. It is also clear that the upper and lower frequency bands have noise present even after the ensemble averaging (as mentioned in Chapter 3) that took place in the testing phase. A closer look a the coherence plot in Figure 4.11 reveals that at the upper and lower frequencies the coherence is considerably less than unity. This shows that there is little confidence in the data collected in this region. The potential causes for the noise are discussed later in this chapter. Figure 4.12 shows the MAC for a damaged bolt 3.

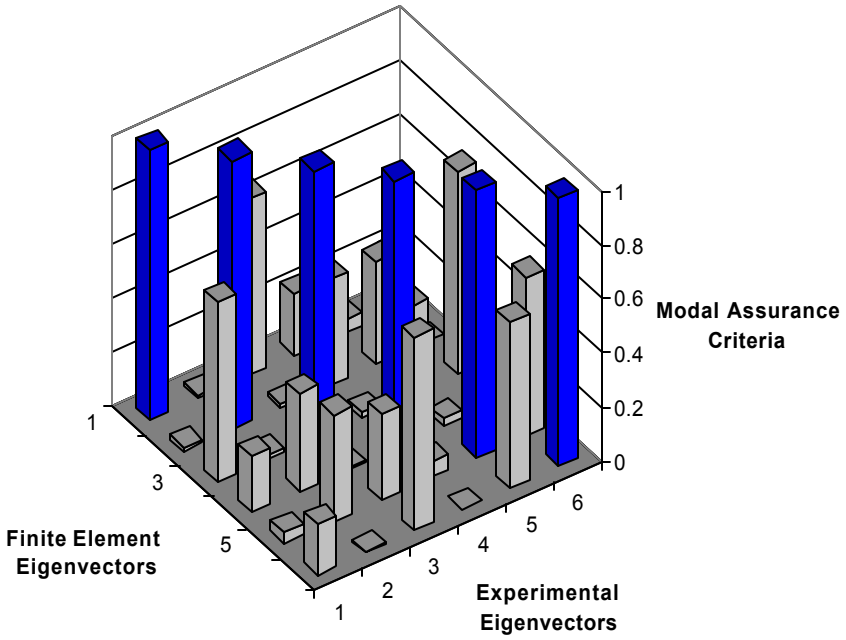

Figure 4.12. MAC for Bolt 3 Removed

Table 4.4 shows the frequencies of the damaged case and compares them to the finite element solutions.

Table 4.4 Bolt 3 Removed Frequency Comparison

Mode	FEA Frequency (Hz)		EXP Frequency (Hz)		Percent Difference
1	91.36		85		-7.48%
2	256.6		245		-4.73%
3	337.73		311.25		-8.51%
4	418.06		403.75		-3.54%
5	458.17		442.5		-3.54%
6	730.5		706.25		-3.43%

It is evident from Table 4.4 that there is a good relationship between the FE and physical models. This evidence is the average 5.21% difference in the natural frequencies. The well correlated MAC modes between the finite element solution and the experimental solution for bolt 3 is found in Figures 4.13 - 4.18 below All frequencies listed in figures are experimental values that compare well to the finite element vectors using the MAC.

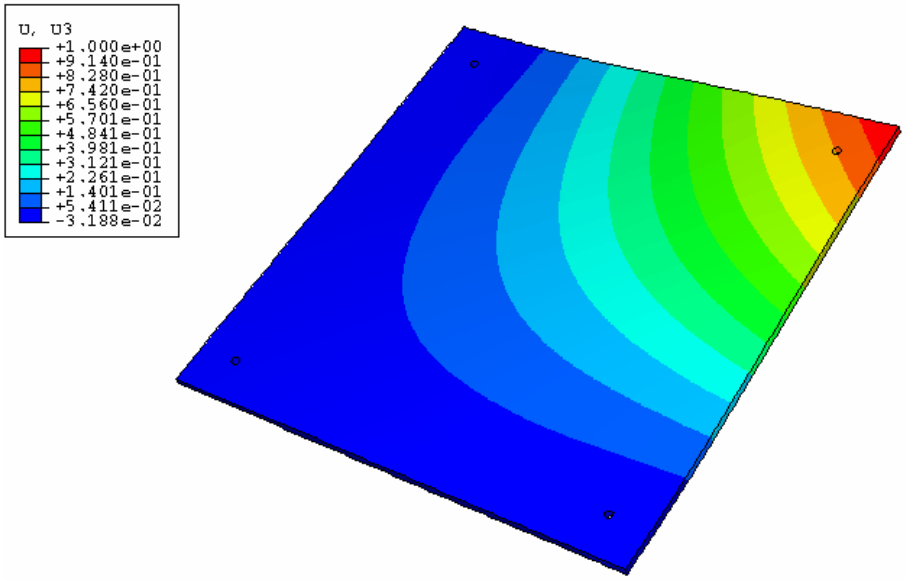

Figure 4.13. First MAC Matching Mode with Bolt 3 Removed 85 Hz

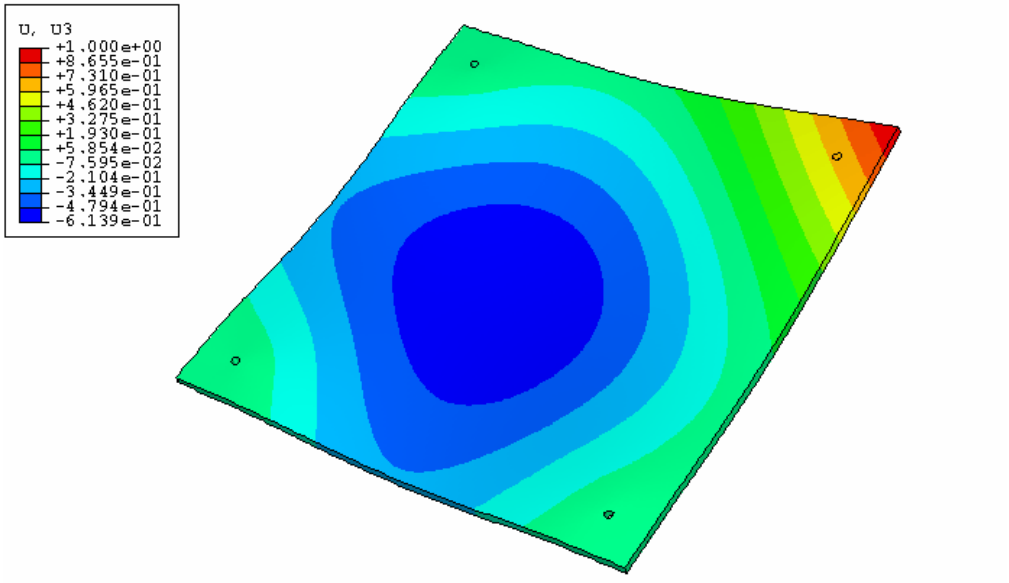

Figure 4.14. Second MAC Matching Mode with Bolt 3 Removed 245 Hz

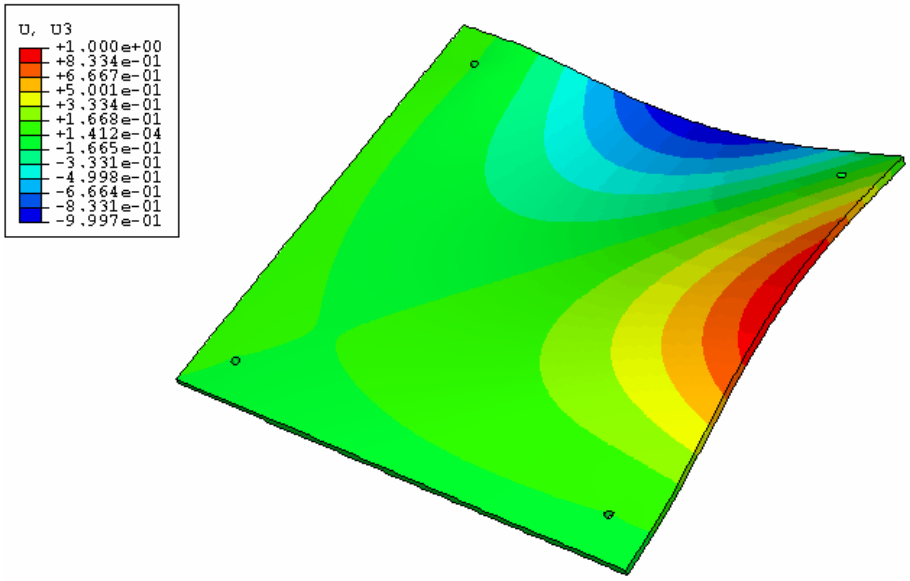

Figure 4.15. Third MAC Matching Mode with Bolt 3 Removed 311.25 Hz

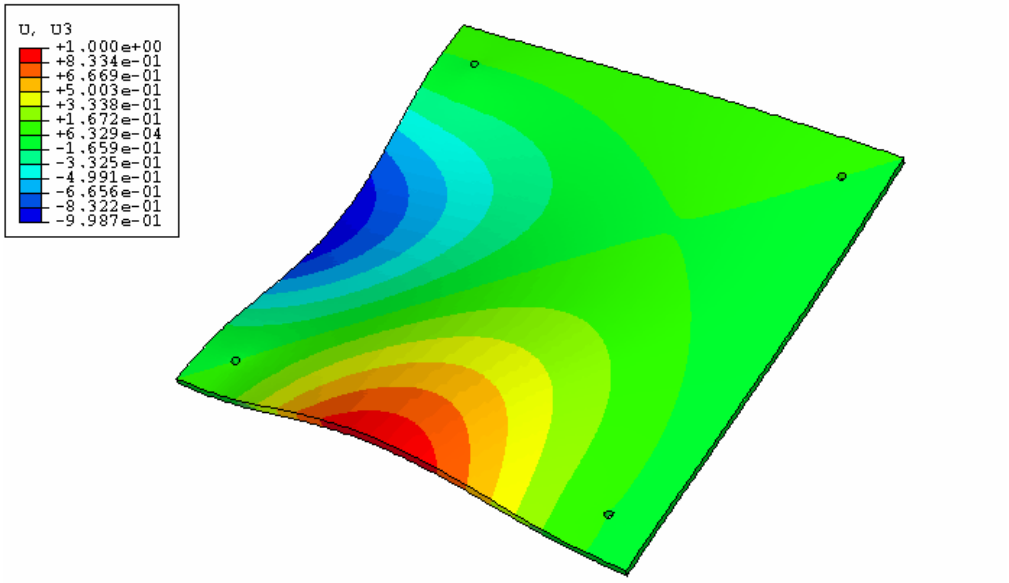

Figure 4.16. Fourth MAC Matching Mode with Bolt 3 Removed 403.75 Hz

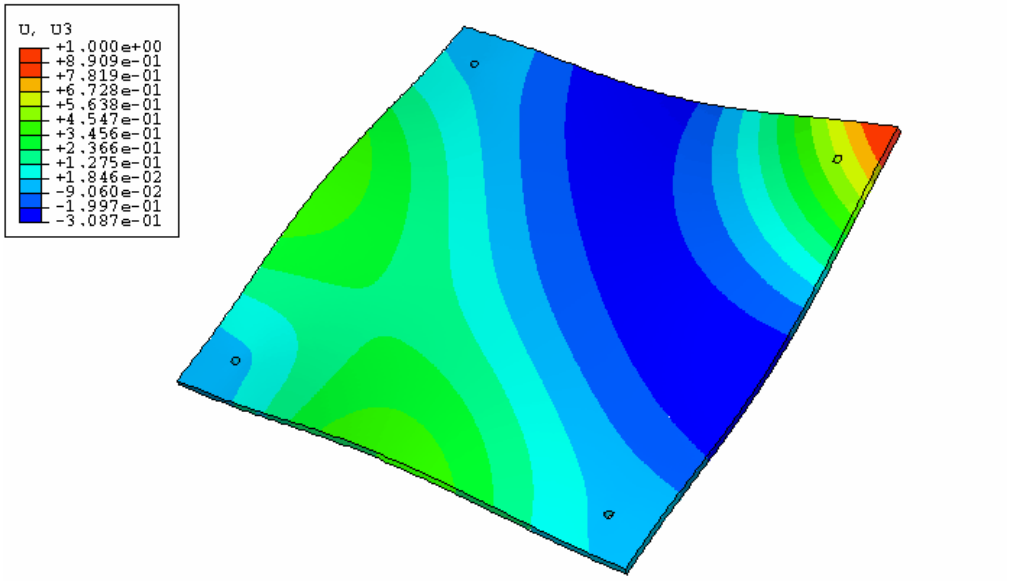

Figure 4.17. Fifth MAC Matching Mode with Bolt 3 Removed 442.5 Hz

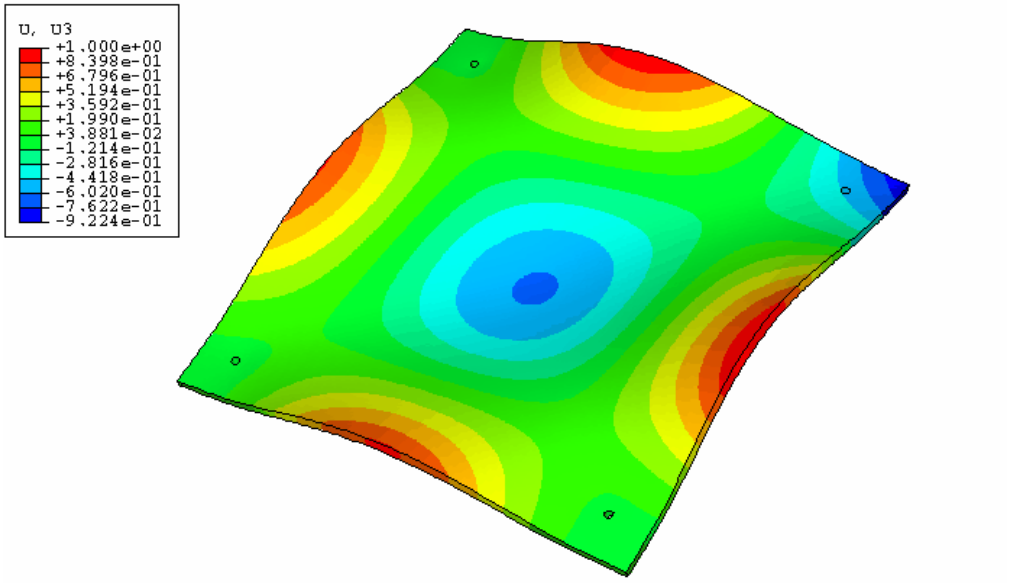

Figure 4.18. Sixth MAC Matching Mode with Bolt 3 Removed 706.25 Hz

The frequencies and mode shapes for the undamaged and damaged cases are then compared to each other. Only those that meet the Modal Assurance Criteria are kept for this process. Table 4.5 shows a side by side comparison of the experimental modal frequencies for modes that have a good MAC.

Table 4.5 MAC Correlated Experimental Frequencies for All Bolts and Bolt 3 Removed

Mode	All Bolts Frequency (Hz)		Bolt 3 Removed
1	230		85
2	391.25		245
3	420		311.25
4	692.5		403.75
5	n/a		442.5
6	n/a		706.25

From this table it is observed that the frequencies of the damaged case where bolt 3 is removed are lower than the undamaged at the same mode number. The graphical evidence of these numbers is found in Figures 4.6-4.9 and Figures 4.13-4.18. It can

further be characterized that as a result of the bolt being removed the structure is less stiff than the undamaged case. Equation (2.4) shows the basis of this statement. The mass matrix, **M**, changes only slightly with the removal of the bolt and spacer and the forcing function, *Q(t)*, ranges with the input to excite the resonant frequencies in the structure. Since damping is neglected in this research, it follows that the natural frequencies are given by the solution to Equation (2.4). If the mass remains constant then the stiffness, **K**, must be lower. This shift in frequencies is the key to detecting damage in the structure. This however is not the method that ABAQUS uses to solve for the eigenvalues and eigenvectors of the system. ABAQUS uses the Lanczos method to solve the eigenproblem. This method simplifies the solution and speeds processing due to the use of multiple vectors spanning a subspace. The process uses iteration, resulting in a diagonal matrix which is used to obtain eigenvalues (9).

Several items are learned from the investigation of case 1. First, the usage of rigid body connections in the finite element model proved to be a valid assumption as shown in Table 4.3. Second, the use of the MAC to compare mode shapes and their associated partial eigenvectors proved justifiable. Finally, the close comparison between the AFRL data and this research data shows the approaches are similar.

Case 2

Increasing in complexity of the model is the 12" by 24" plate system. This system is larger and has a greater unsupported area in the center of the plate. As such, the system is anticipated to be less stiff than the 12" x 12" plate system. As seen in the results below this is indeed the case.

As with the 12” x 12” plate, the first step in examining the 12” x 24” plate is to model it using ABAQUS CAE®. A global mesh seeding size of 0.125” is used for this system resulting in 93600 elements and 3 rotational and 3 translational degrees of freedom per node.

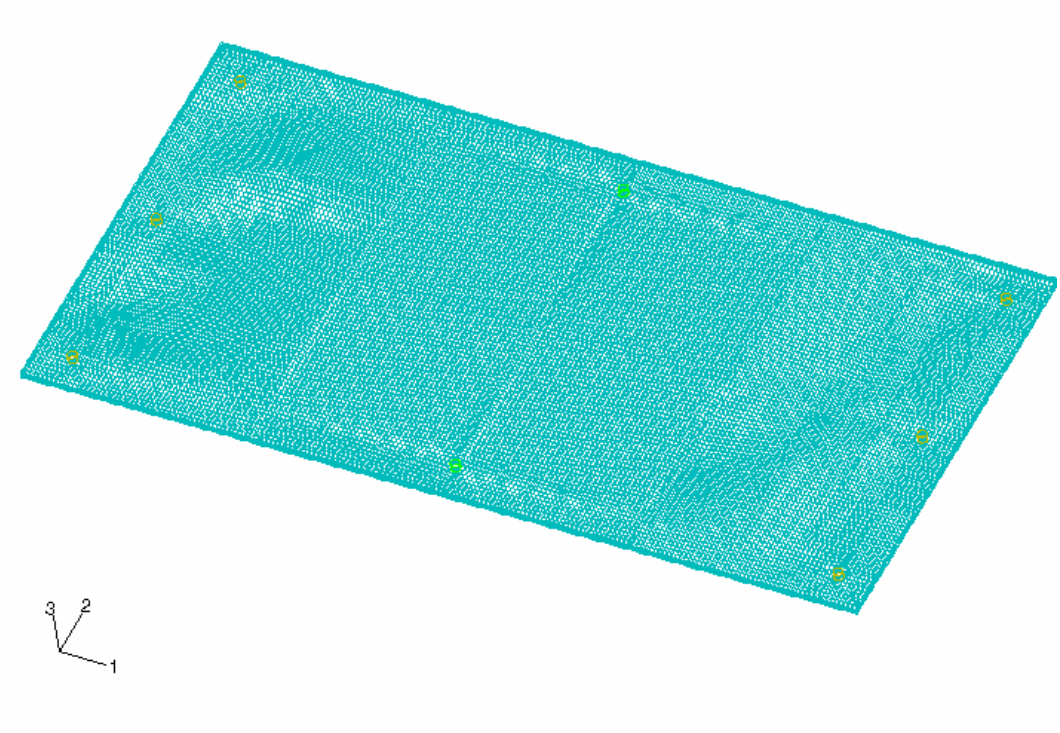

Figure 4.19. 12” x 24” Mesh

The above figure shows the mesh for the 12” x 24” plate. As with the 12” x 12” case the mesh is very dense. This leads to a more accurate result when the solution to the eigenproblem is found. With the plate meshed at this seed size (ABAQUS terminology), the process of plate 1 is repeated. The first 15 modes of the plate are found for the undamaged, all bolts tight, case and for the cases where bolts 1, 2 and 4 are removed (see Figure 4.20)

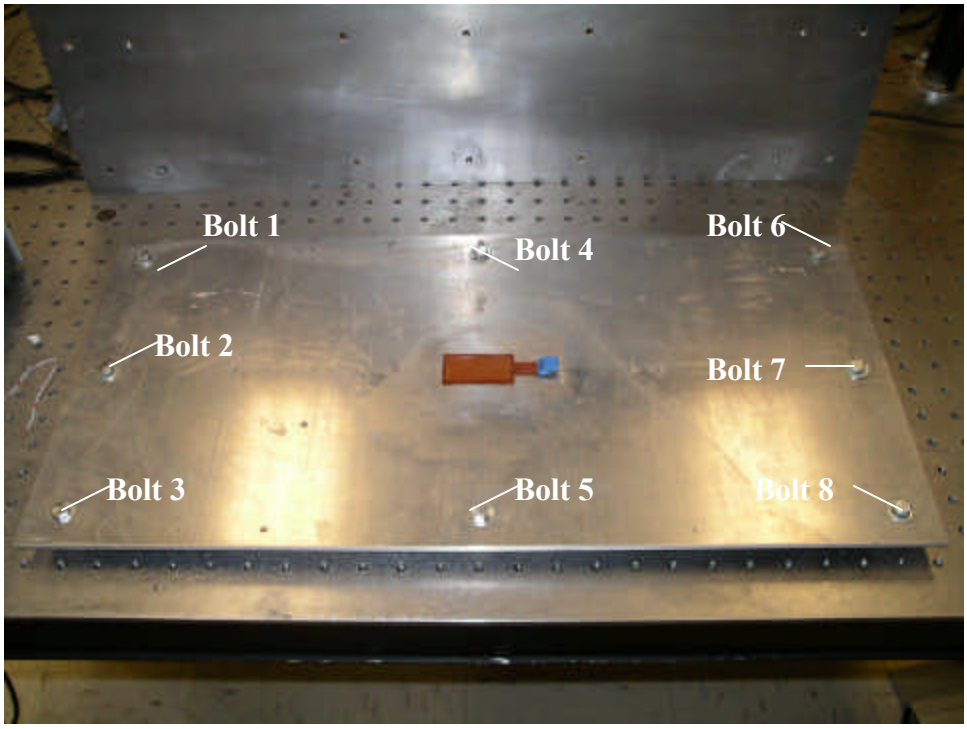

Figure 4.20. Bolt Numbering Scheme for Case 2

. The experimental testing process remains the same as in the 12" x 12" plate. Each test begins with the bolts being torqued to 50 in-lb and bolts are removed as necessary for each condition. The first mode of the undamaged case is shown in Figure 4.21 for reference. The first mode of the damaged cases are located in Figures 4.22-4.24. The remaining mode shapes are located in Appendix A.

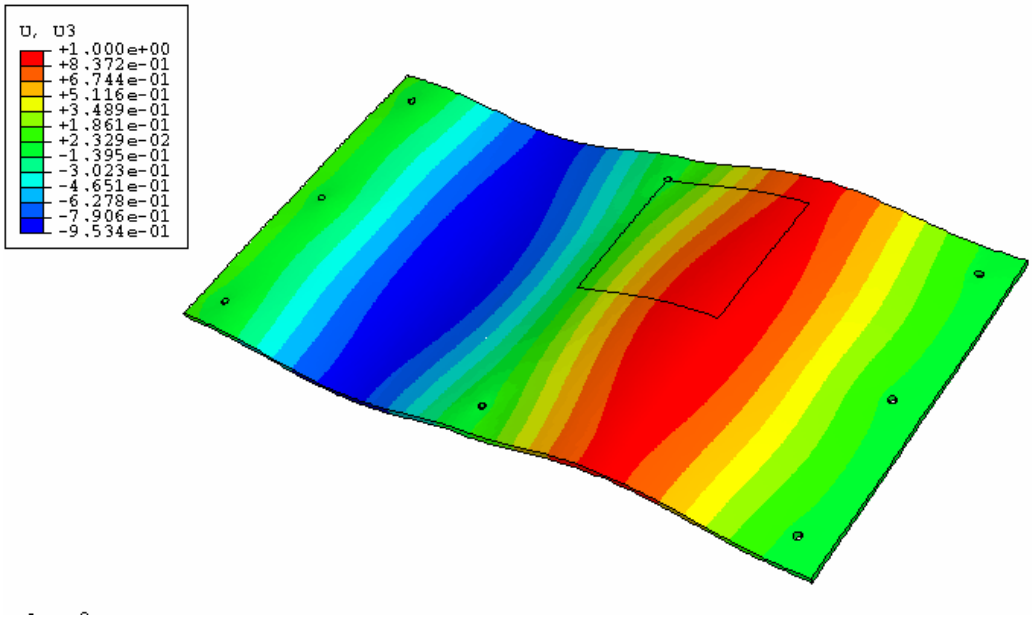

Figure 4.21. First Undamaged Mode 246.09 Hz Experimental

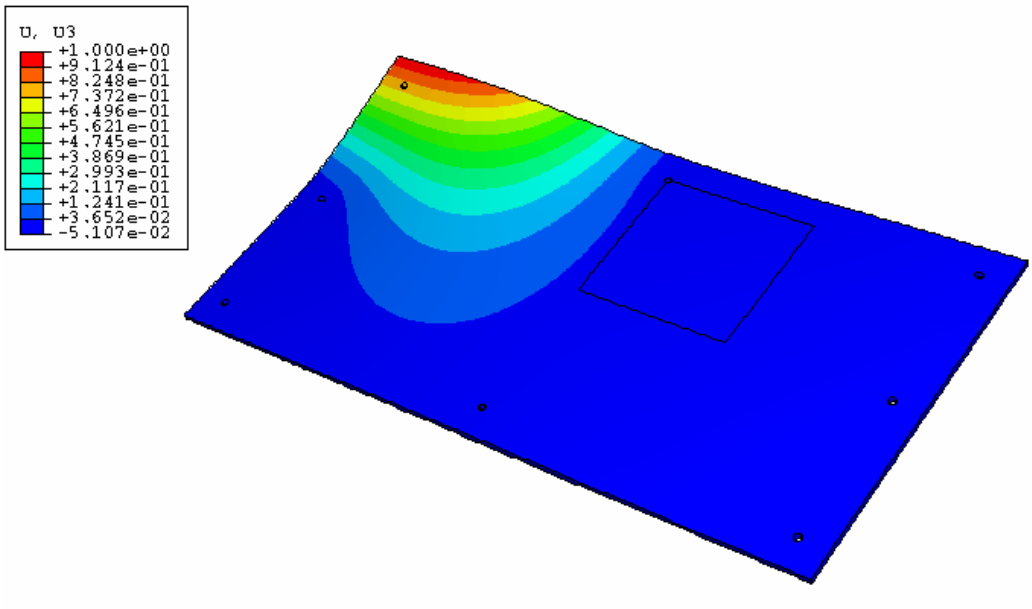

Figure 4.22. First Mode for Bolt 1 Removed 174.22 Hz Experimental

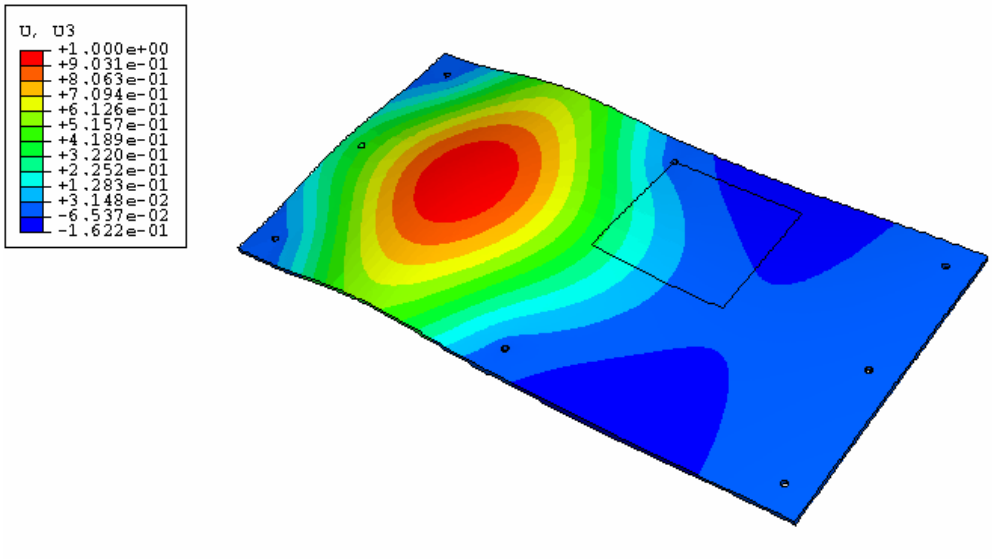

Figure 4.23. First Mode for Bolt 2 Removed 221.09 Hz Experimental

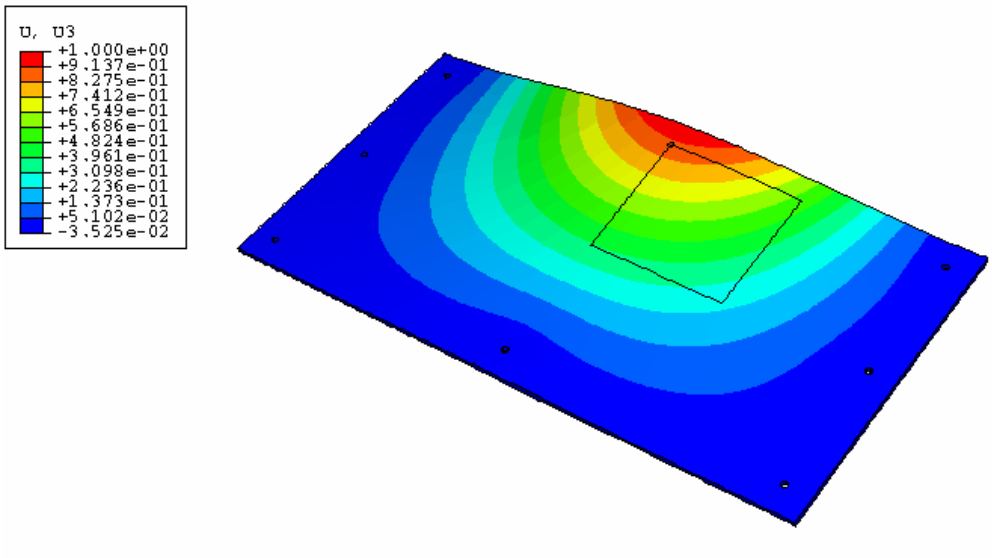

Figure 4.24. First Mode for Bolt 4 Removed 101.56 Hz Experimental

There are 12 accelerometers located on the plate as seen in Figure 4.25.

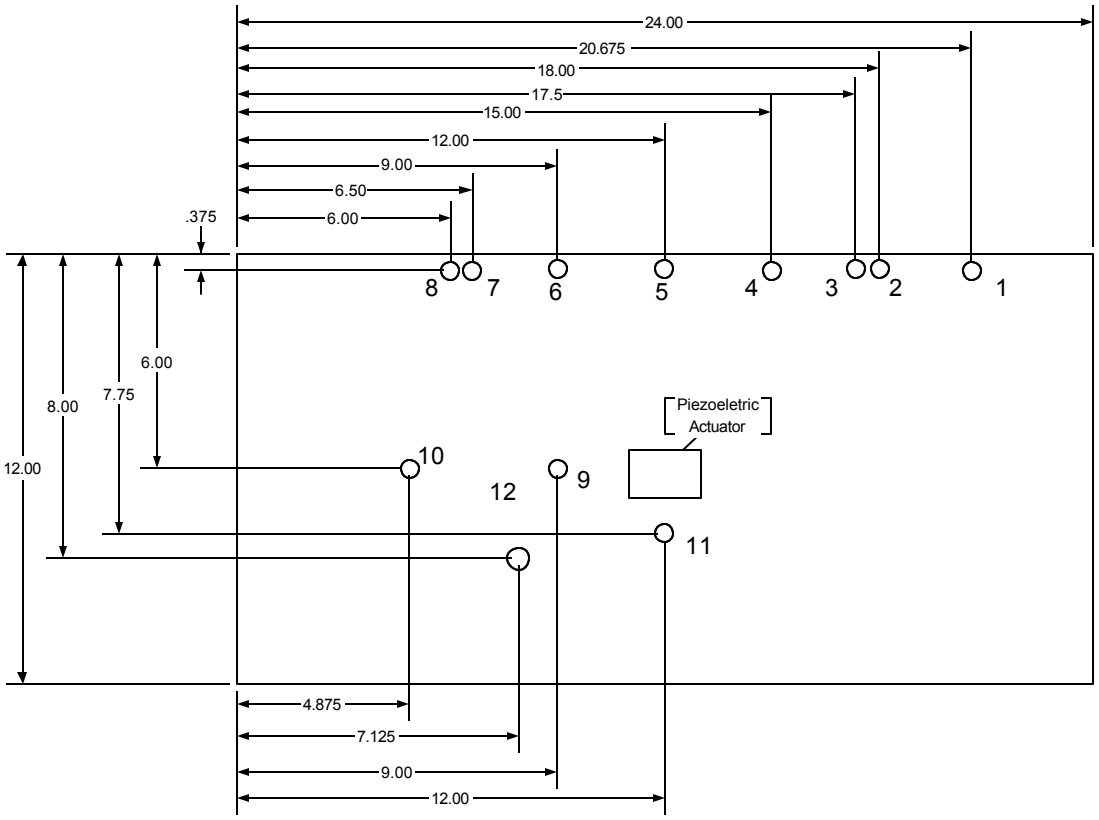

Figure 4.25. 12" x 24" Plate Schematic (Sensors labeled 1-12)

The sensors are placed in a line across the plate to gain a picture of the behavior of the system across its span. Additionally, the location of the accelerometers is also a result of examining the FEA responses to determine the positions with maximum deflection. A typical frequency response for the undamaged case is shown in Figure 4.26 below.

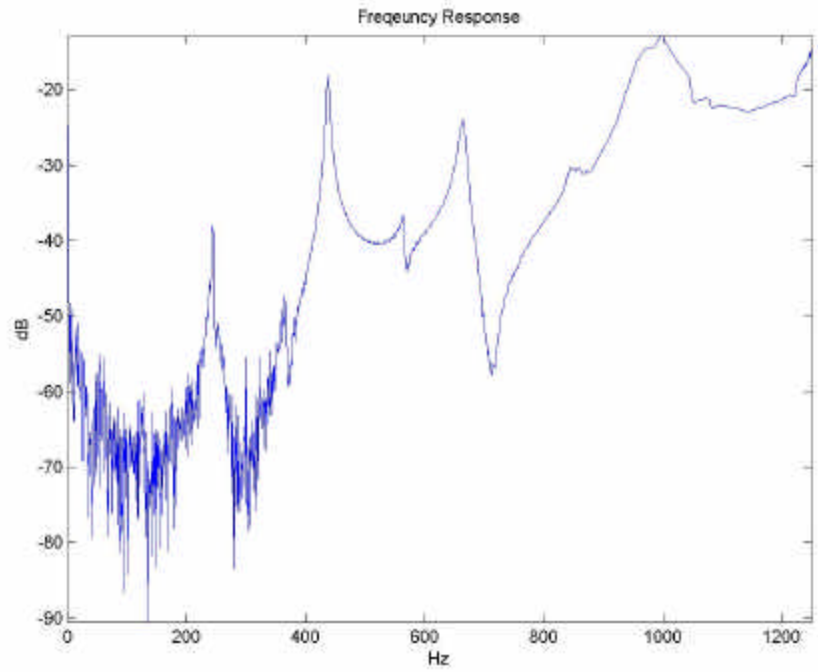
Freqeuncy Response
dB
-20
-30
-40
-50
-60
-70
-80
-90
0
200
400
600
800
1000
1200
Hz

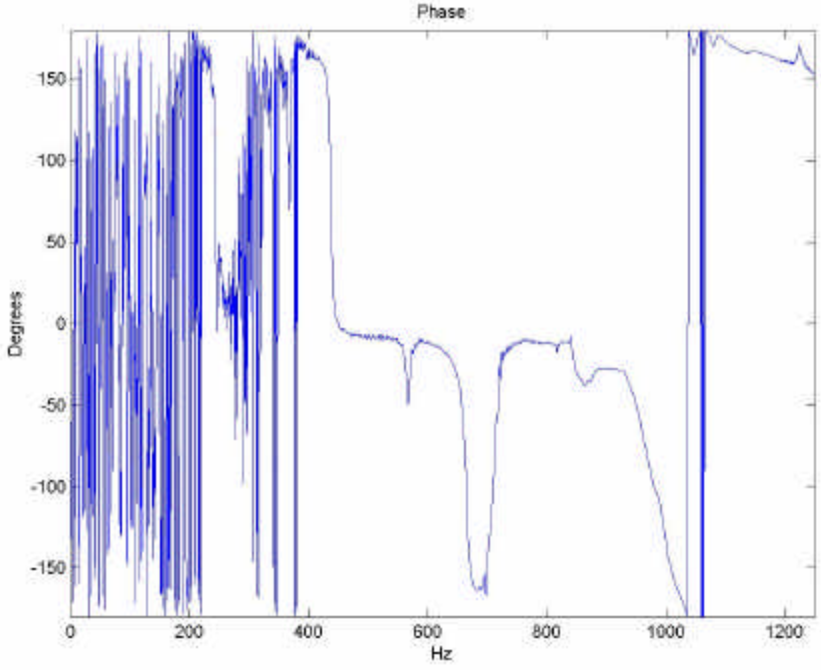
Phase
Degrees
150
100
50
0
-50
-100
-150
0
200
400
600
800
1000
1200
Hz

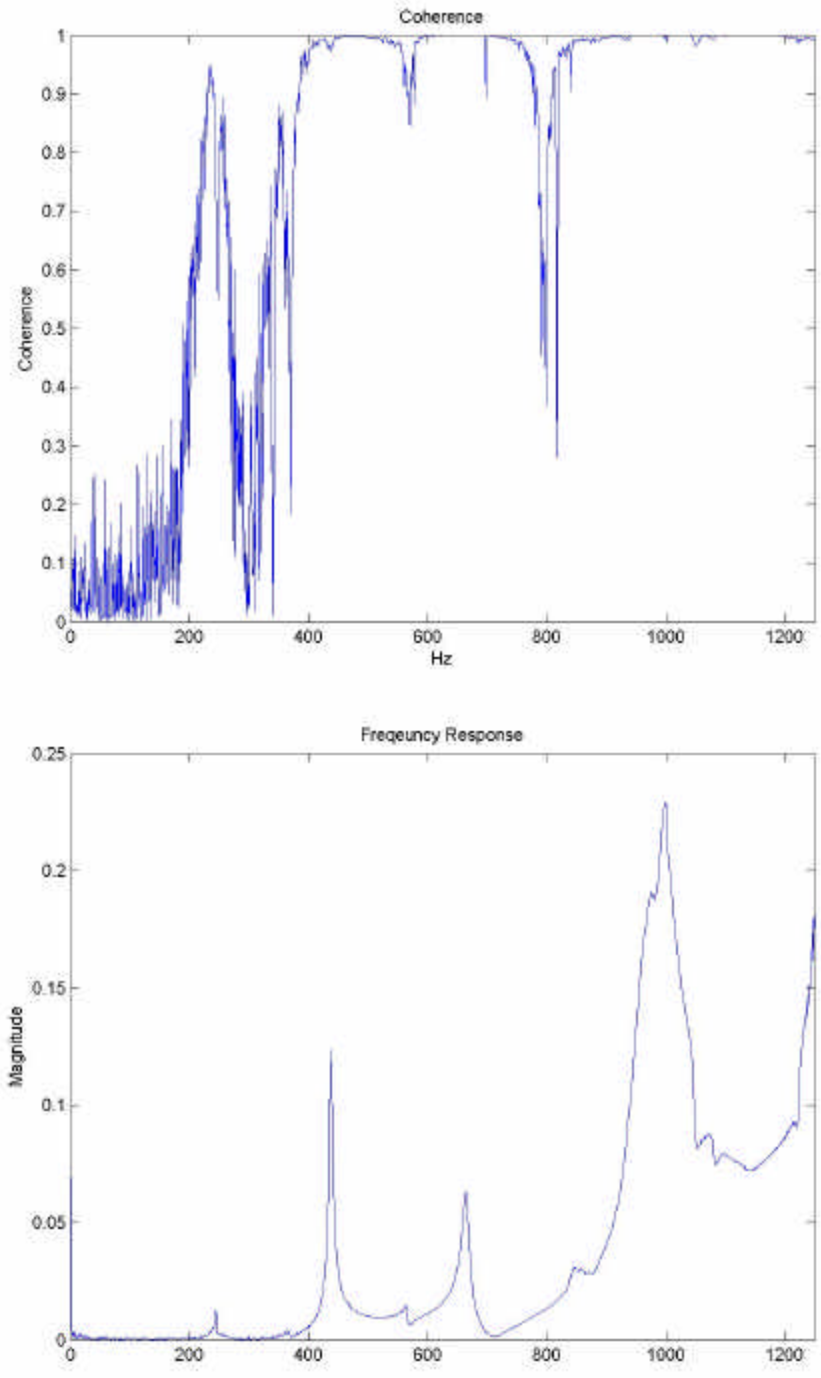

Figure 4.26. Frequency Response and Coherence for Accelerometer 1, All Bolts Fixed

These graphs show the magnitude, phase and coherence of sensor 1. It is evident that there is poor coherence below 200 Hz which is classified as noise. The phenomenon of noise in the responses of all test cases is discussed in a separate section of this chapter. The peaks, representing the resonant frequencies are also visible in the graphs. Due to the number of sensors recorded for each test, the graphs associated with these tests are very cluttered. In order to make them more visually appealing and legible, they would have to be shown with limited sensor responses per graph. This would result in a extraordinarily large Results section or Appendix to contain the remainder of the response graphs. As a result these graphs are not included, but the figures in the text of the thesis show the typical response characteristics of the plates.

The process of finding the Modal Assurance Criteria for both the experimental versus the finite element and undamaged experimental versus damaged experimental is performed in the same manner as for the 12" x 12" plate.

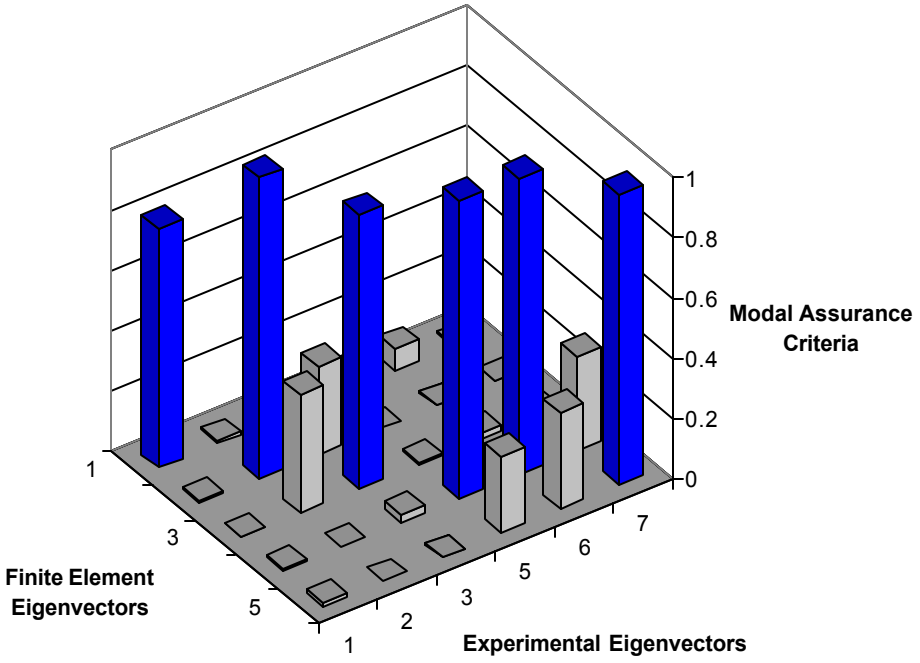

Figure 4.27. MAC For Undamaged Case

Figure 4.27 shows the MAC for the undamaged case. It is seen in the figure that for finite element mode number four there are 3 experimental eigenvectors that correspond well. It is difficult to determine from the eigenvectors and the MAC which mode is the best fit. The frequency ranges from 4.43% to 1.49% from experimental modes 4 to 6. The average percent difference in the frequencies of the MAC modes that agree is 4.29%.

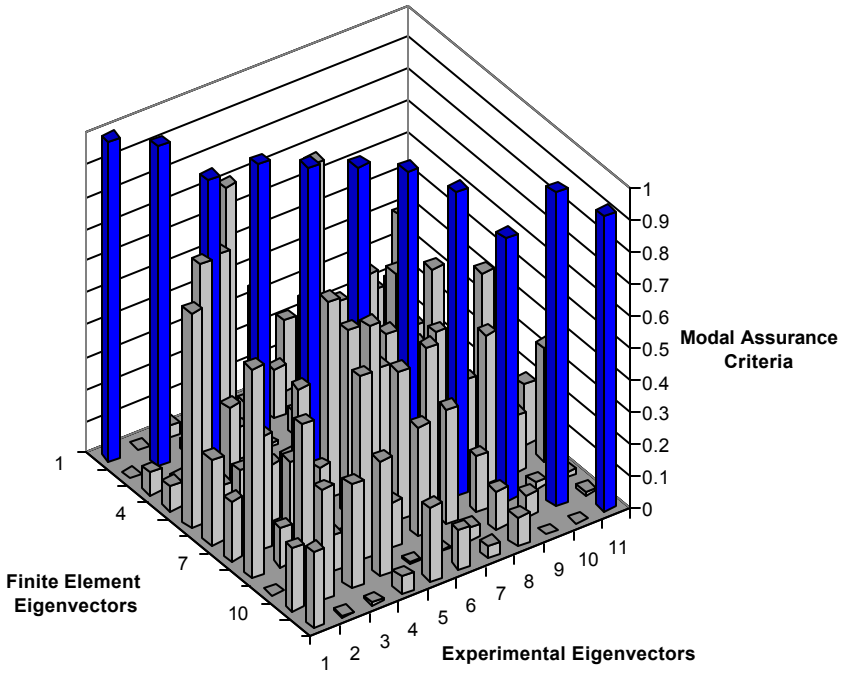

Figure 4.28. MAC for Bolt 1 Removed

Figure 4.28 shows the Modal Assurance Criteria for the case where bolt 1 is removed from the system. Examination of the figure shows that there is correlation of 11 modes for the FE and experimental models. Further exploration of the modes reveals that there is a 3.32% average percent difference between the physical and FE modes.

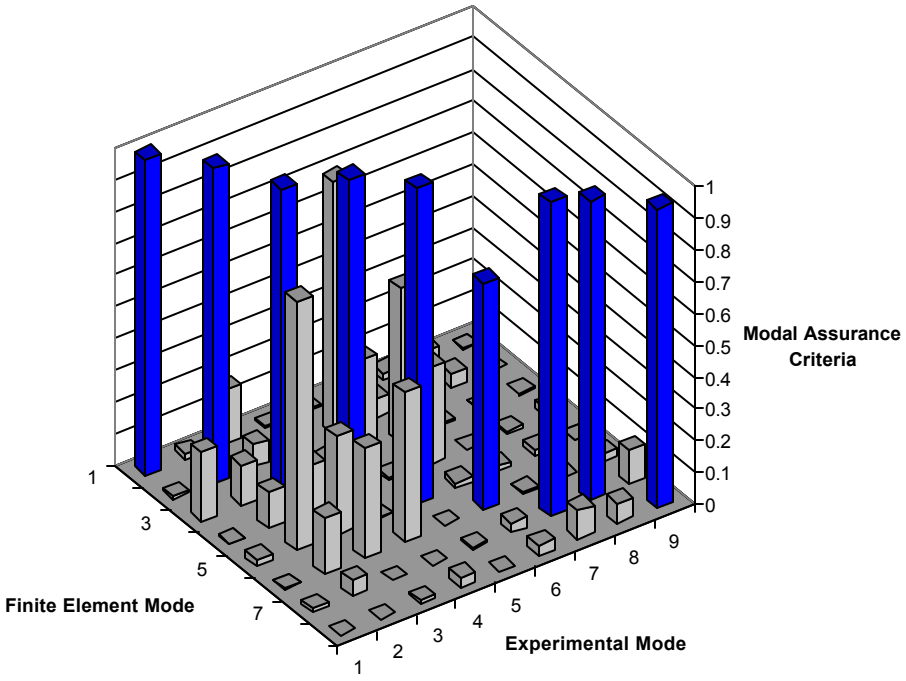

Figure 4.29. MAC for Bolt 2 Removed

The MAC shown in Figure 4.29 is the comparison between the physical and finite element results for the case where bolt 2 is removed from the system. The figure shows good correlation between the two models. There is a 3.22% average difference in the frequencies for the modes that meet the criteria.

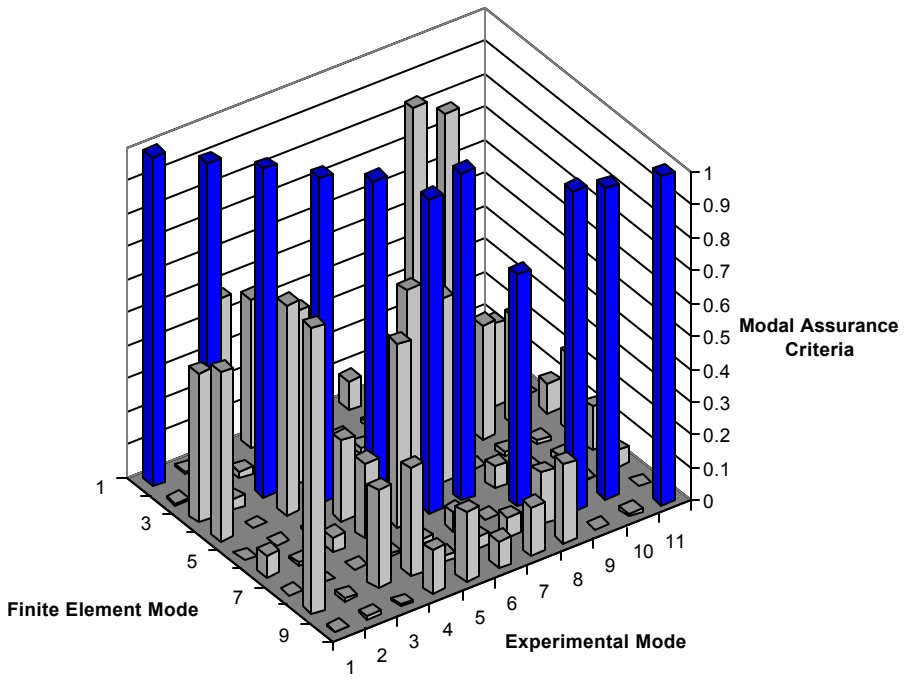

Figure 4.30. MAC for Bolt 4 Removed

The final case examined is shown in Figure 4.30 where bolt 4 is removed from the system. This figure shows the correlation between the FE and physical models. There is an average percent difference of 4.63% between the modes that have good agreement. The results for the frequencies that compare between the finite element and experimental modes are listed below in Table 4.6.

Table 4.6 Experimental Frequencies for Correlated Modes

Mode	All Bolts		Bolt 1 Removed		Bolt 2 Removed		Bolt 4 Removed
	Frequency (Hz)						
1	246.09		174.22		221.09		101.56
2	437.5		246.88		246.09		217.19
3	664.84		257.03		395.31		289.06
4	926.56		348.44		437.5		418.75
5	970.31		392.19		578.91		464.06
6	998.44		446.09		719.53		657.03
7	1221.88		657.81		991.41		716.41
8	n/a		942.97		1028.13		828.91
9	n/a		972.66		1210.16		864.06
10	n/a		994.53		n/a		873.44
11	n/a		1150		n/a		1065.63

Table 4.6 shows the natural frequencies of the MAC agreeing modes. The shifts in frequencies are not random and do, in fact, follow a logical order. Refer to Figure 4.20 for the bolt numbering scheme. The case with all bolts present has the highest frequency when looking at mode 1. This is because this mode has the most constraints placed on it. Similarly, the case where bolt 2 is removed has the next highest frequency and from Figure 4.20 this is logical as removing this bolt does not greatly increase any free span between bolts. The case where bolt 1 is removed eliminated the constraint at the corner and as seen in Figure 4.22 shows that the deflection occurring is at that location. Finally, the case where bolt 4 is removed, Figure 4.24, provides a large span with no support and as such the system is less stiff resulting in the lowest first mode frequency. As with the 12" x 12" case there is a noticeable drop in the frequency of the modes compared to the baseline where no damaged is present. This allows the detection of damage in the system

by revealing to the engineer or technician that there is something wrong with the system since there is a shift in the natural frequencies.

Case 3

This case set is the most complicated of the experimentation in this research. The first step as with the other two cases is the development of the finite element model. This model presents an additional technical variable in the joining of the two plates in the model. The model of the bolts connecting the bottom plate to the table are the same as the previous cases with the nodes of the bolt hole being constrained to allow no rotation or displacement. The connection between the upper and lower plate is examined next. Several investigations into the best method to connect the two plates follow.

The first method of joining the plates is to tie all the nodes of the bolt hole on the upper plate to the corresponding nodes of the bolt hole in the lower plate.

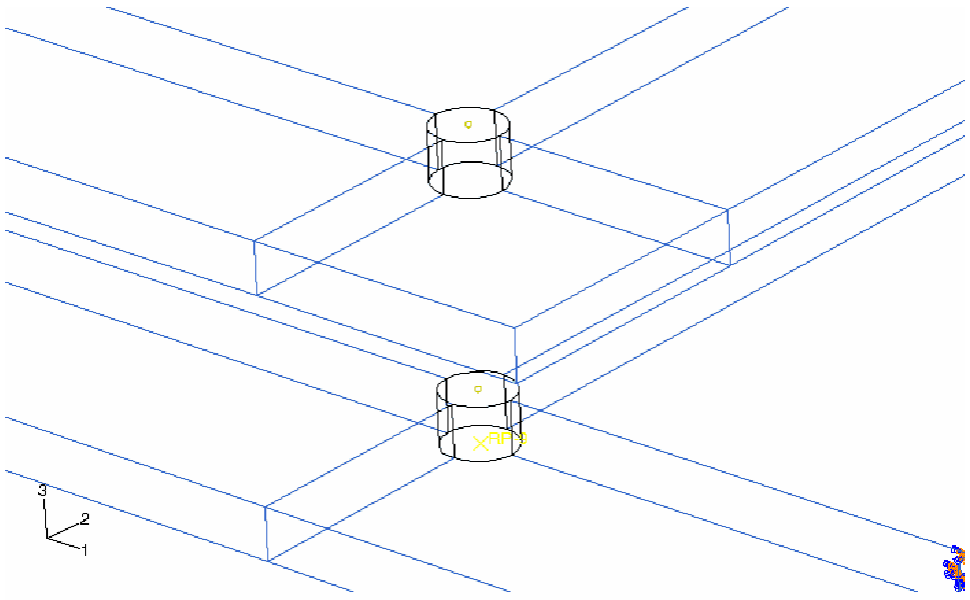

Figure 4.31. All Bolt Hole Nodes Joined Method

This method is compared to the physical case where all bolts are present, i.e. no damage. The processed MAC for this method is in Figure 4.32 below.

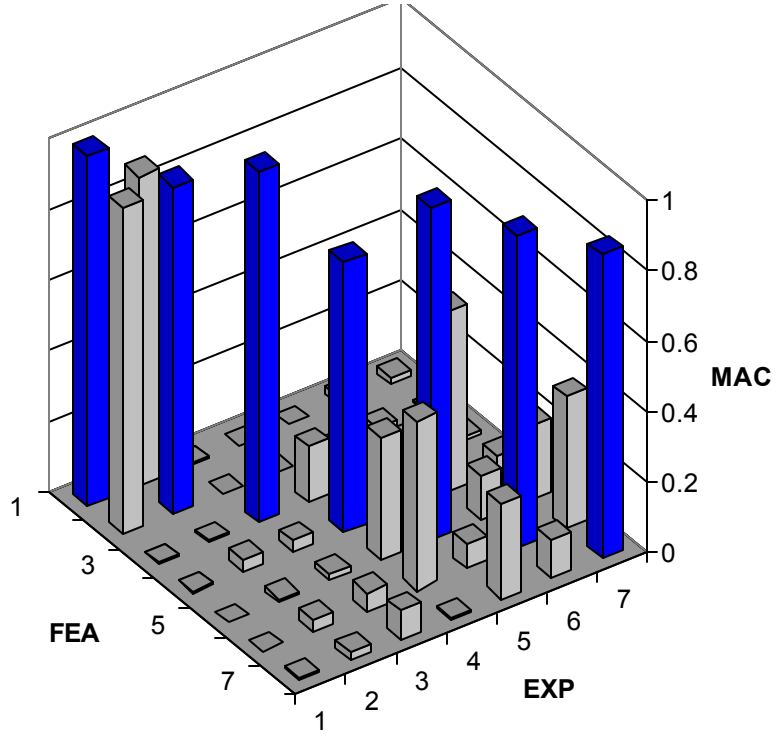

Figure 4.32. MAC for Bole Hole Tie

It is observed that there is a high degree of correlation between the finite element and experimental eigenvectors. The next method only ties the nodes of each hole together that face the cavity between the two plates.

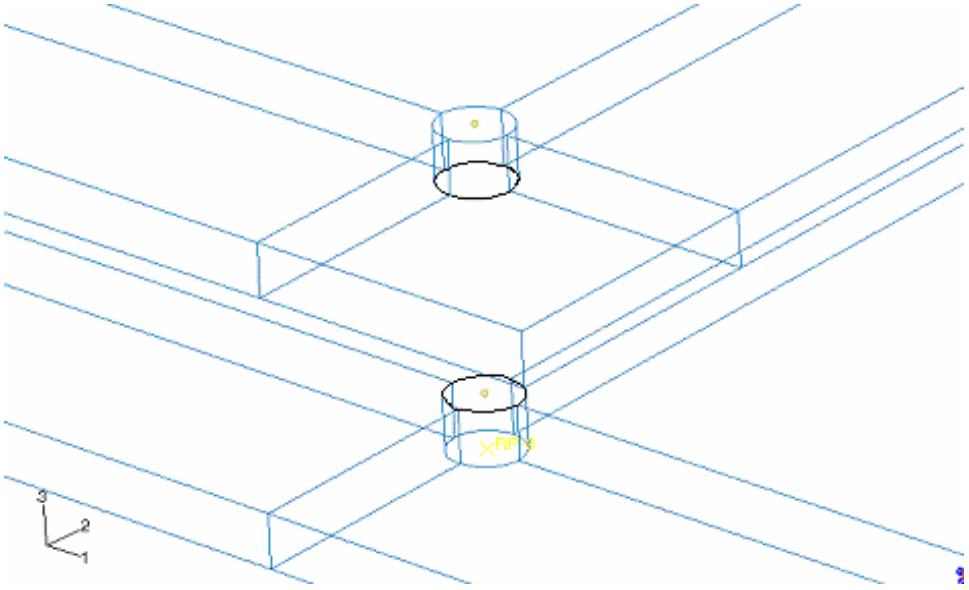

Figure 4.33. Bolt Holes Edge Nodes Joined

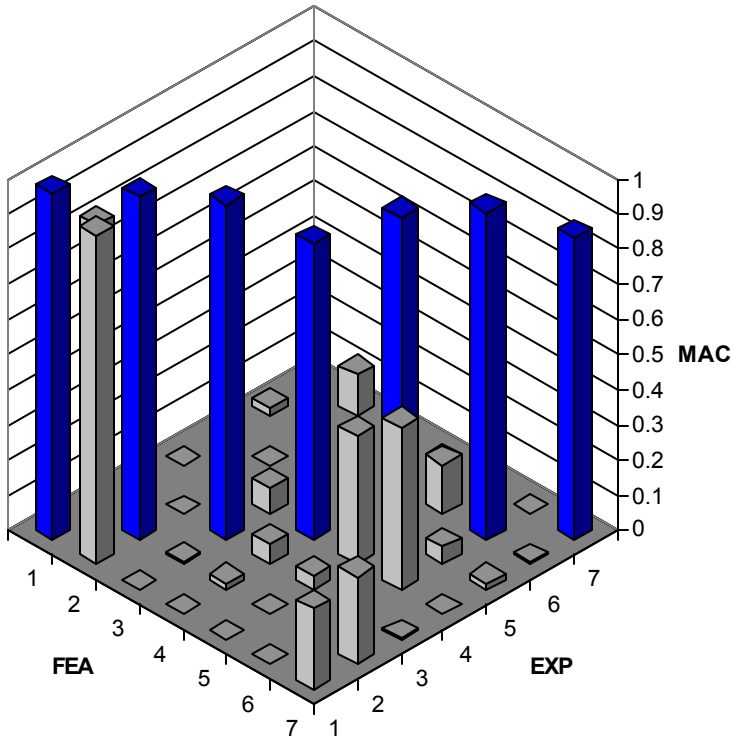

Figure 4.34. MAC for Bole Hole Edge Tie

This method also shows a high degree similarity in the mode shapes. Since these two methods both show good correlation in the MAC a comparison in the percent difference of the frequencies associated with the diagonal MAC correlations is performed. This comparison shows that method 2, edge nodes tied, has a 7.19% average difference between the frequency of the physical modes and the finite element modes. Similarly, method 2, all bolt hole nodes tied, shows a 9.81% difference in the average correlation frequencies. Analyzing the MAC and frequency comparisons the decision to use method 2 is chosen.

The preceding investigation's results are carried forward into the remainder of the finite element analyses. The first 20 modes are found in this analysis using a global mesh spacing of 0.18", leading to 99440 elements in the model and 6 degrees of freedom per node.

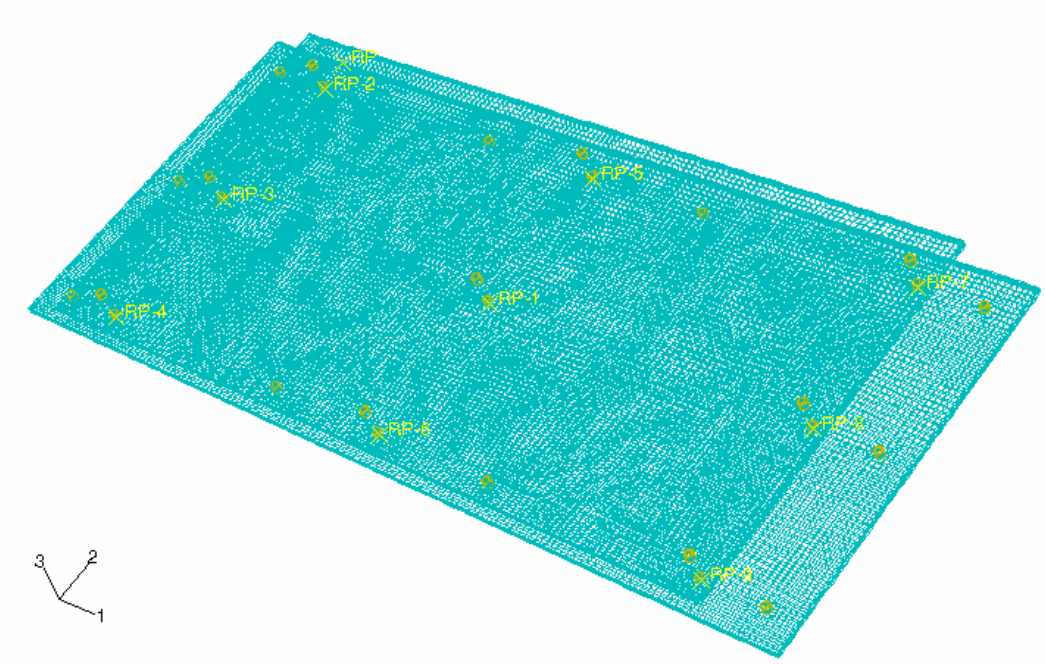

Figure 4.35. Joined Plates Mesh

As with before, constraints are removed as necessary to simulate the removal of bolts from the system. In this case, bolts 1, 2, 3, 4, 10, 11 and 13 are removed from the upper and lower plates as shown in Figure 4.36

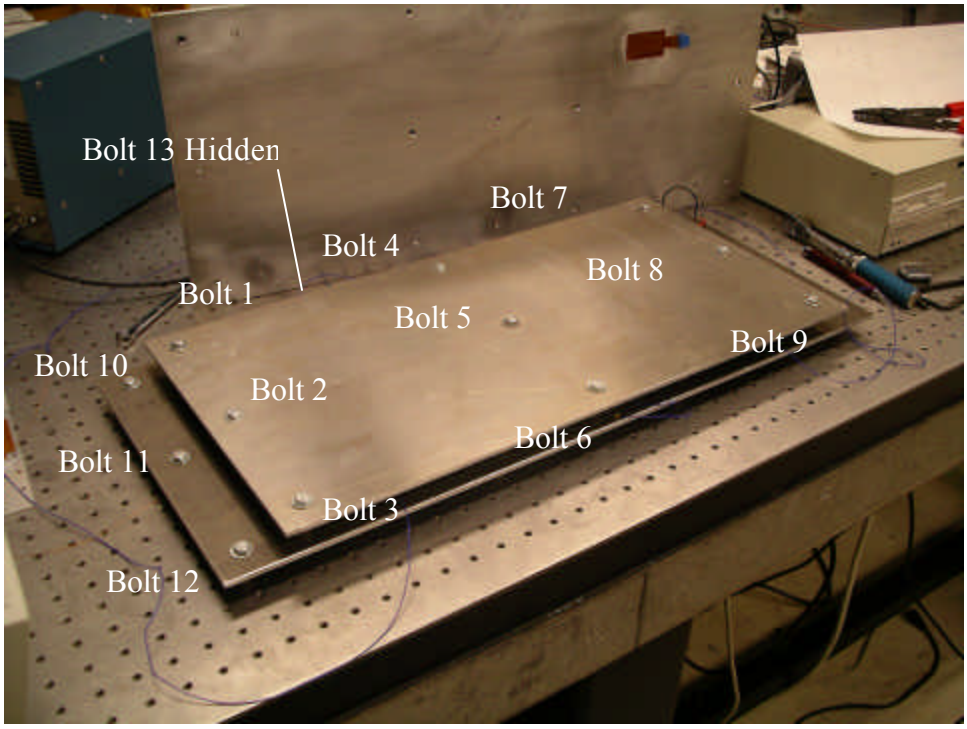

Figure 4.36. Bolt Diagram for Joined Plates

. The relevant mode shapes for these cases are found in Appendix B. The first correlated mode shape between the FE and experimental cases are located in the following figures.

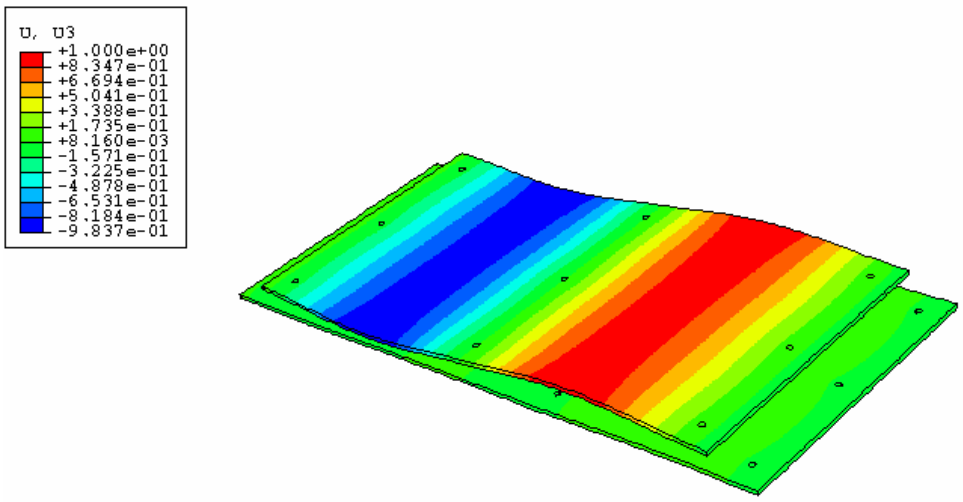

Figure 4.37. All Bolts First Mode 239.06 Hz

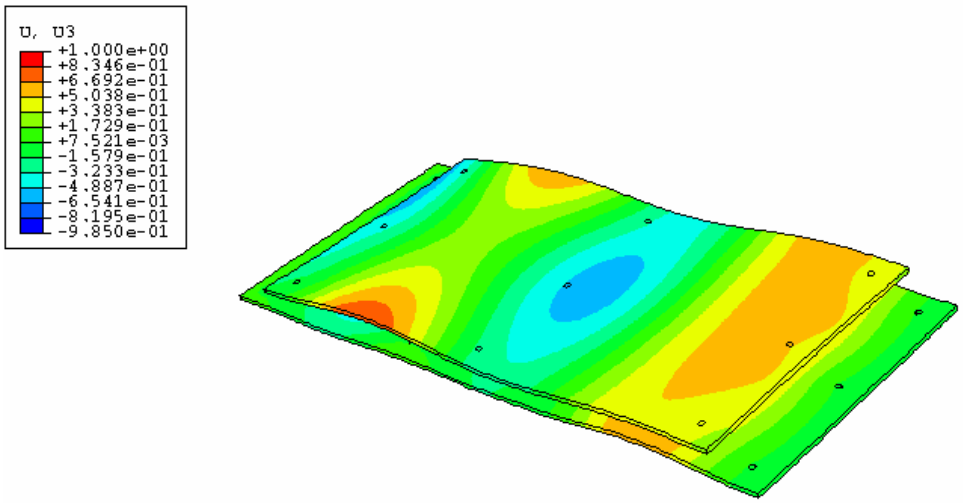

Figure 4.38. Bolt 1 First Mode 328.13 Hz

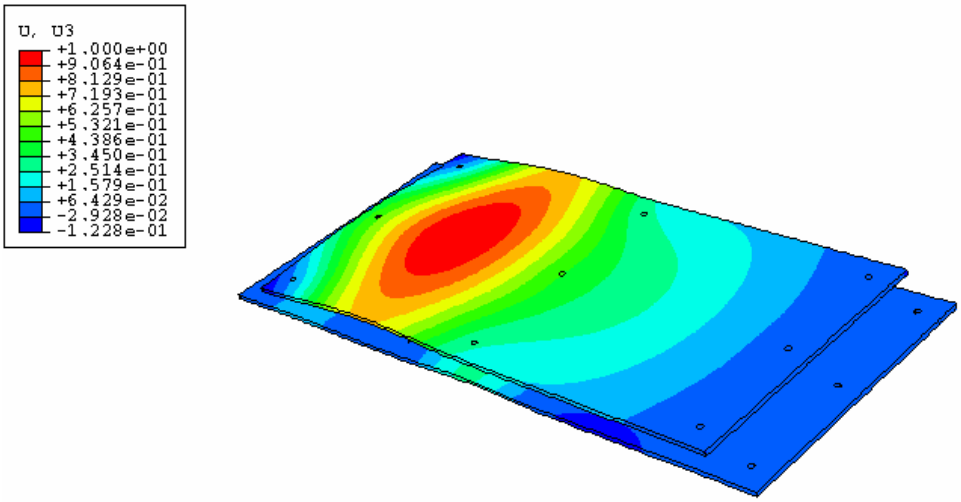

Figure 4.39. Bolt 2 First Mode 185.16 Hz

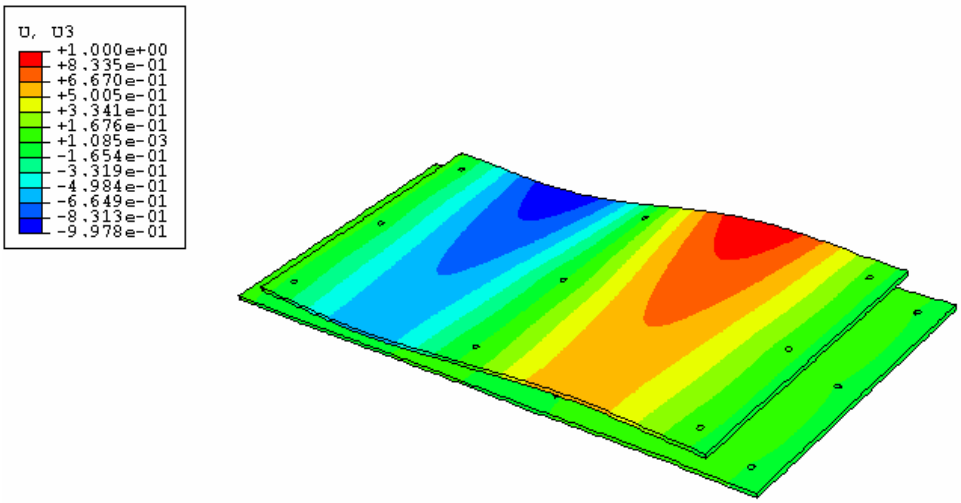

Figure 4.40. Bolt 4 First Mode 214.06 Hz

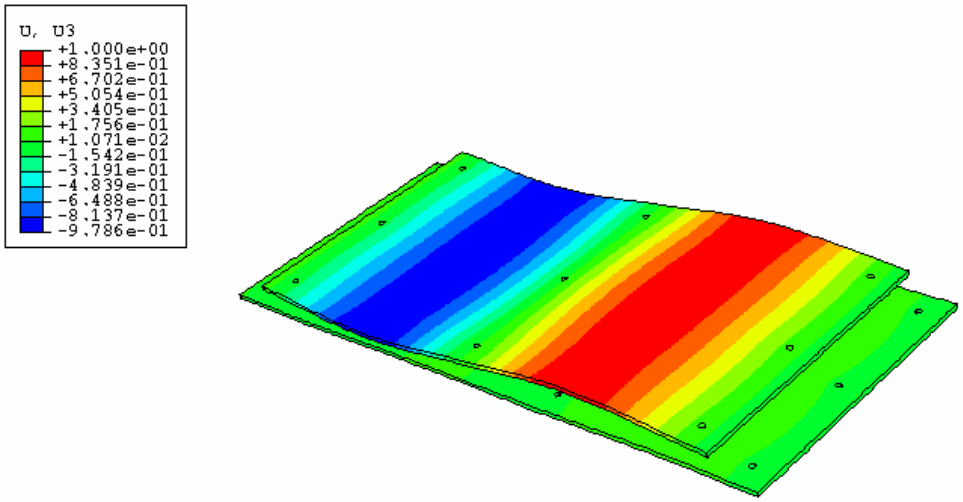

Figure 4.41. Bolt 5 First Mode 217.19 Hz

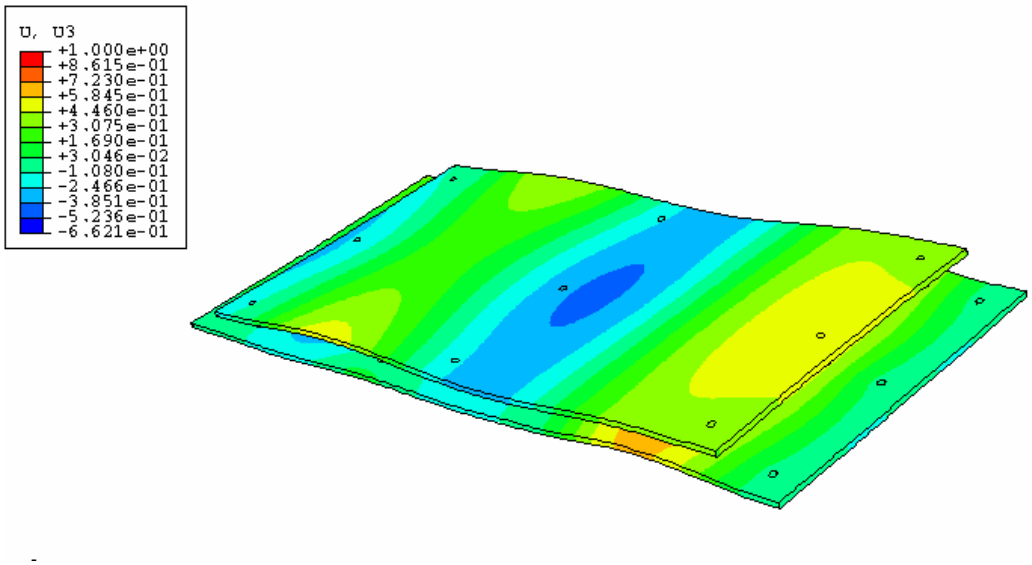

Figure 4.42. Bolt 10 First Mode 341.41 Hz

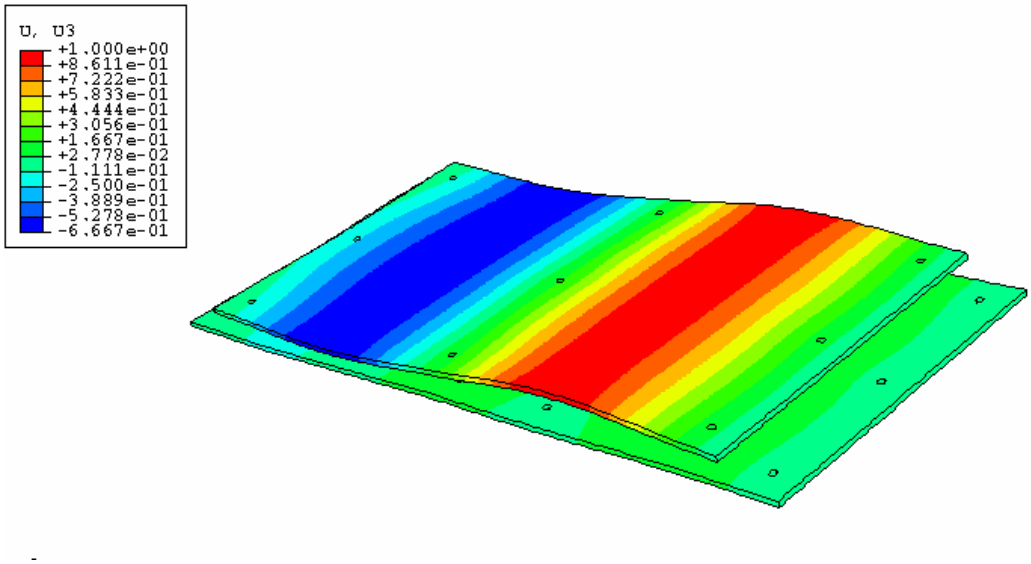

Figure 4.43. Bolt 11 First Mode 230.47 Hz

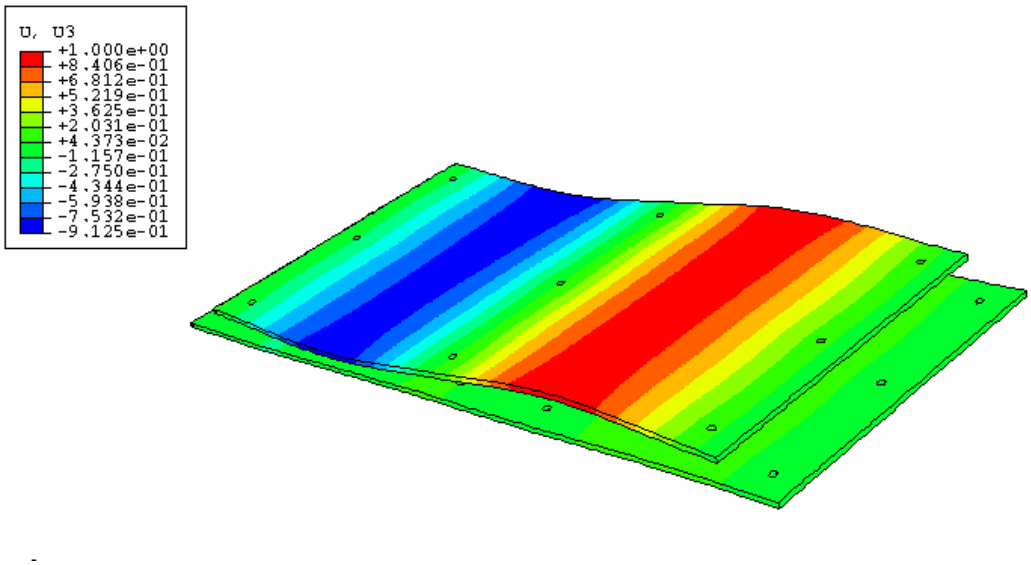

Figure 4.44. Bolt 13 First Mode 234.38 Hz

As with the 12” x 24” plate, there are 12 accelerometers on the joined plate structure. The locations are shown in Figure 4.45 below.

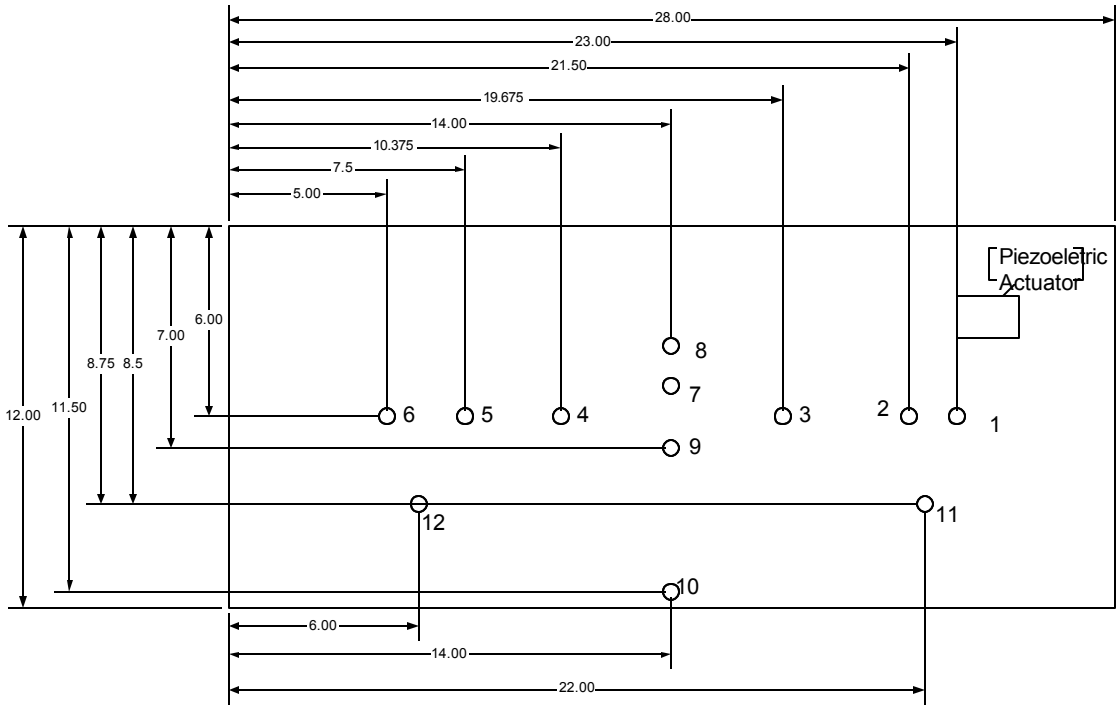

Figure 4.45. Joined Plates Schematic, Lower Plate Only (Sensors labeled 1-12)

Due to the plethora of sensors there are more data collected than is prudent to present in this chapter. A typical set of frequency response graphs are shown in Figure 4.46 below. As discussed in case 2, the remaining graphs are not shown due to the large quantity, but the figure below represents the typical response.

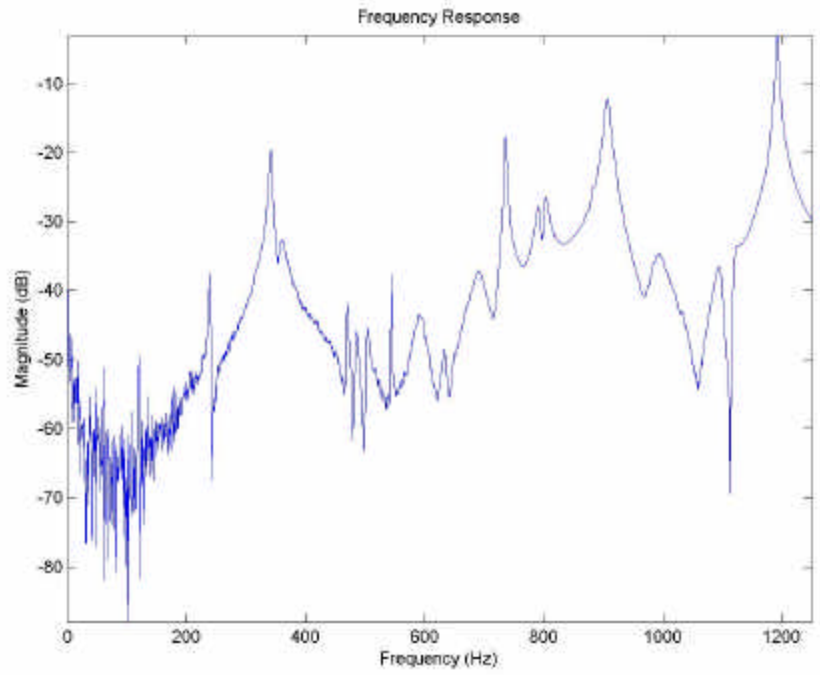
Frequency Response
Magnitude (dB)
-10
-20
-30
-40
-50
-60
-70
-80
0
200
400
600
800
1000
1200
Frequency (Hz)

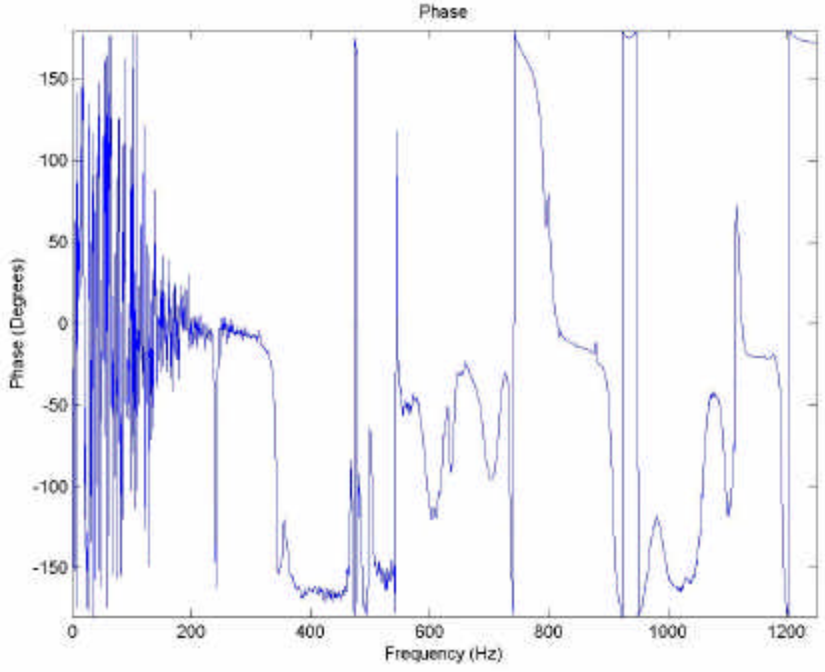
Phase
Phase (Degrees)
150
100
50
0
-50
-100
-150
0
200
400
600
800
1000
1200
Frequency (Hz)

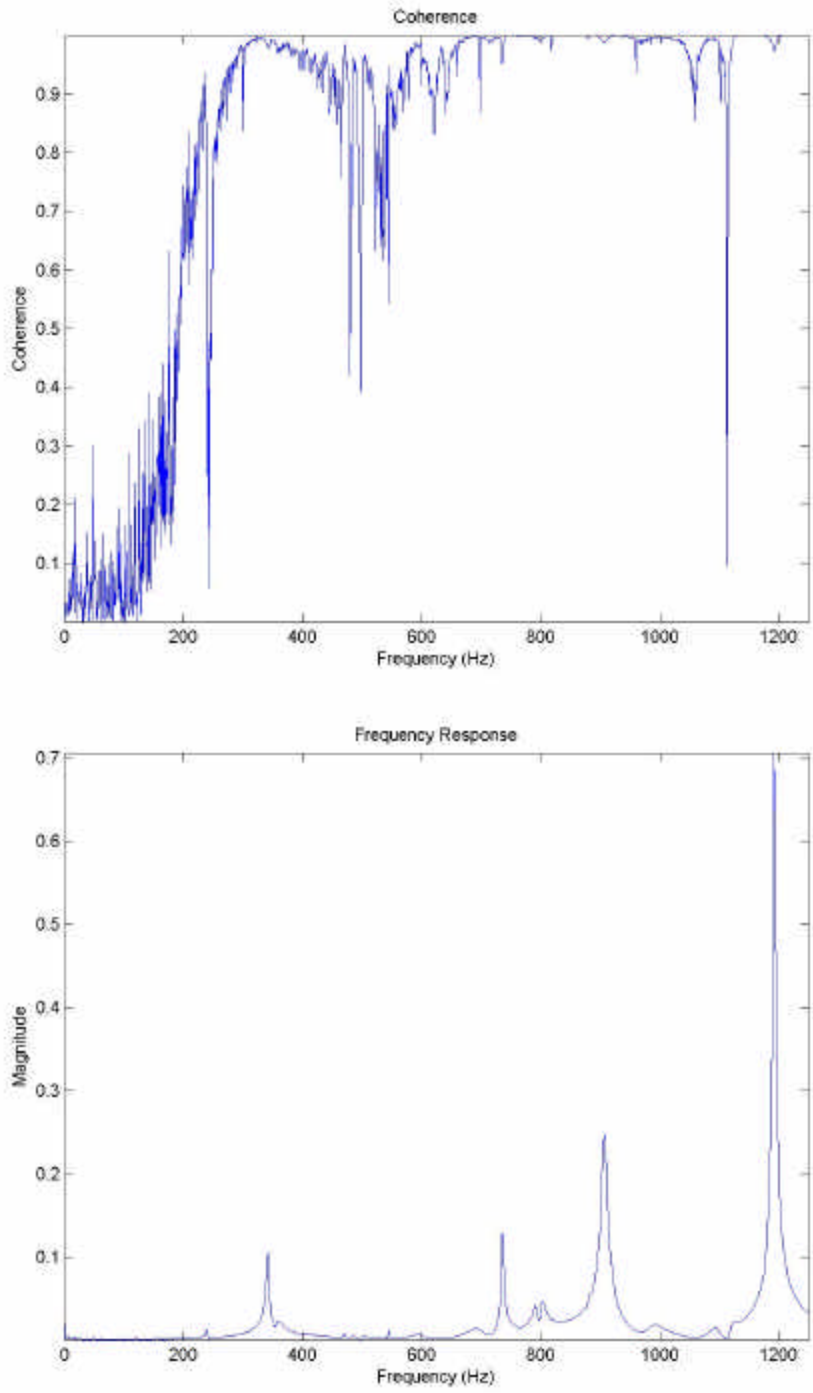

Figure 4.46. Frequency Response and Coherence for Accelerometer 1

It is seen in the graphs the level of noise in the lower range of the frequency band, below 250 Hz. This is discussed later in this chapter. It is also noticed that there is good coherence in the data.

With all data collected, the next step is calculating the MAC between the FE and experimental solutions. The edited results of this comparison are found in Figures 4.47 through 4.54.

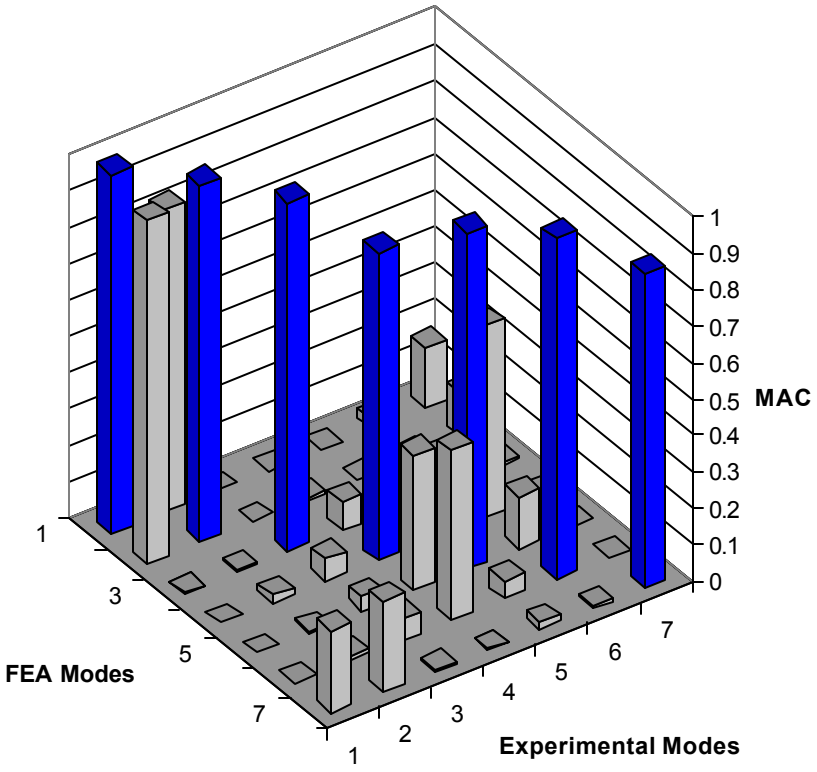

Figure 4.47. MAC Results All Bolts

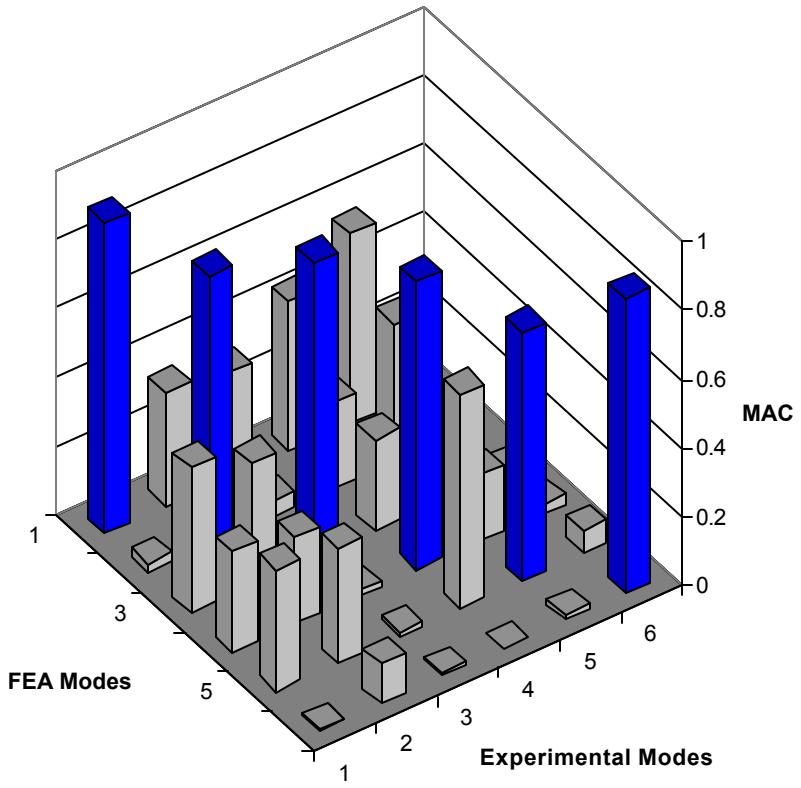

Figure 4.48. MAC Results Bolt 1 Removed

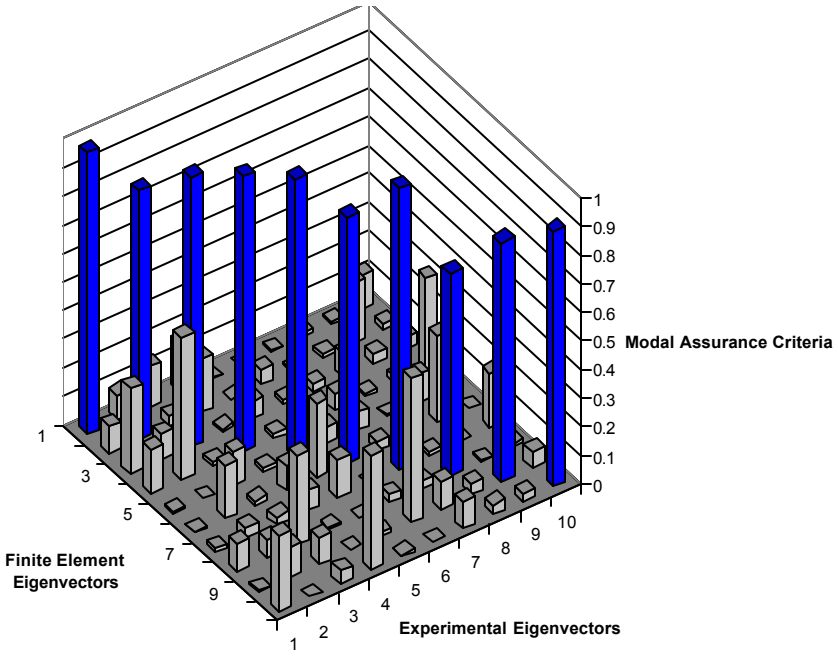

Figure 4.49. MAC Results Bolt 2 Removed

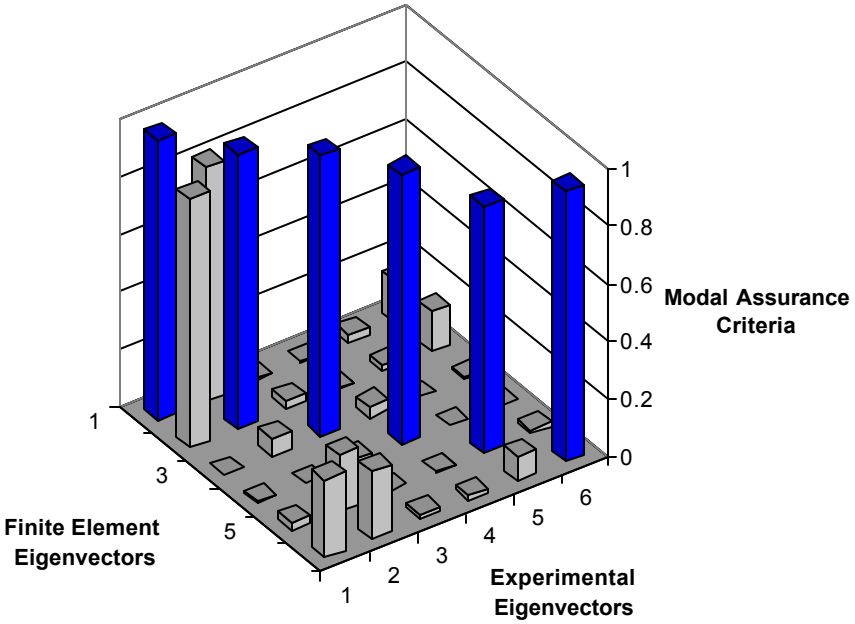

Figure 4.50. MAC Results Bolt 4 Removed

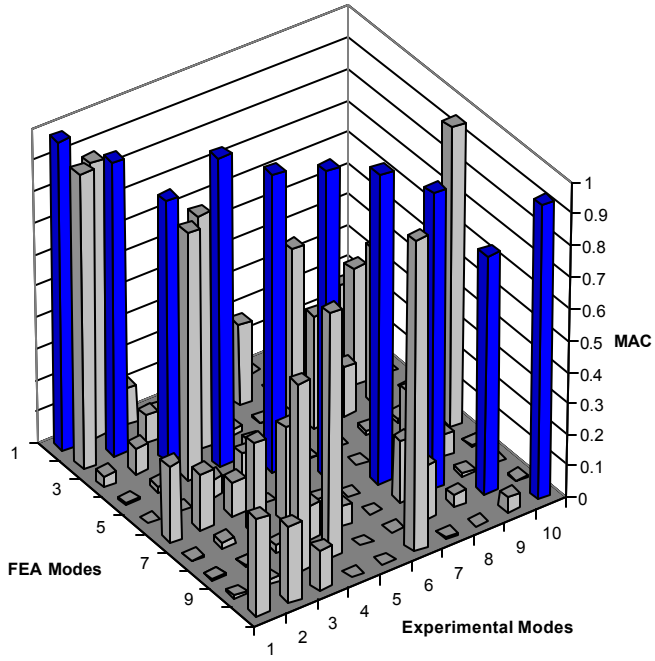

Figure 4.51. MAC Results Bolt 5 Removed

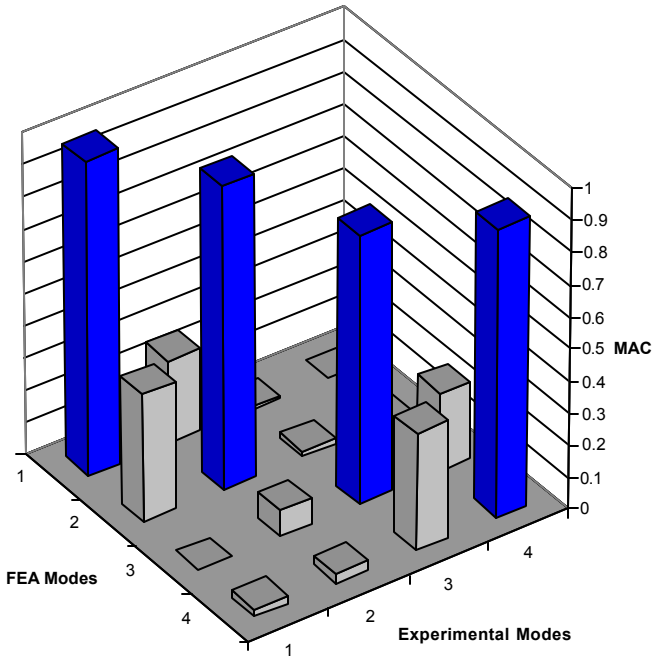

Figure 4.52. MAC Results Bolt 10 Removed

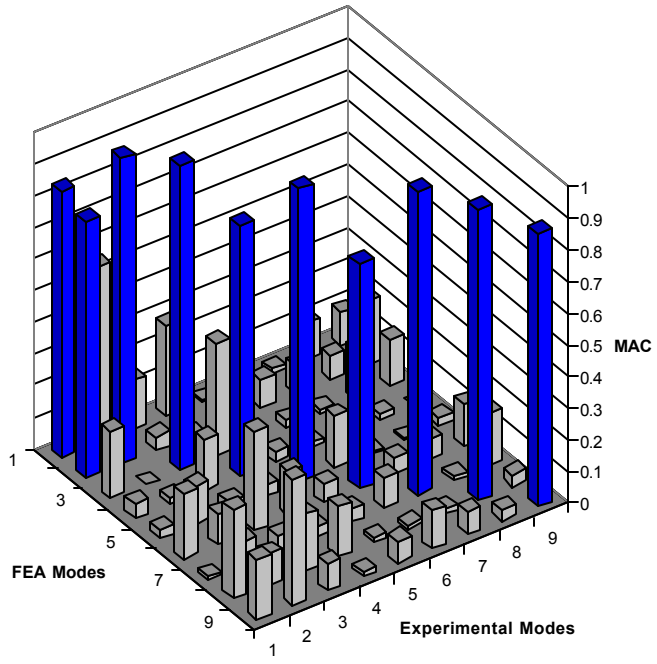

Figure 4.53. MAC Results Bolt 11 Removed

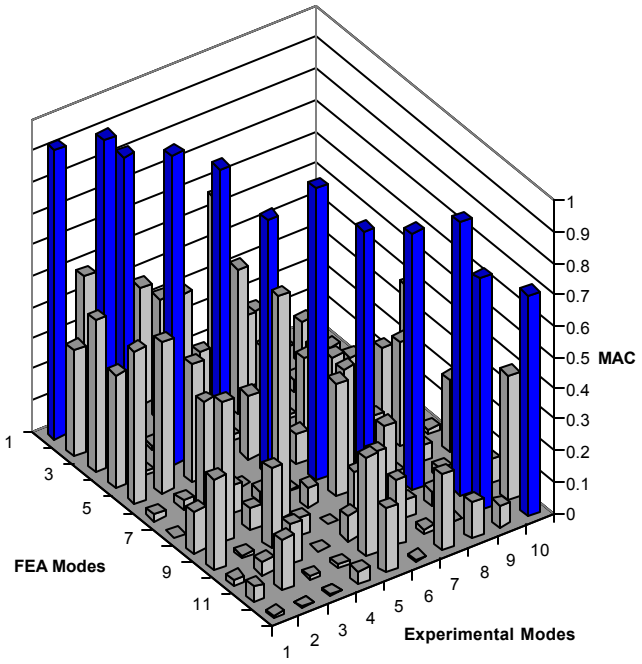

Figure 4.54. MAC Results Bolt 13 Removed

Examining the above figures shows that there is good correlation between the finite element model and the actual joined plate system. Another good indicator of the similarity between the modeled and physical system is the closeness of their natural frequencies. The average difference in frequency of the modes that correlate using the MAC is 3.94%. Further examination reveals the average frequency difference in Table 4.7.

Table 4.7. Average Percent Difference for MAC Correlated Frequencies

Damage Case	Percent Difference
Undamaged	7.19
Bolt 1 Removed	1.86
Bolt 2 Removed	2.60
Bolt 4 Removed	4.27
Bolt 5 Removed	6.84
Bolt 10 Removed	2.60
Bolt 11 Removed	3.22
Bolt 13 Removed	2.94

Table 4.8 Experimental Modal Frequencies for Joined Plates

	All Bolts		Bolt 1 Removed		Bolt 2 Removed		Bolt 4 Removed
Mode	Frequency (Hz)						
1	239.06		328.13		185.16		214.06
2	341.41		338.28		332.03		339.84
3	469.53		378.13		347.66		424.22
4	503.91		462.5		402.34		476.56
5	633.59		512.5		457.03		685.16
6	735.16		536.72		483.59		732.03
7	1120.31		646.88		596.88		n/a
8	n/a		n/a		686.72		n/a
9	n/a		n/a		709.38		n/a
10	n/a		n/a		735.16		n/a
	Bolt 5 Removed		Bolt 10 Removed		Bolt 11 Removed		Bolt 13 Removed
Mode	Frequency (Hz)						
1	217.19		341.41		230.47		234.38
2	332.81		474.22		302.34		296.09
3	353.91		502.34		341.41		347.66
4	432.81		620.31		358.59		472.66
5	456.25		n/a		470.31		492.19
6	485.16		n/a		510.94		519.53
7	549.22		n/a		612.5		544.53
8	600.78		n/a		725.78		667.19
9	676.56		n/a		744.53		729.69
10	1120.31		n/a		n/a		757.81

Table 4.8 shows that with the exception of bolts 1 and 10 that the first mode for the damaged cases has a lower frequency than the baseline case. There is however, a change in frequency in the bolt 1 and bolt 10 removed cases leading to the detection of damage. The frequencies of the bolts 1 and 10 removed cases could have matched at lower frequencies than found using the MAC to match modes. As discussed in the subsequent paragraph, bolts 1 and 10 (see Figure 4.36) are located a large distance from the actuator

and the excitation may not be great enough to excite these modes. Poor coherence may be to blame or perhaps the placement of the piezoactuator too far away to properly excite these lower modes. The lack of better correlation between bolts 1 and 10 and their respective finite element models may be a result of a forcing function that lacks power in the low-frequency band. This feature is observed in the response graphs, which show the accelerometers not sensing at low frequencies.

Noise in Experimental Data

Modal analysis testing introduces several means for noise to appear in the end result. Some noise can be attributed to equipment and possibly environmental conditions. In this research large stiff structures are being excited with a small piezoelectric patch. While the voltage to the actuator is amplified, the output signal from the patch is still quite small. The noise in the graphs shown in this chapter show noise in the lower frequency range. All of the plots are using the FFT of the signals to produce the plots. At low frequencies, the response of the system is not forced strongly and thus does not respond in a powerful manner. When this response is divided by a small FFT of the input, the "noise" of the structural response is amplified by this fact. Add to this the transfer functions of the actuator, amplifiers, accelerometers and the remaining equipment and the potential for unwanted signal alteration increases. A solution to this problem may be to use a larger piezopatch capable of imparting a greater force on the system. It is also observed in the graphs shown in this chapter that the coherence is very low in the regions where the noise occurs. This means there is poor correlation between the input and output signals. The phase plots for the accelerometer signals also show that

the sensors are moving considerably in the regions with poor coherence. This is an indicator that the system response is not adequate for the MAC.

Summary

The results presented in this research reaffirm that the use of frequency shifts to detect damage is valid. The impact of the research goes beyond this fact though. The goal of this thesis is to detect damage in a structure by monitoring the frequency response of the support structure for the system of interest. Frequency is the means by which all damage comparison are made in cases 1-3. The results of case 3 show that it is possible to accomplish the above task by using the eigenvectors of the FE and experimental cases, both undamaged and damaged, to find the MAC and modal frequencies. The MAC is the tool by which the eigenvectors of the experimental and FEA results are compared and quantified. The associated modal frequencies for the damaged and undamaged cases are the basis for detection of damage in the system. The ability to sense damage in the skin of a vehicle from the support structure has the benefit of allowing removal and replacement of the protective skin while allowing the sensor cluster to remain intact and unaltered. It also prevents the sensor array from being exposed to high temperatures and pressures associated with some vehicle maneuvers.

V. Conclusions and Recommendations

Damage Detection

It is found through this research that a shift in resonant frequencies does indeed provide insight into a change in the system that may ultimately be characterized as damage. Examining the Modal Assurance Criteria to determine the degree to which the mode shape of the experiment agrees with the finite element model is the baseline for validating responses. Eliminating the modes that do not correlate leads to graphical results from the FE model that relate to the experiment. The frequencies are then compared to note any changes that signify damage to the system. It is observed from the data in Chapter 4 that frequency can be used to detect damage to the skin of a vehicle by sensing from its superstructure. A change in frequency indicates a change in system response and thus a change in eigenvectors. This process should be investigated more thoroughly using some of the recommendations below. Also, it is shown that an accurate FE model is possible to represent the behavior of a joined systems response. This is of great use to future developments as remote or stand-off sensing needs to be further developed.

Finite Element Modeling

The use of the Modal Assurance Criteria to show the relationship between the finite element and experimental results proved invaluable! Modes that matched between the physical and finite element showed average percent differences in frequencies of 4.06% for all models. While the finite element modeling technique utilized in this

research provides accurate results in comparing to the physical case some improvements may be possible. First, while the bolts in these tests are modeled as rigid bodies, this may not be the case in all instances. More examination into the performance of deformable bolts and spacers along with contact and connection conditions is possible. This may account for some of the modes from the physical testing that do not align themselves with the FEA results. Perhaps the piezo patch could be modeled and the forcing function used in the test could be used in the solution. While the author has limited exposure to ABAQUS there exists the ability in the program to model peizo actuators. The forcing function applied in the laboratory could be applied to the finite element model actuator to simulate the same excitation. With this performed, the operating responses may be better matched to the finite element responses.

Future Research

Several interesting cases were discovered during the course of this research that bear further investigation. First, as mentioned in the previous section, more experimentation with the finite element model could provide even better results. The joined plate case in particular with several type of connections and contact conditions could benefit from further investigation. Second, more work could be done in the arena of representing damage by merely reducing the torque on the bolts. A small case was done in the 12" x 12" plate, but that was merely to determine if the bolt behaved as a rigid body. Third, exploration of the effect of cracks on the system is another potential damage that could be explored. Fourth, the use of energy methods to determine the amount of energy present in the plates at any time could be an indicator of damage in the

system. Finally work with different plate structures and perhaps the actual Thermal Protection System tiles should be accomplished.

With the proper finite element model and physical representation, research into the flight conditions of the applicable vehicle can be explored to determine effects on the sensing of damage. A limited flight test case can be fielded to determine the effects of other aircraft parameters on the performance of the accelerometer sensitivity and response. With this data, a better ground testing protocol can be developed to further the research effort.

Appendix A

All frequencies listed are the experimental correlated frequencies.

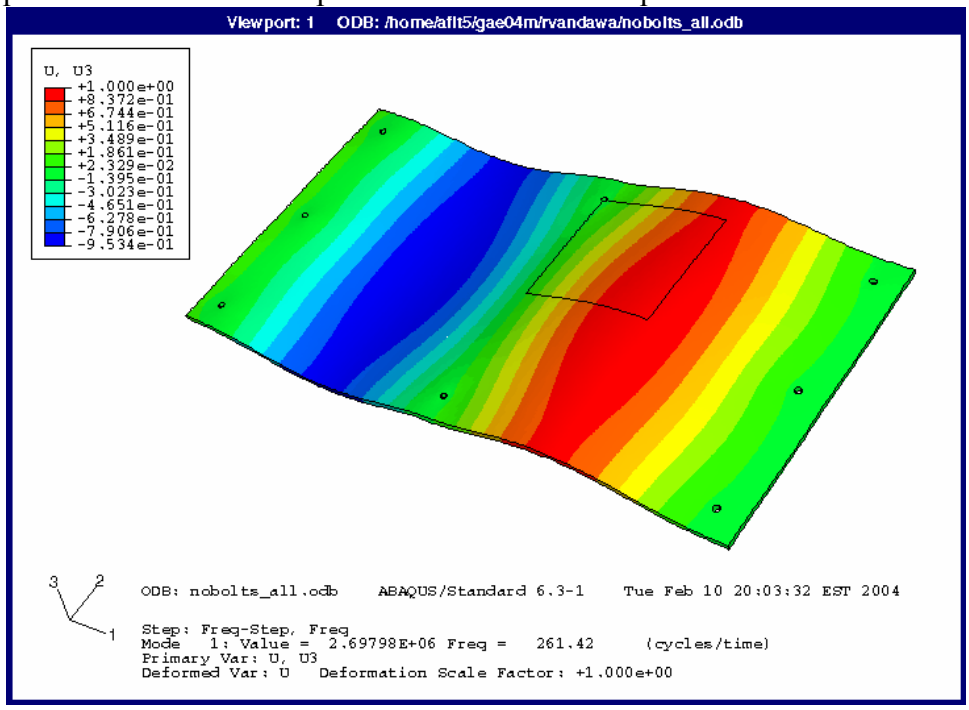

1st Correlated MAC Mode for All Bolts. 246.09 Hz

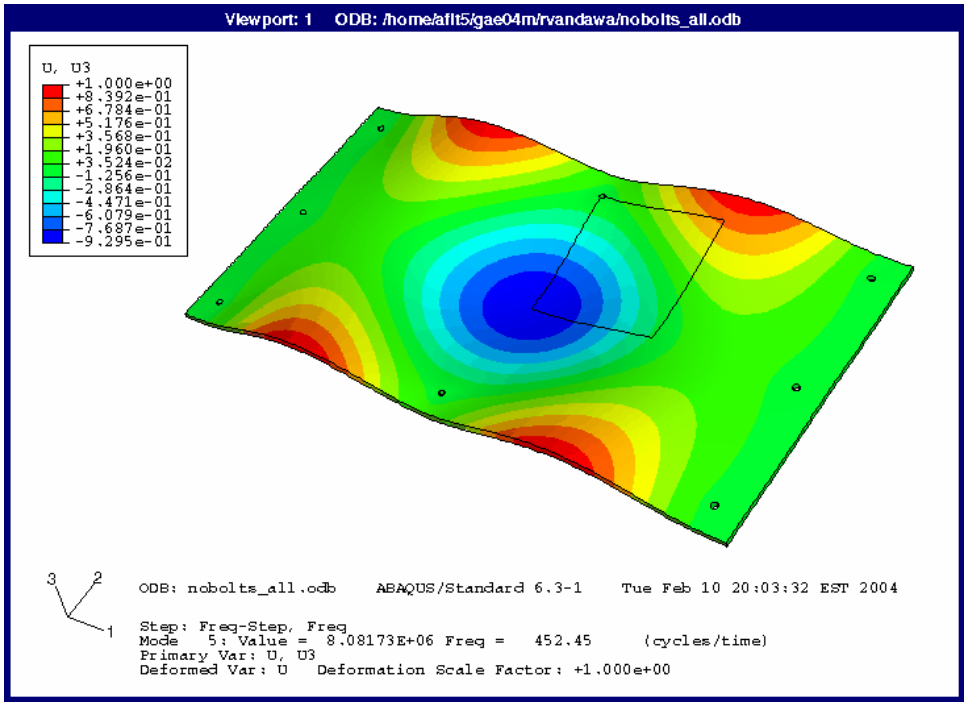

2nd Correlated MAC Mode for All Bolts. 437.50 Hz

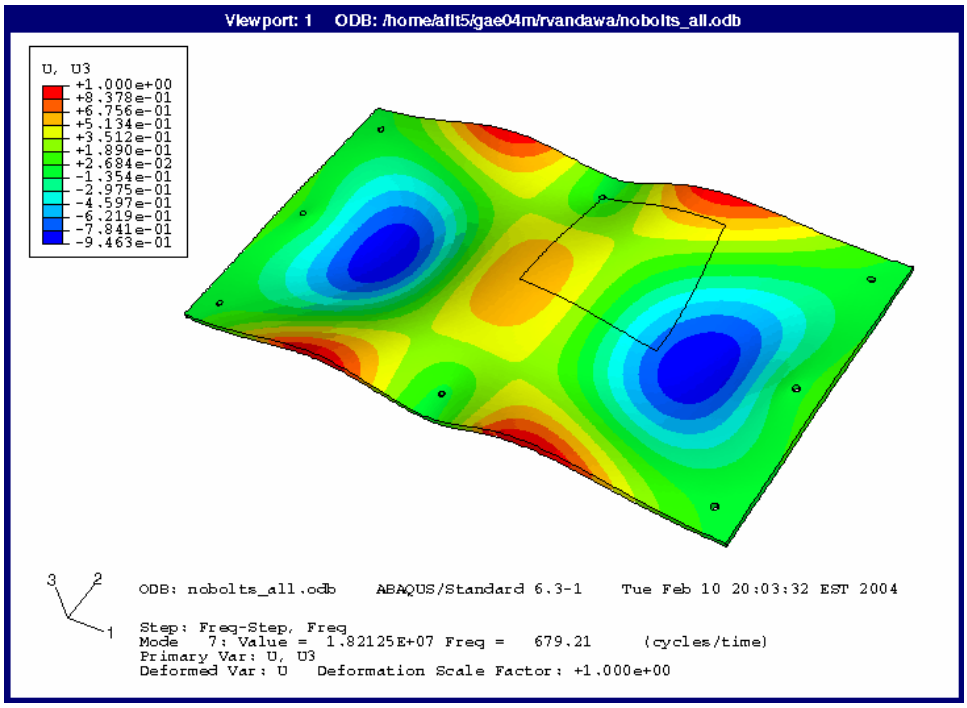

3rd Correlated MAC Mode for All Bolts. 664.84 Hz

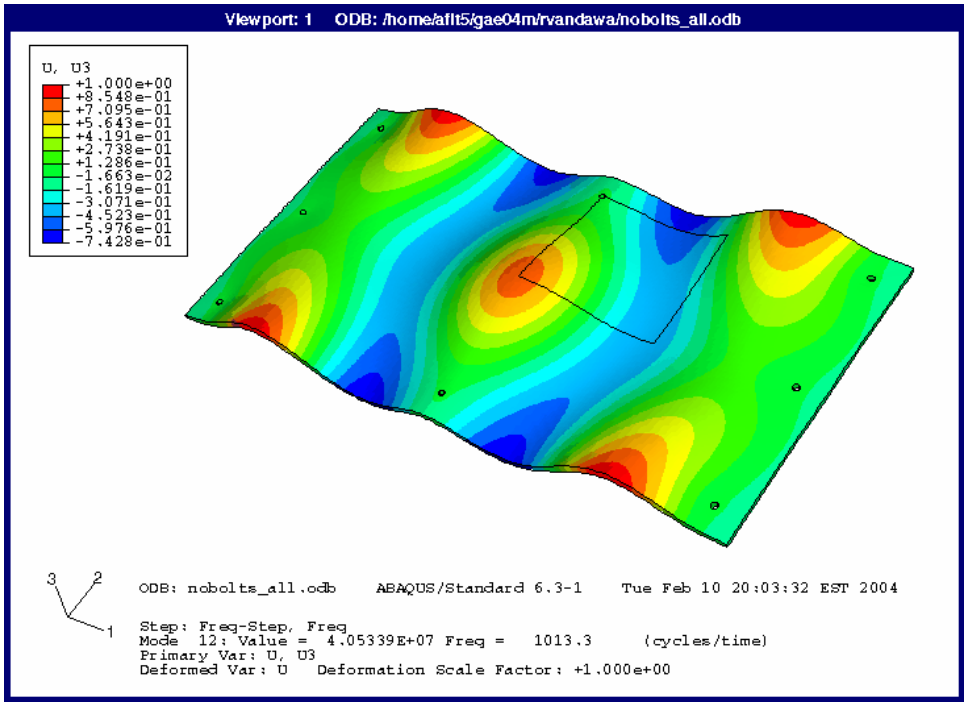

4th Correlated MAC Mode for All Bolts. 926.56, 970.31, 998.44 Hz

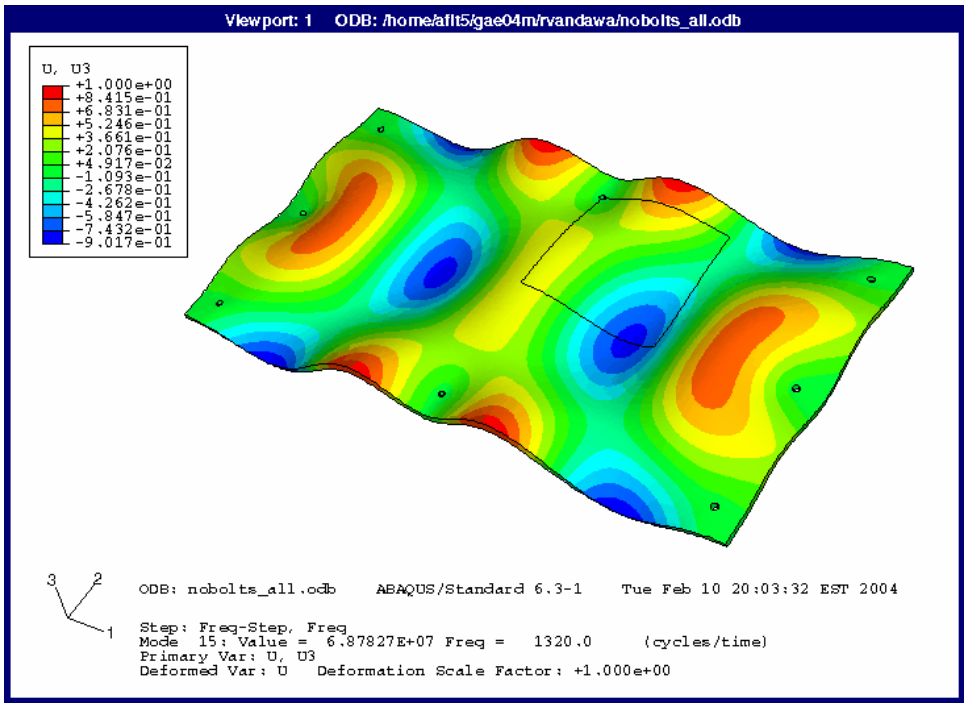

5th Correlated MAC Mode for All Bolts. 1221.88 Hz

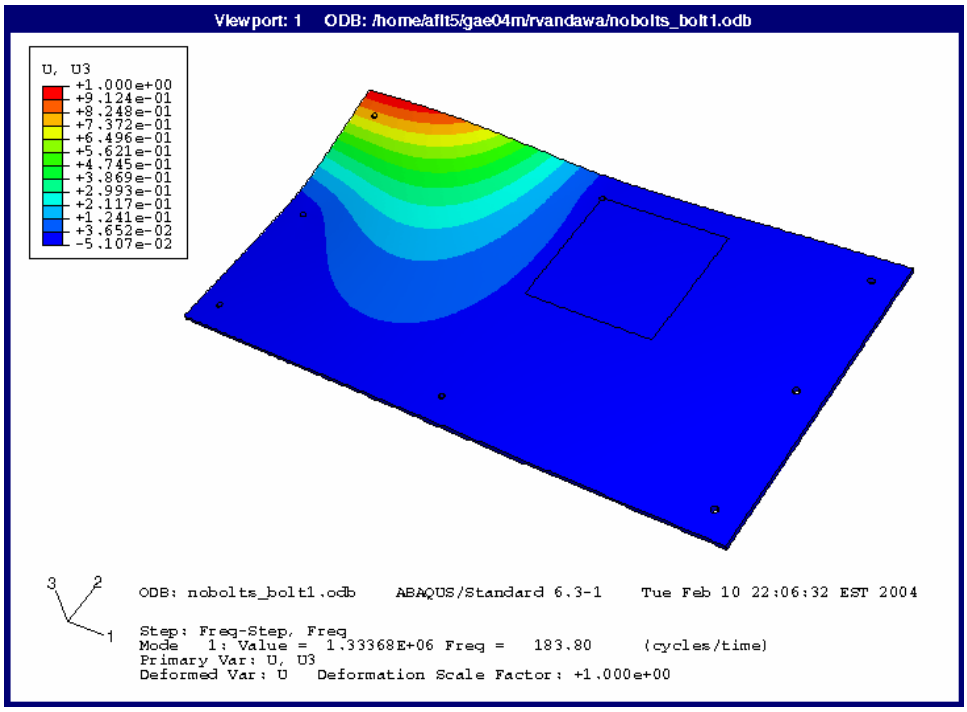

1st Correlated MAC Mode for Bolt 1 Removed. 174.22 Hz

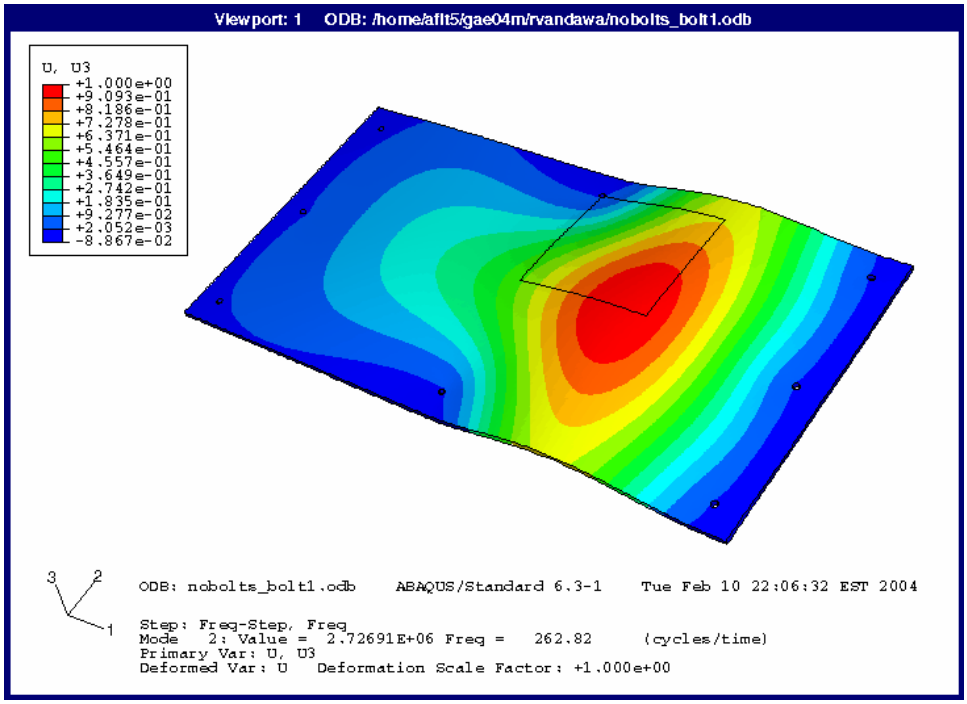

2nd Correlated MAC Mode for Bolt 1 Removed. 246.88 Hz

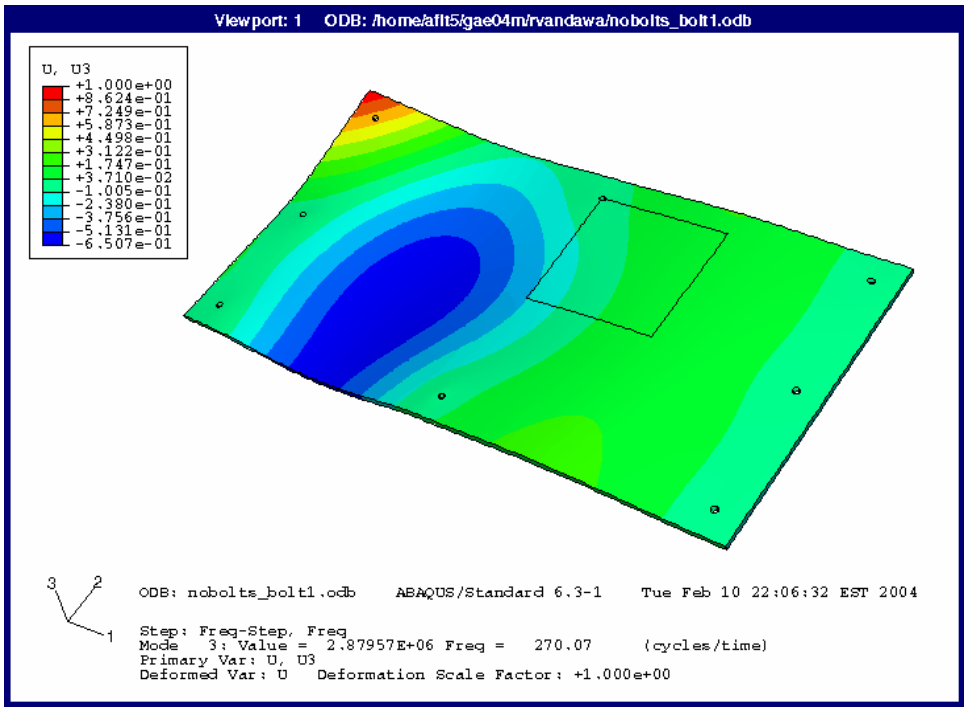

3rd Correlated MAC Mode for Bolt 1 Removed. 257.03 Hz

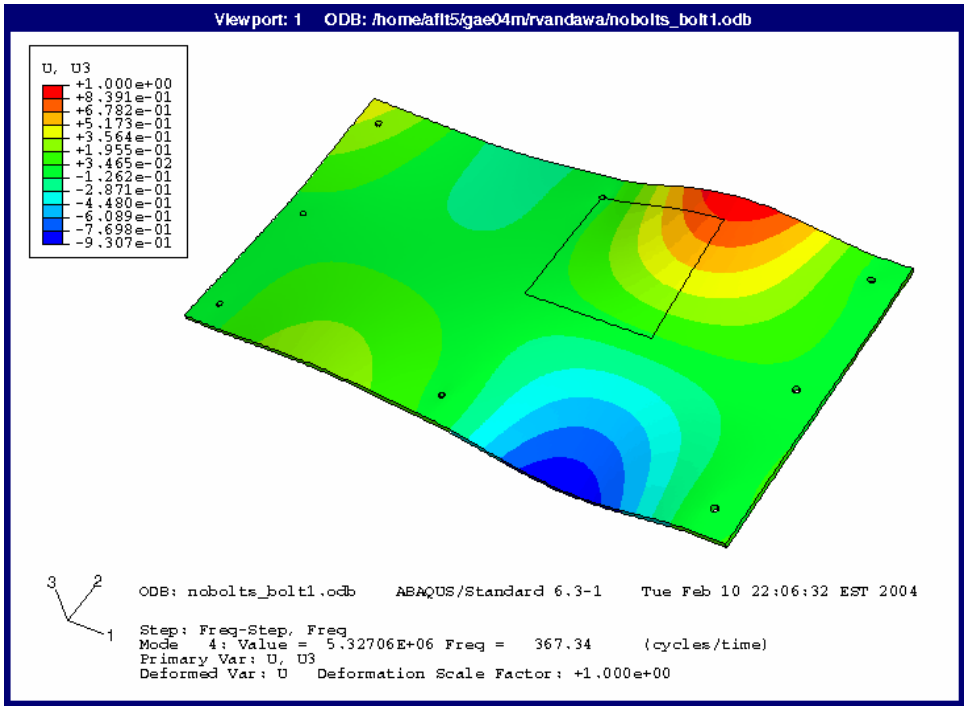

4th Correlated MAC Mode for Bolt 1 Removed. 348.44 Hz

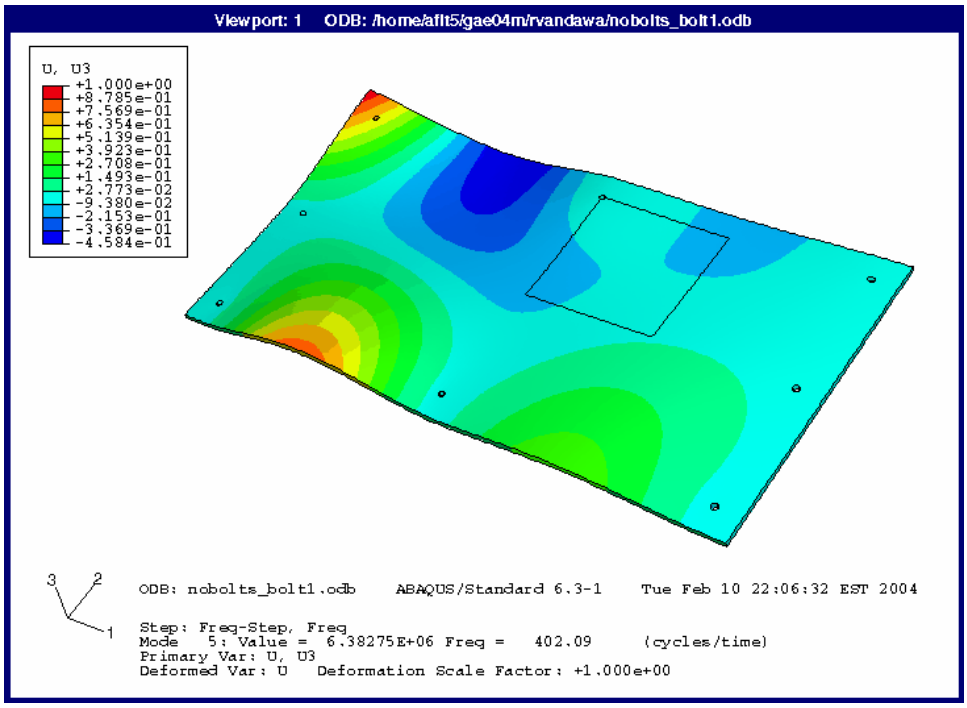

5th Correlated MAC Mode for Bolt 1 Removed. 392.19 Hz

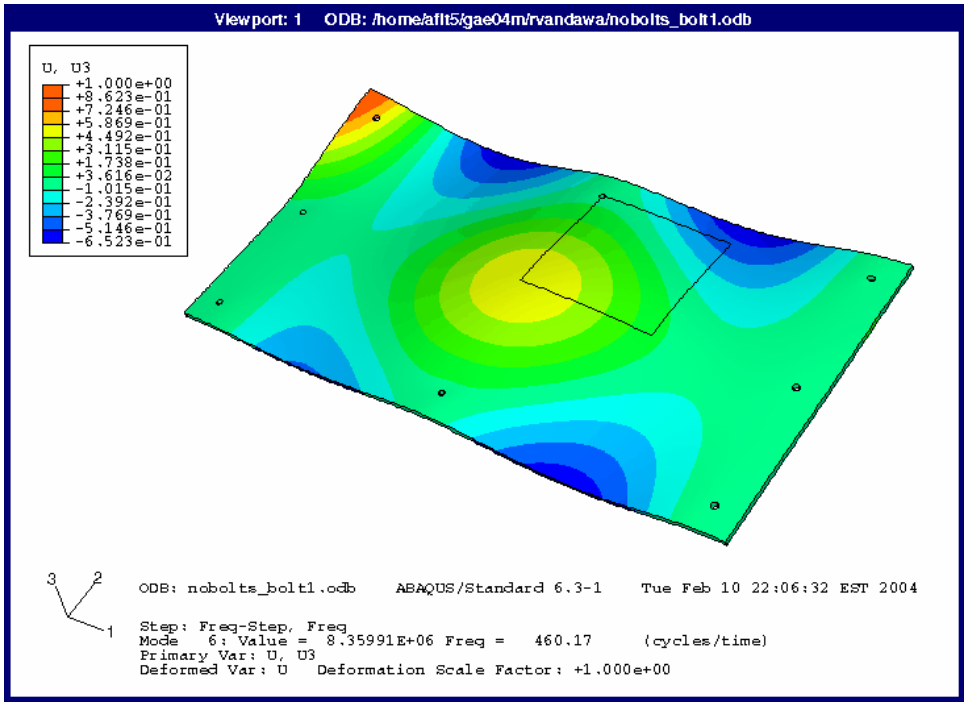

6th Correlated MAC Mode for Bolt 1 Removed. 446.09 Hz

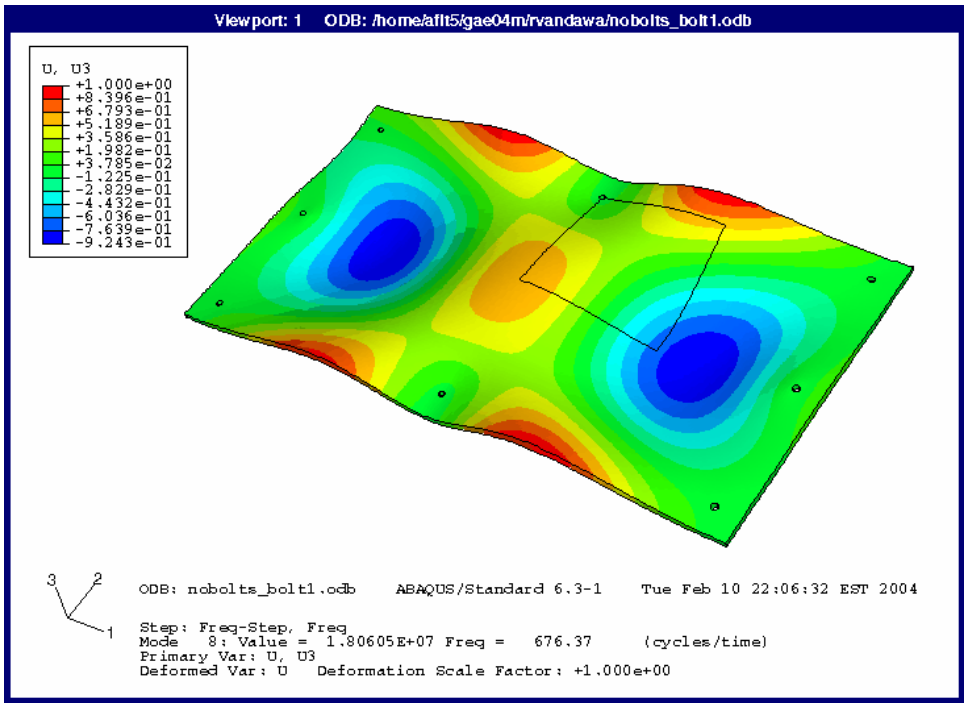

7th Correlated MAC Mode for Bolt 1 Removed. 657.81 Hz

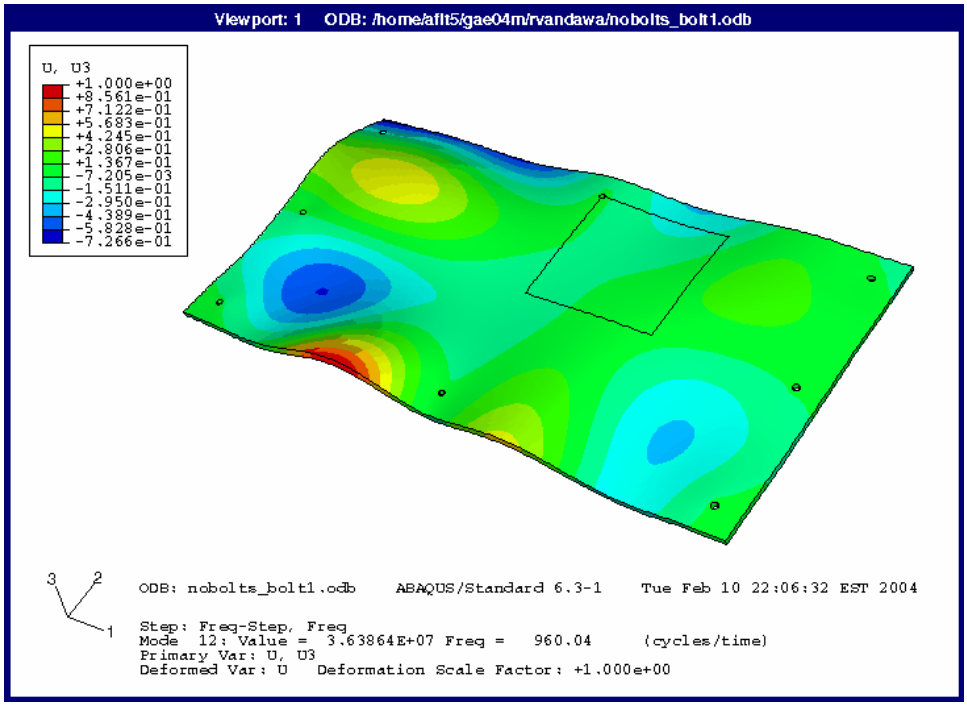

8th Correlated MAC Mode for Bolt 1 Removed. 942.97 Hz

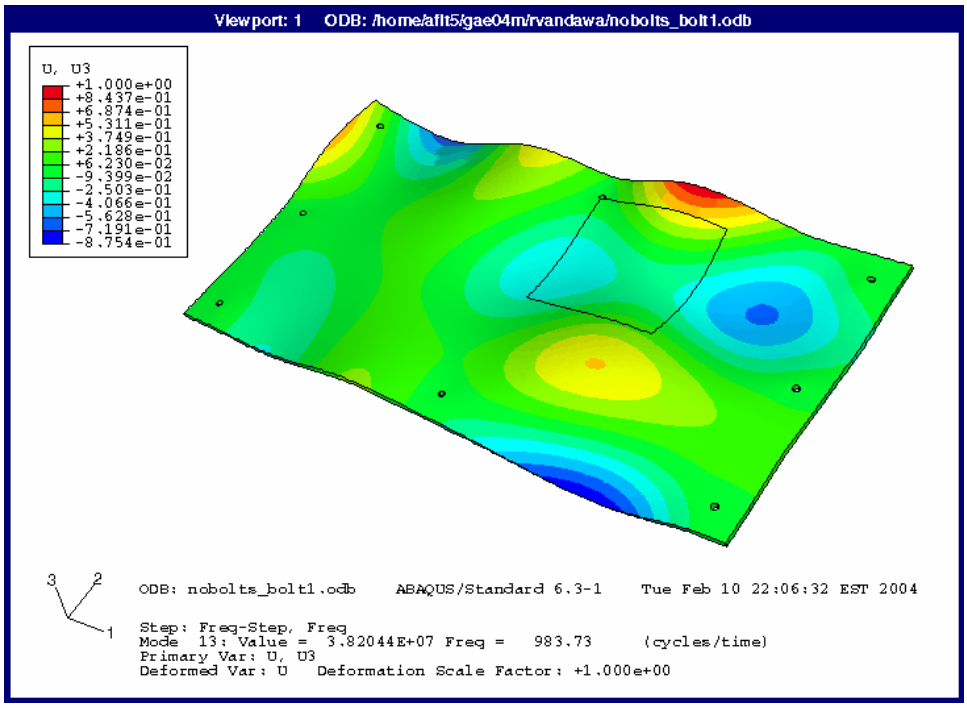

9th Correlated MAC Mode for Bolt 1 Removed. 972.66 Hz

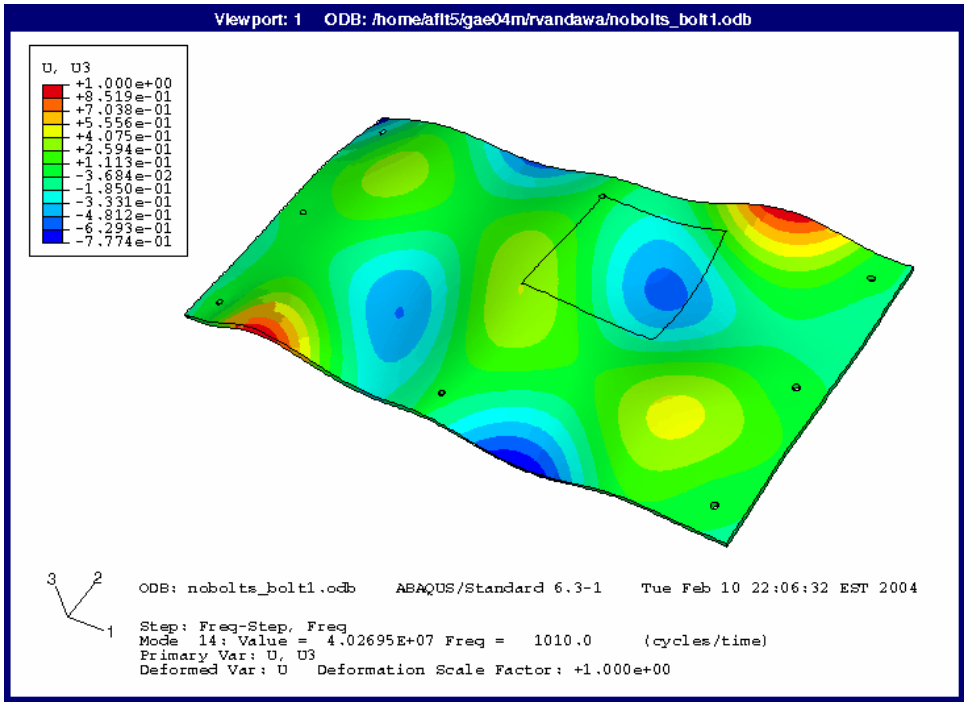

10th Correlated MAC Mode for Bolt 1 Removed. 994.53 Hz

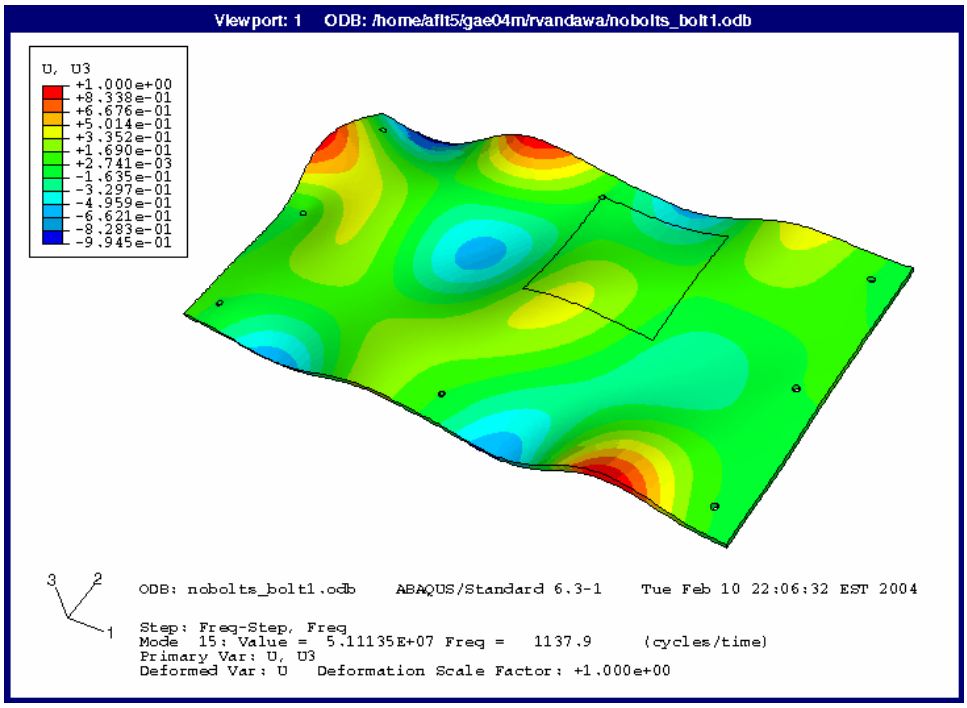

11th Correlated MAC Mode for Bolt 1 Removed. 1150 Hz

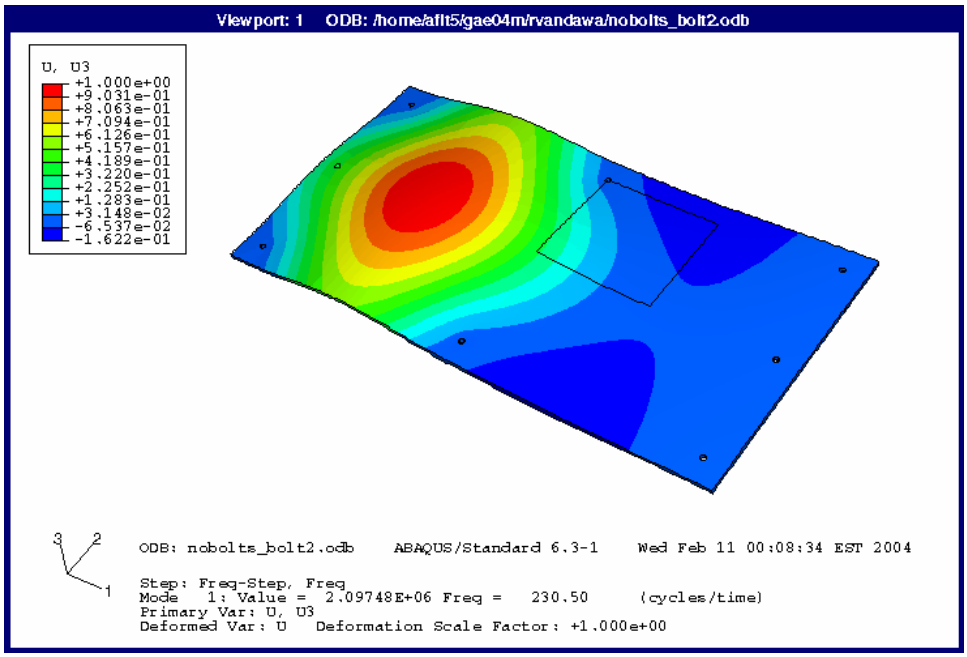

1st Correlated MAC Mode for Bolt 2 Removed. 221.09 Hz

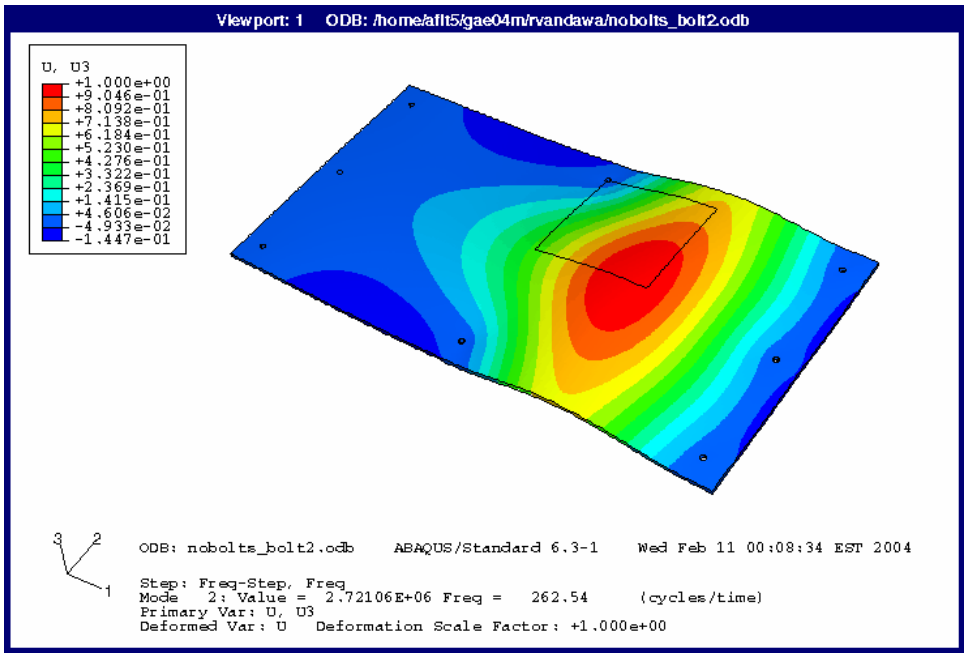

2nd Correlated MAC Mode for Bolt 2 Removed. 246.09 Hz

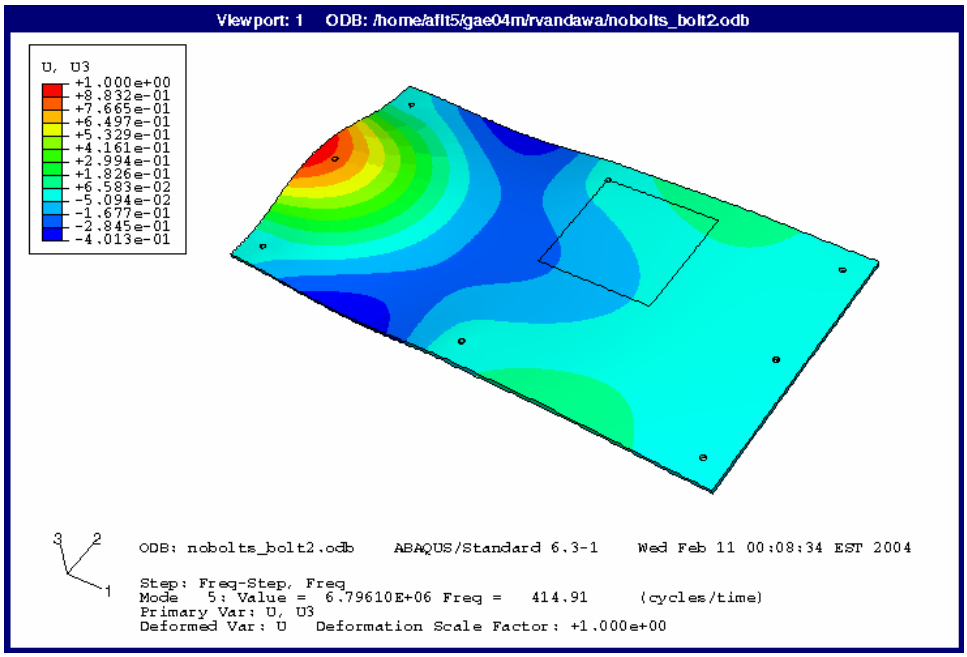

3rd Correlated MAC Mode for Bolt 2 Removed. 395.31 Hz

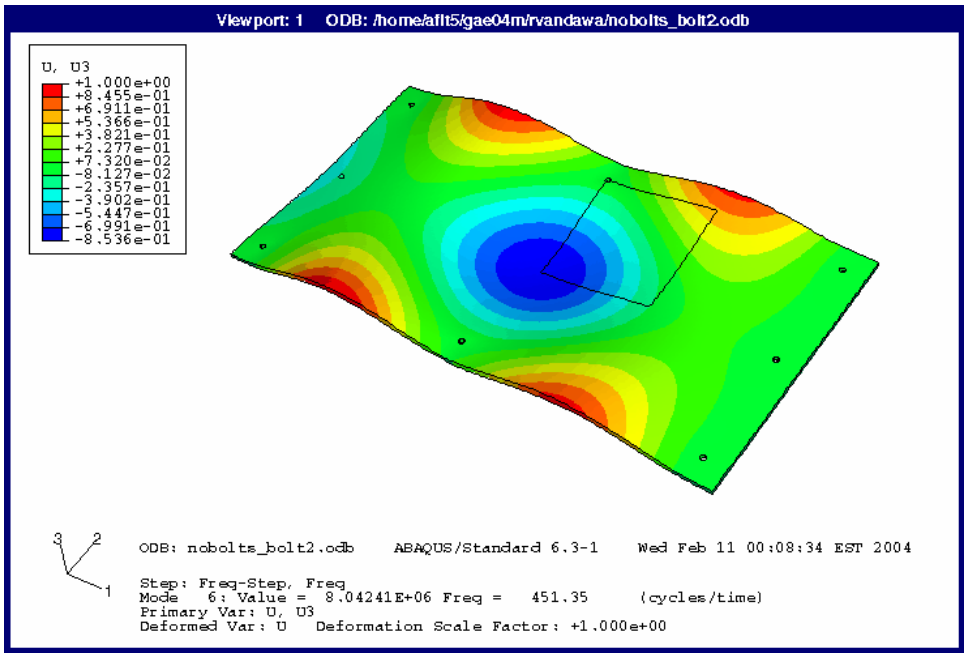

4th Correlated MAC Mode for Bolt 2 Removed. 437.50 Hz

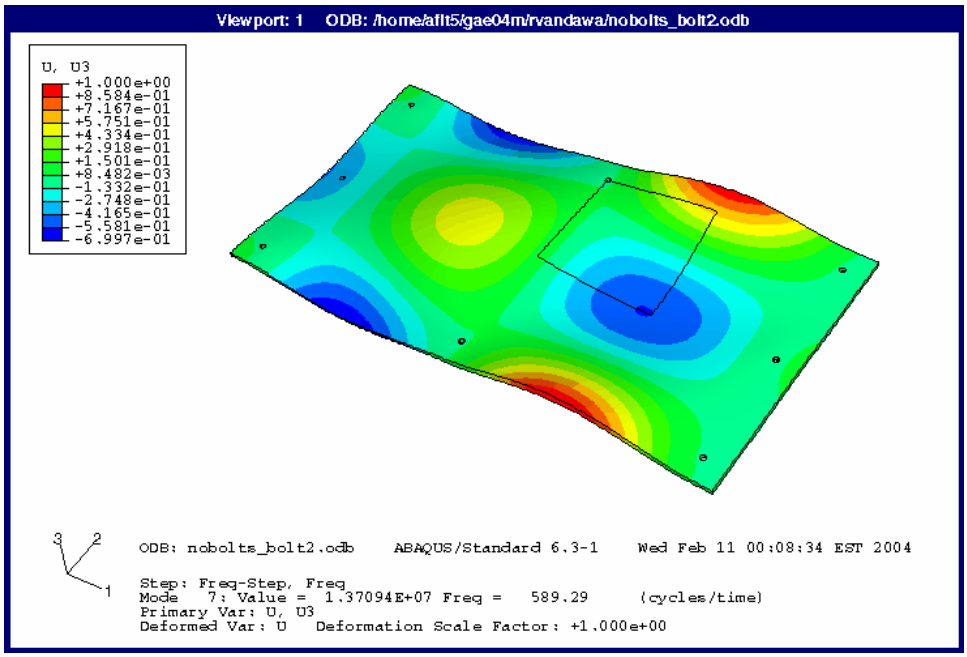

5th Correlated MAC Mode for Bolt 2 Removed. 578.91 Hz

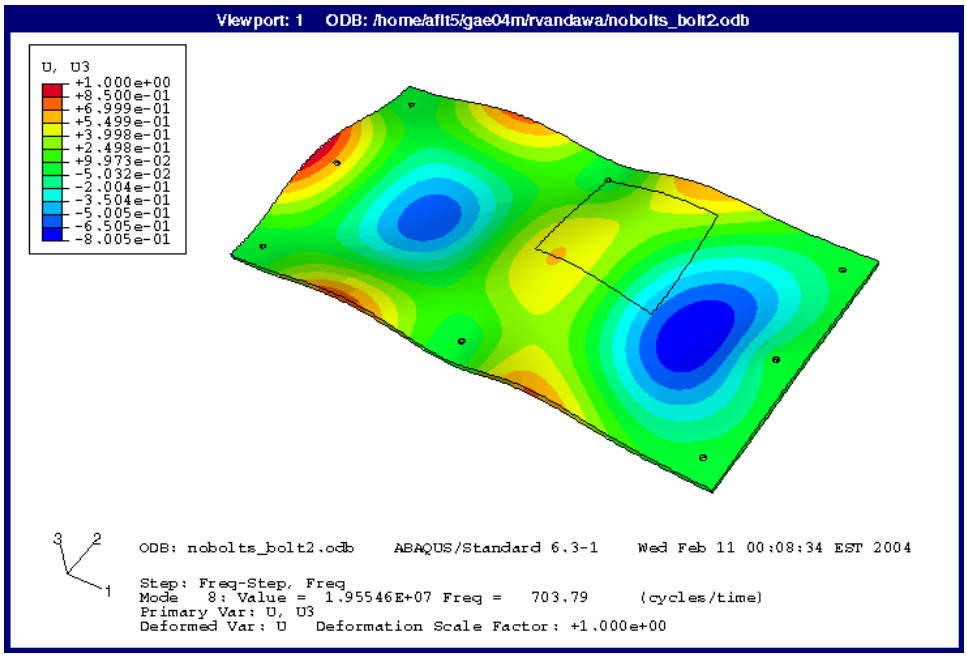

6th Correlated MAC Mode for Bolt 2 Removed. 719.53 Hz

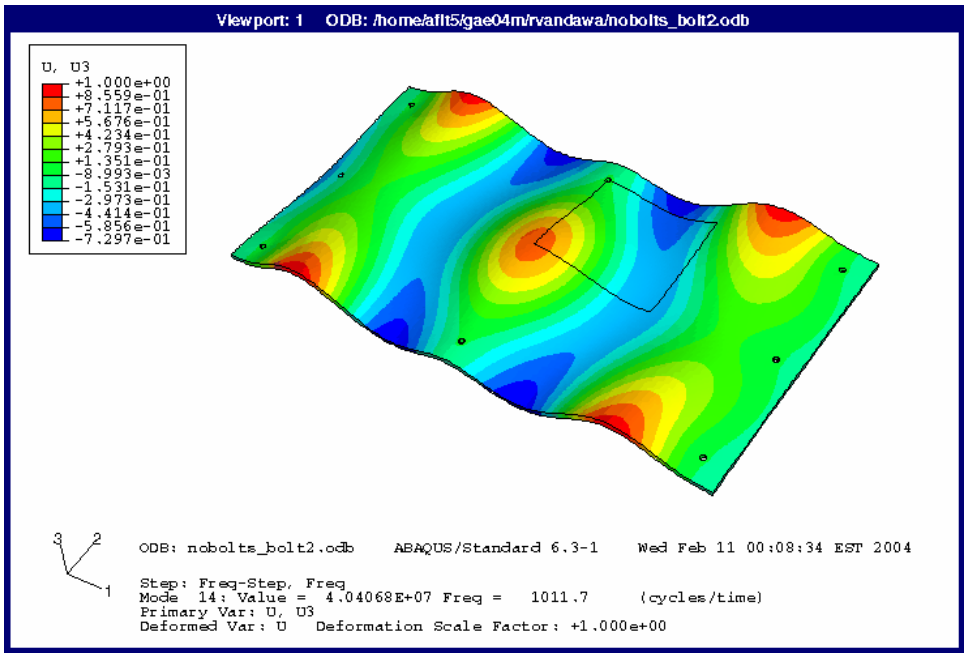

7th Correlated MAC Mode for Bolt 2 Removed. 991.41, 1028.13 Hz

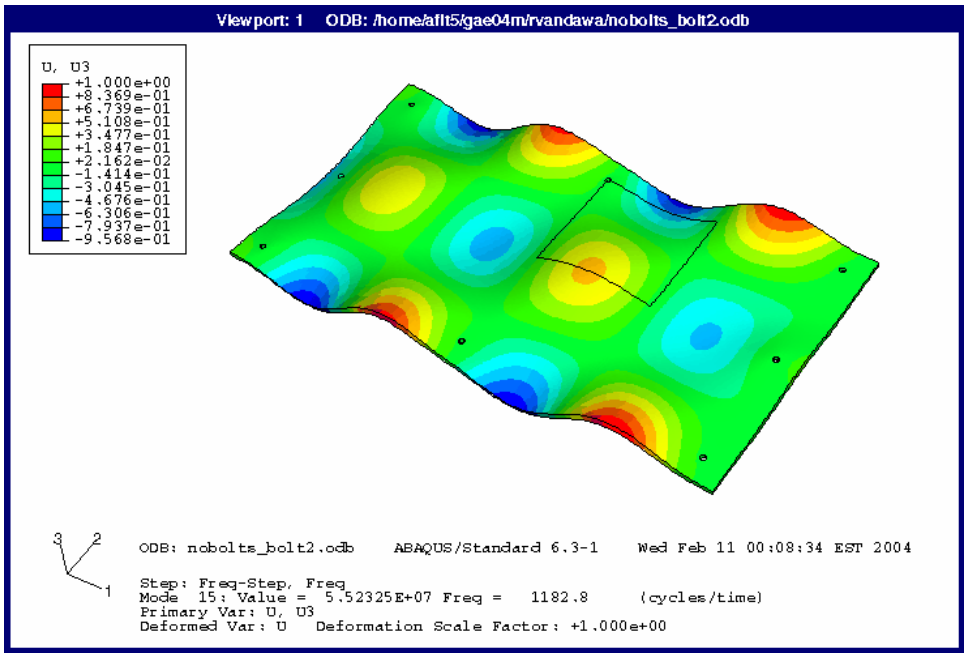

8th Correlated MAC Mode for Bolt 2 Removed. 1210.16 Hz

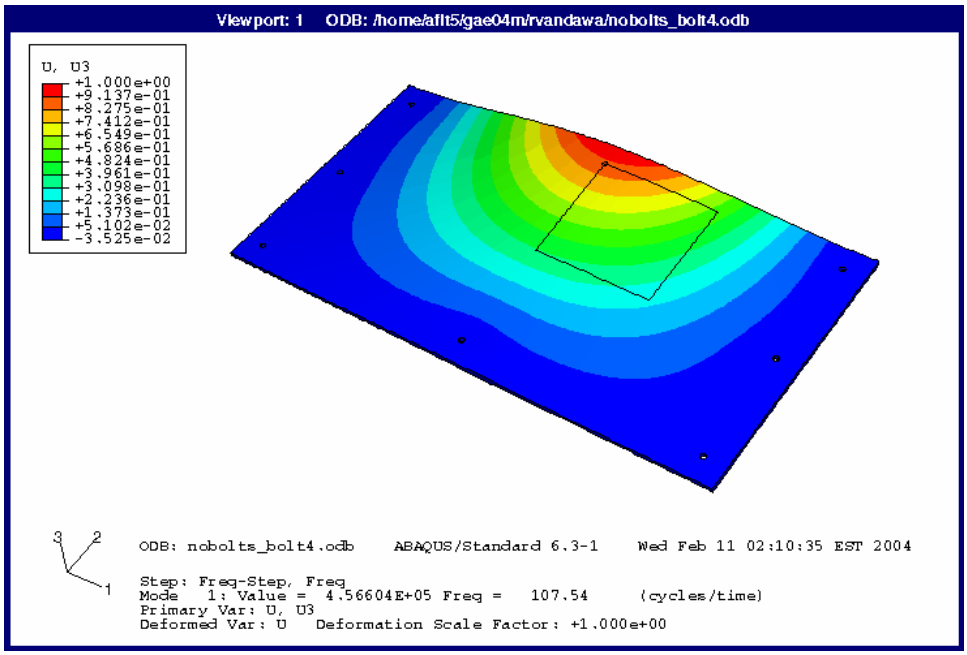

1st Correlated MAC Mode for Bolt 4 Removed. 101.56 Hz

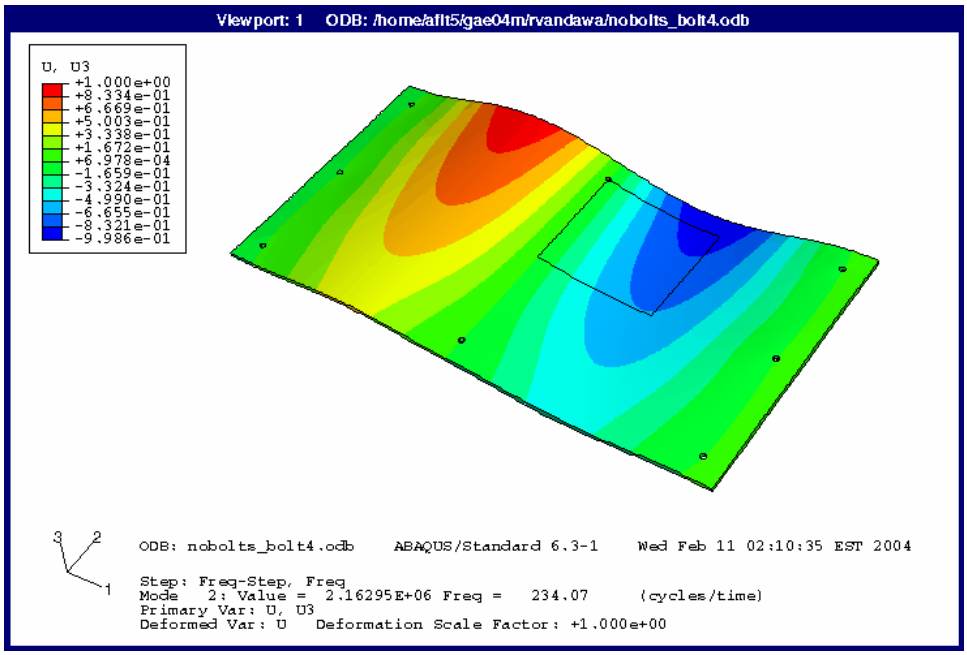

2nd Correlated MAC Mode for Bolt 4 Removed. 217.19 Hz

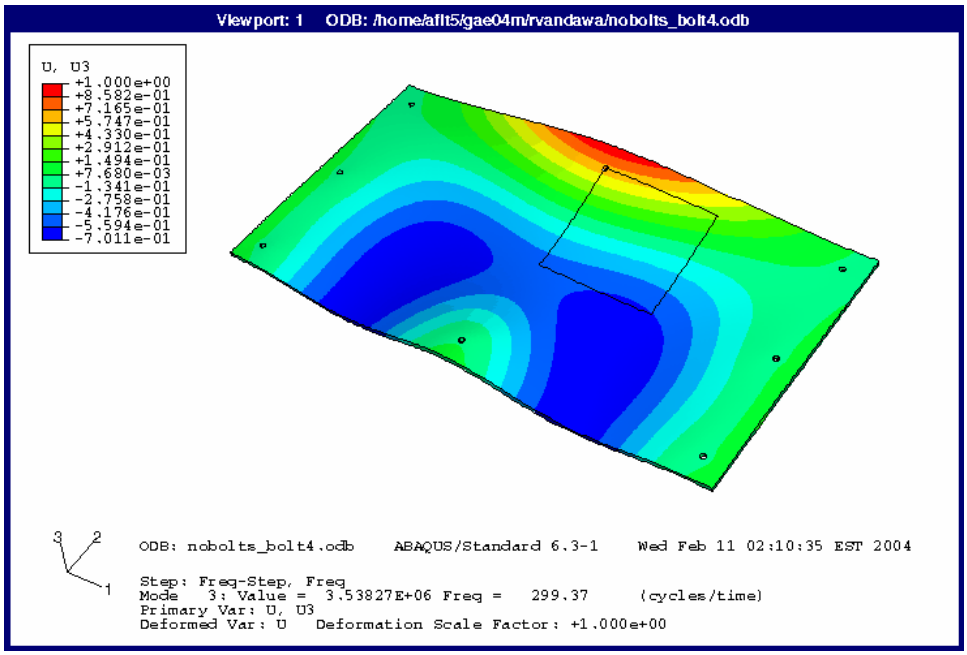

3rd Correlated MAC Mode for Bolt 4 Removed. 289.06 Hz

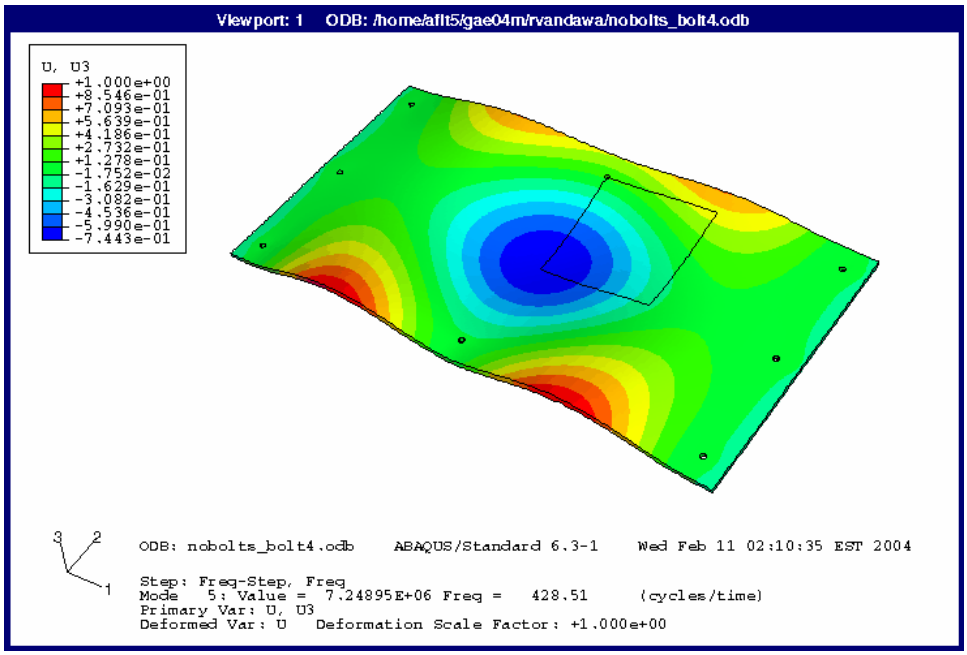

4th Correlated MAC Mode for Bolt 4 Removed. 418.75 Hz

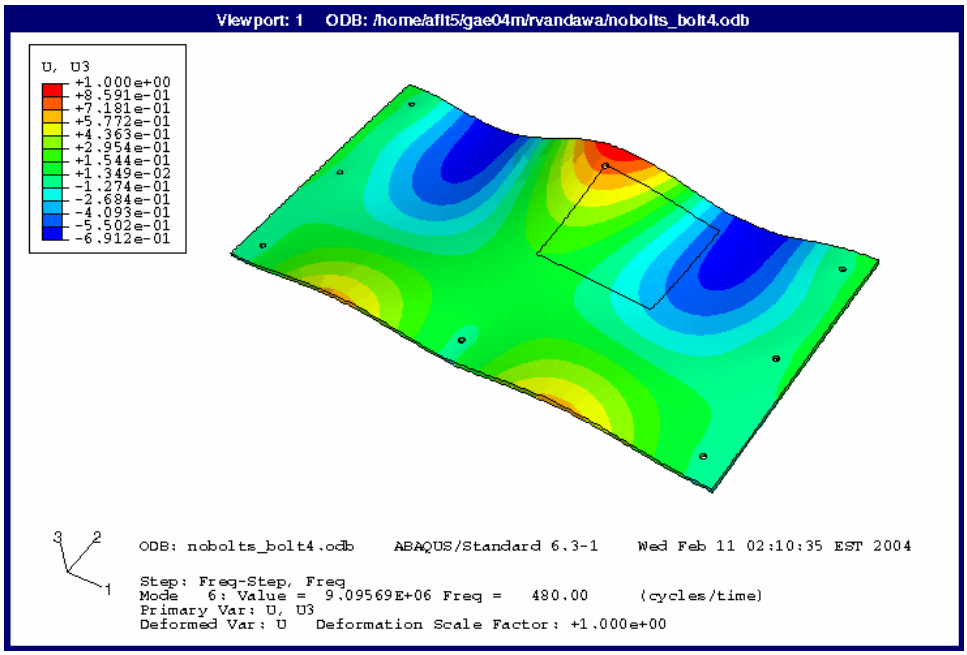

5th Correlated MAC Mode for Bolt 4 Removed. 464.06 Hz

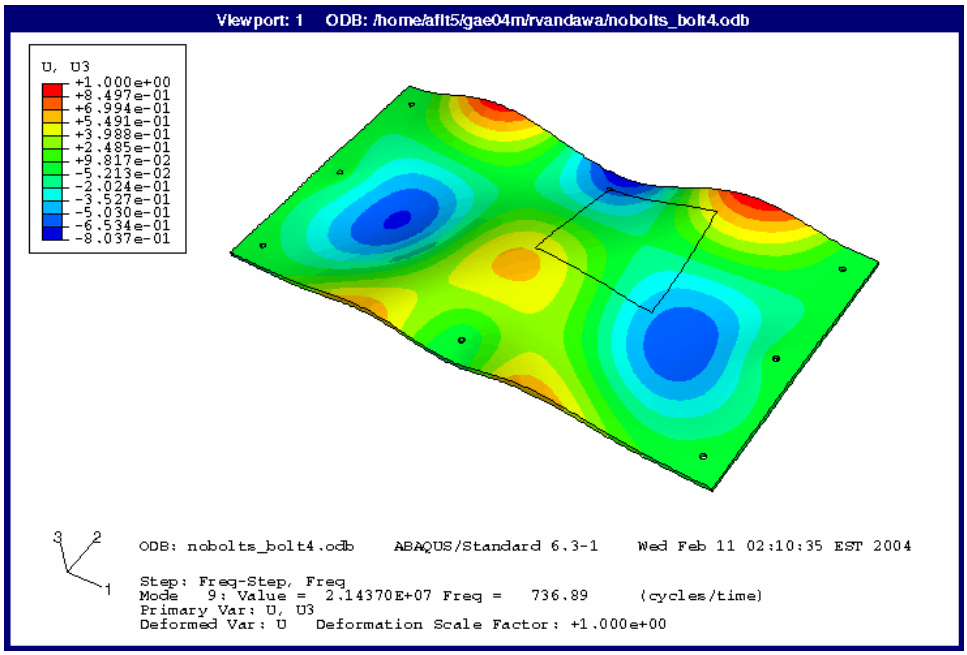

6th Correlated MAC Mode for Bolt 4 Removed. 657.03, 716.41 Hz

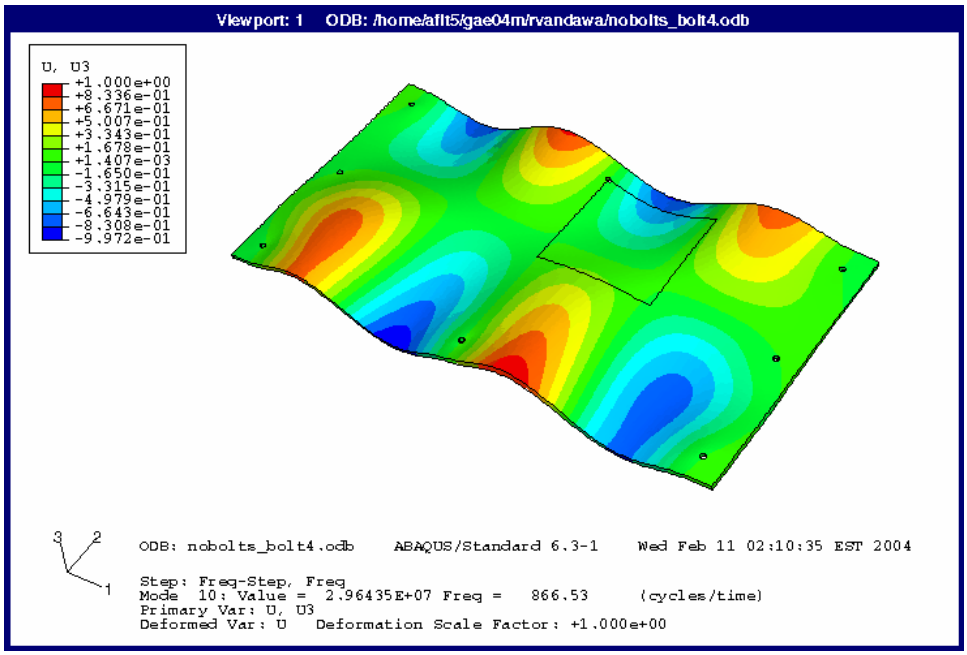

7th Correlated MAC Mode for Bolt 4 Removed. 828.91 Hz

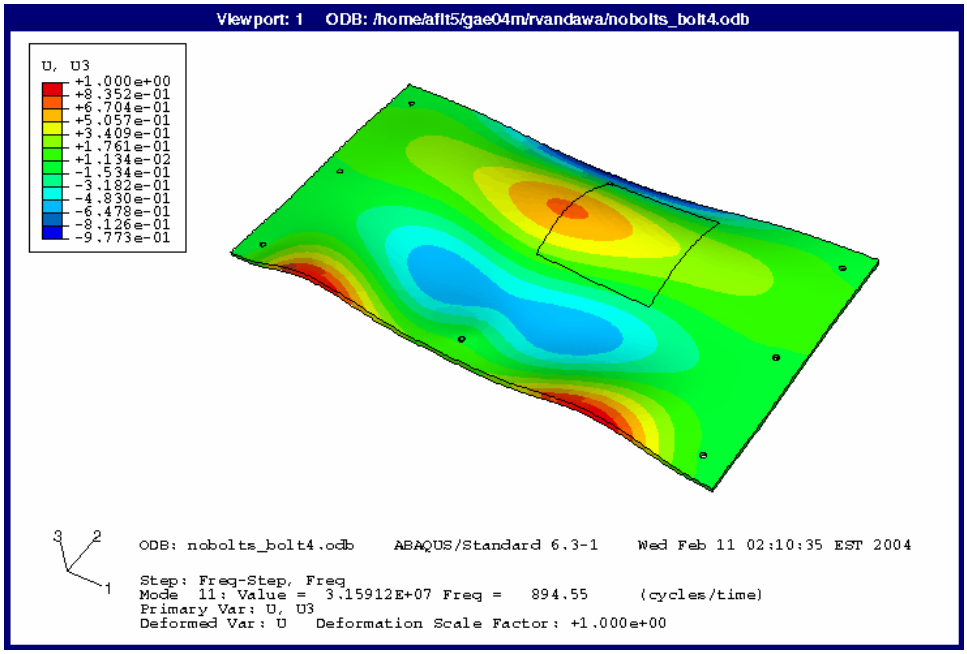

8th Correlated MAC Mode for Bolt 4 Removed. 864.06, 873.44 Hz

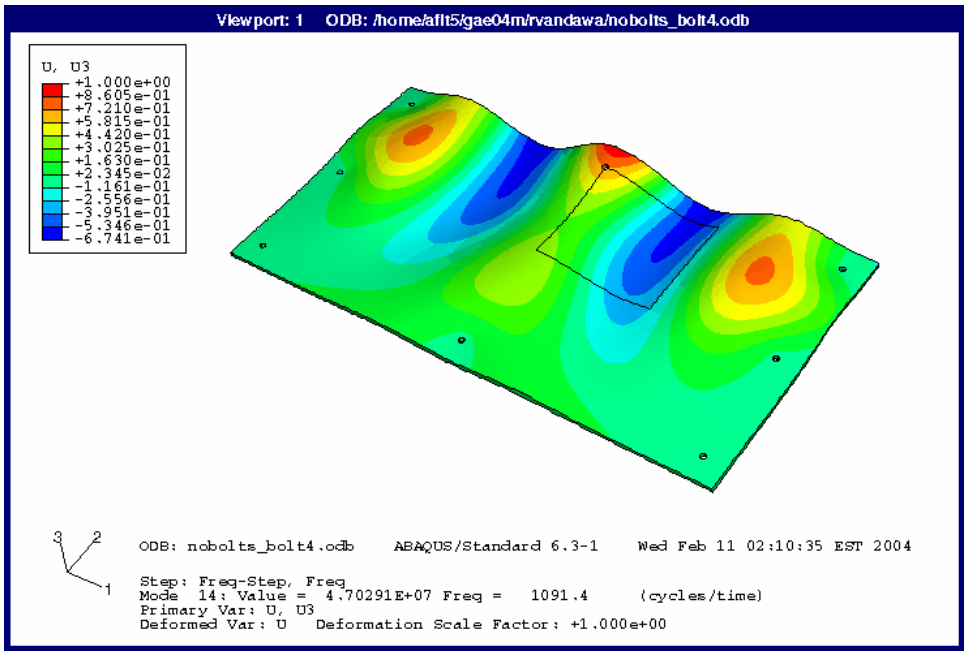

9th Correlated MAC Mode for Bolt 4 Removed. 1065.63 Hz

Appendix B

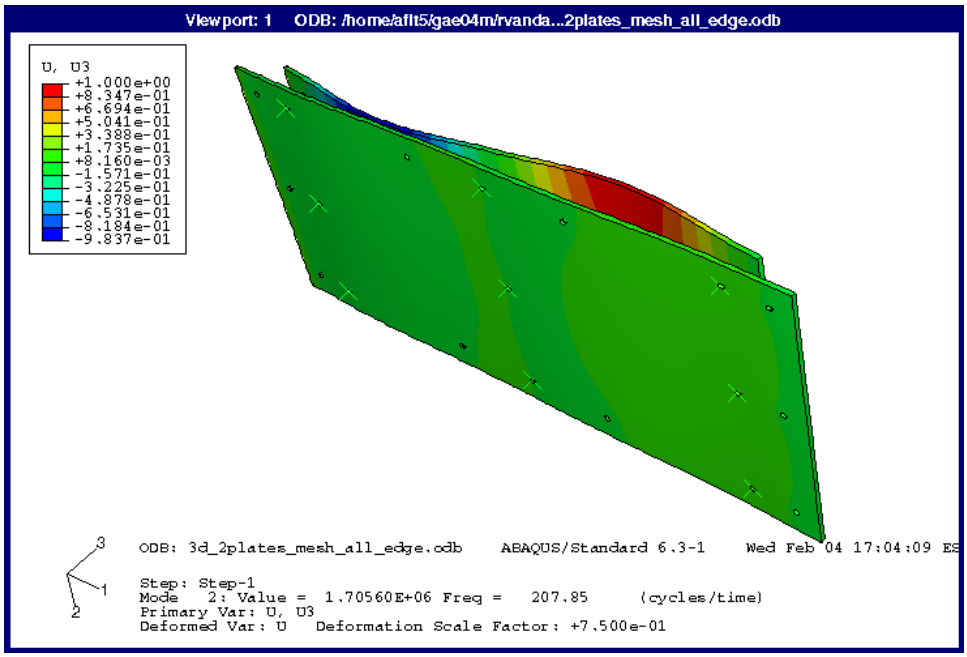

1st Correlated MAC Mode for All Bolts. 239.06 Hz

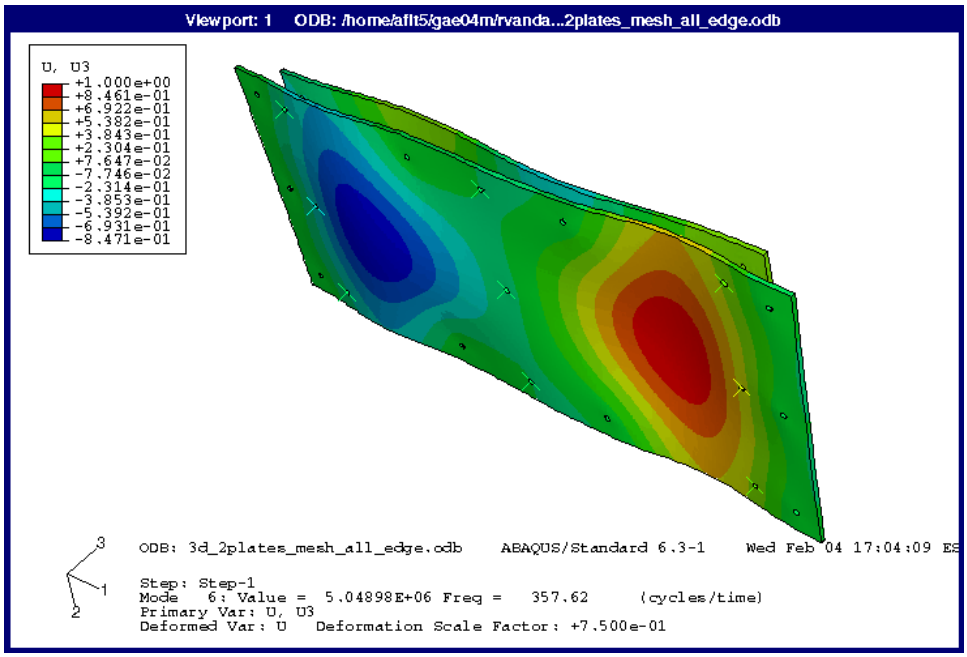

2nd Correlated MAC Mode for All Bolts. 341.41 Hz

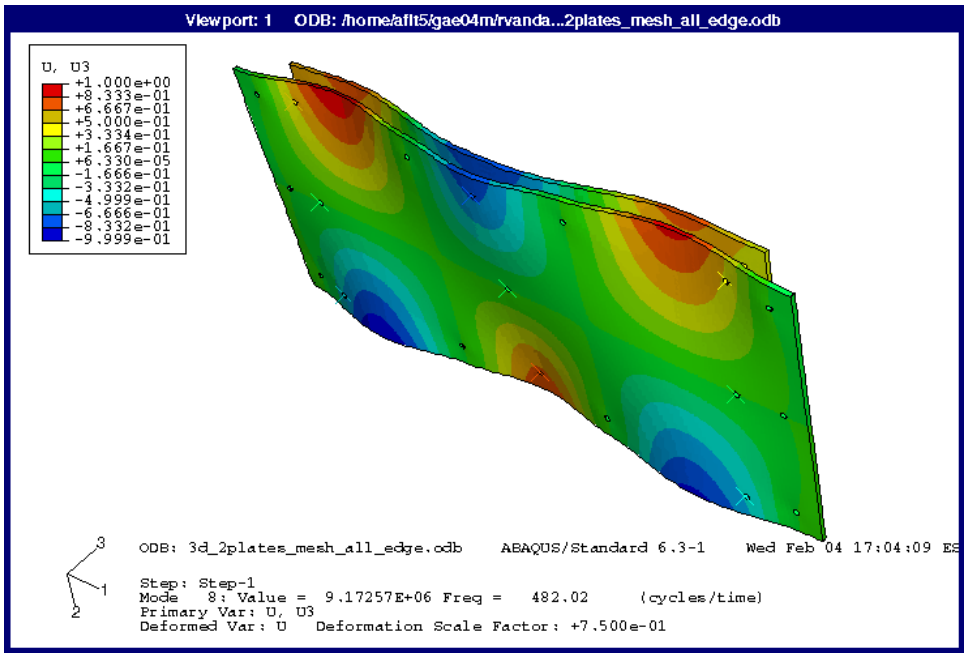

3rd Correlated MAC Mode for All Bolts. 469.53 Hz

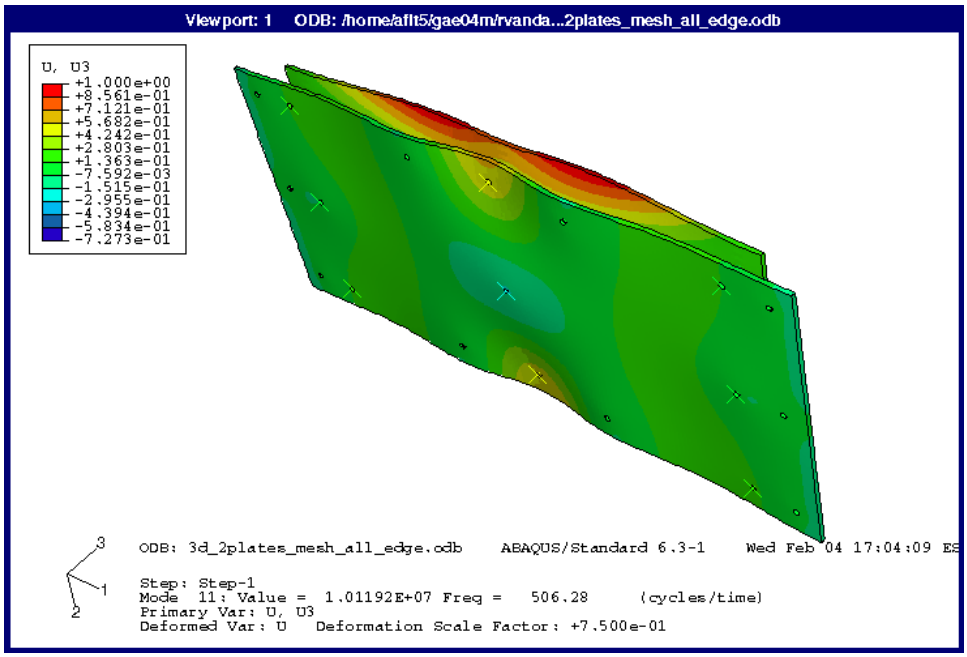

4th Correlated MAC Mode for All Bolts. 503.91 Hz

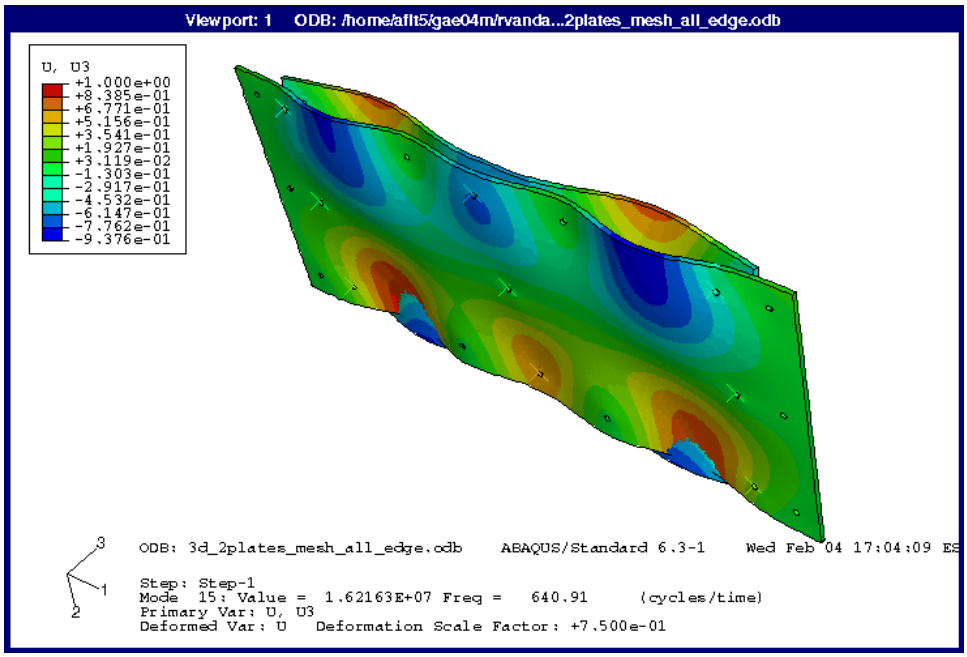

5th Correlated MAC Mode for All Bolts. 633.59 Hz

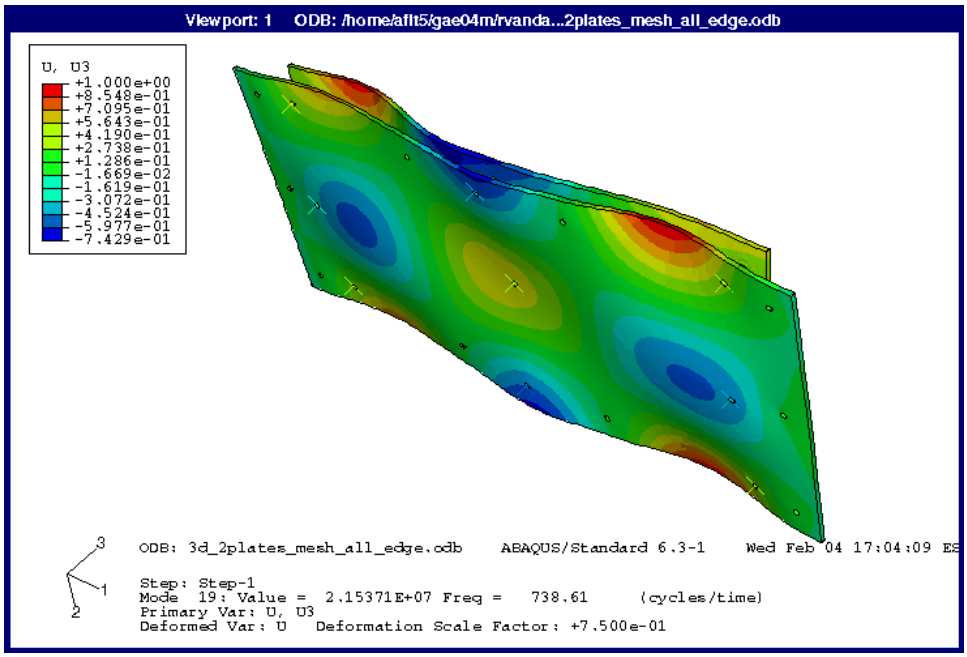

6th Correlated MAC Mode for All Bolts. 735.16 Hz

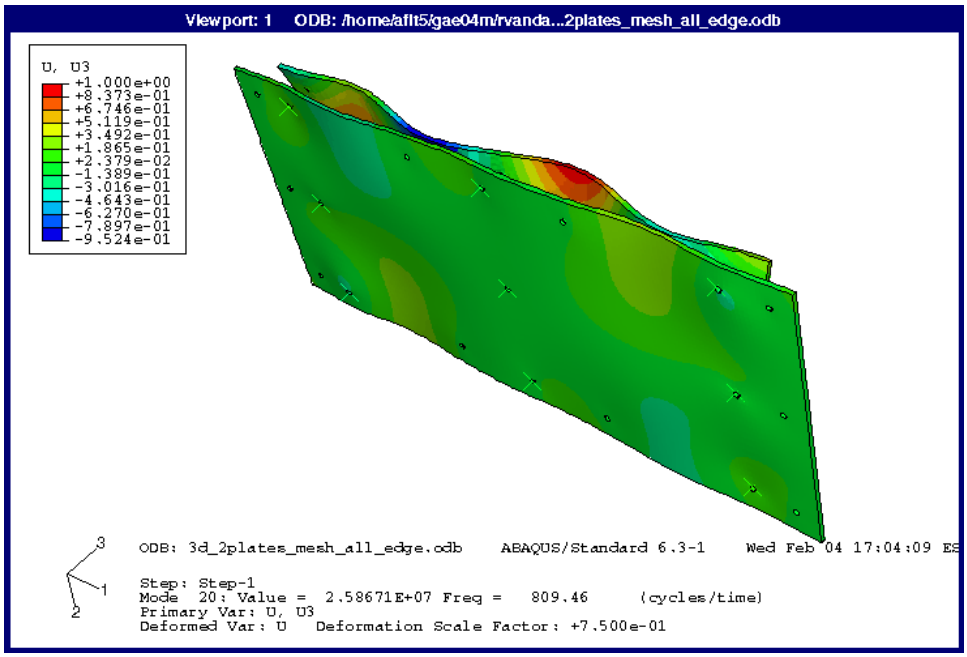

7th Correlated MAC Mode for All Bolts. 1120.31 Hz

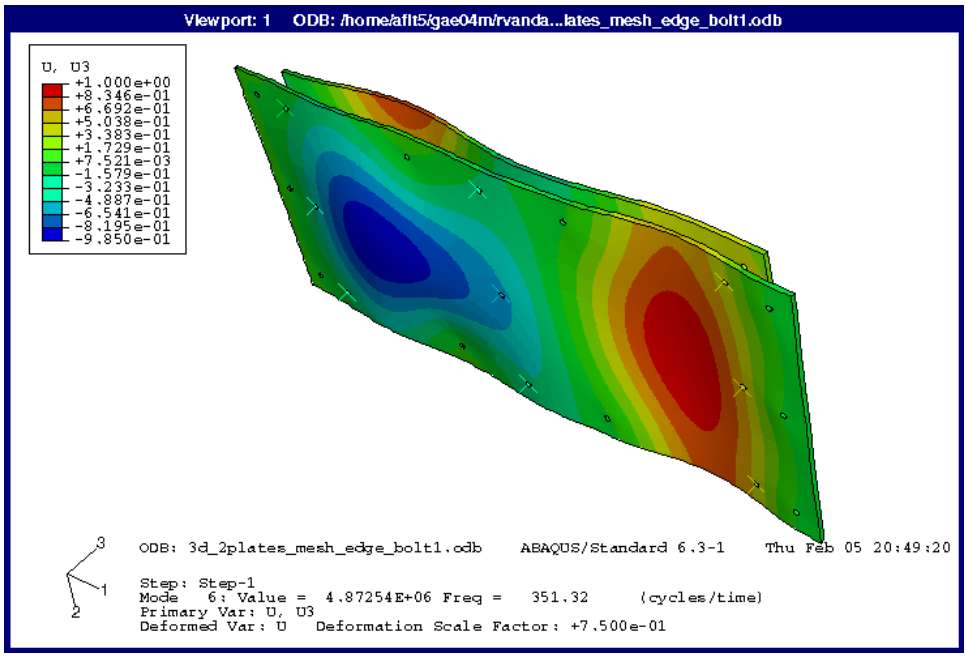

1st Correlated MAC Mode for Bolt 1 Removed. 328.13, 338.28 Hz

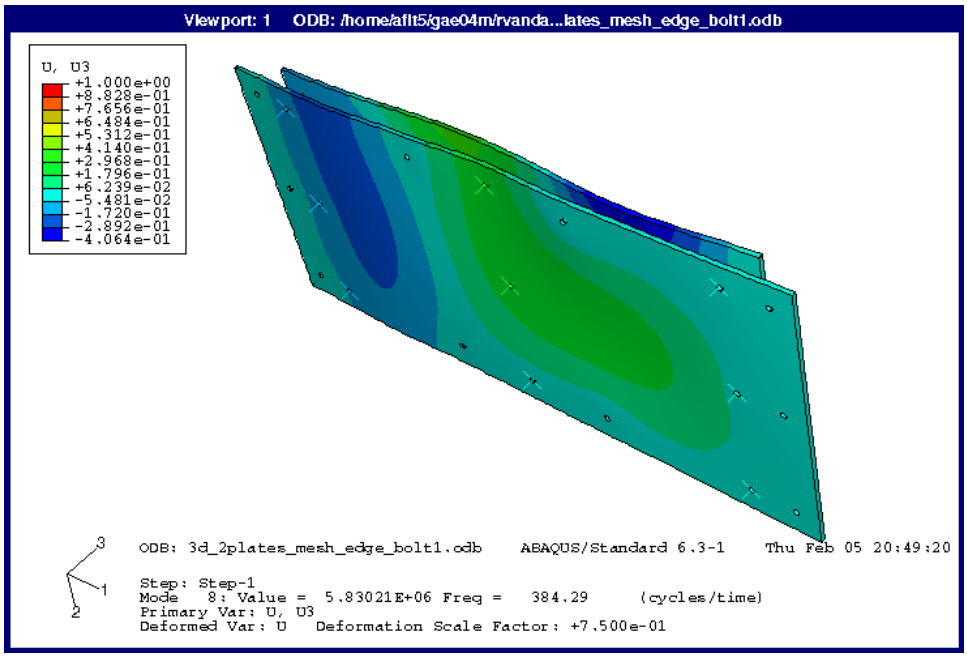

2nd Correlated MAC Mode for Bolt 1 Removed. 378.13 Hz

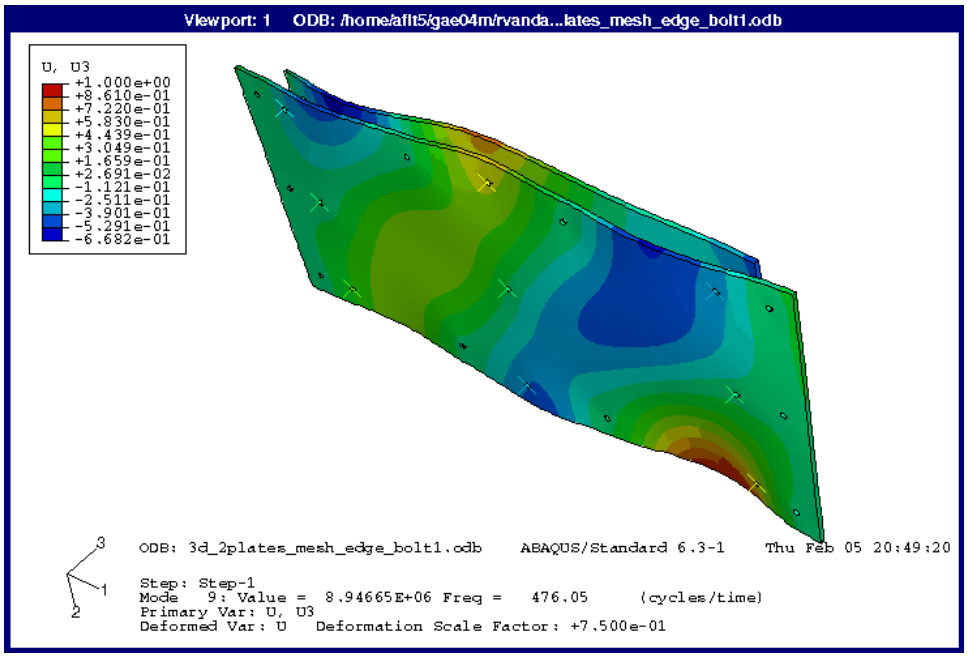

3rd Correlated MAC Mode for Bolt 1 Removed. 462.50 Hz

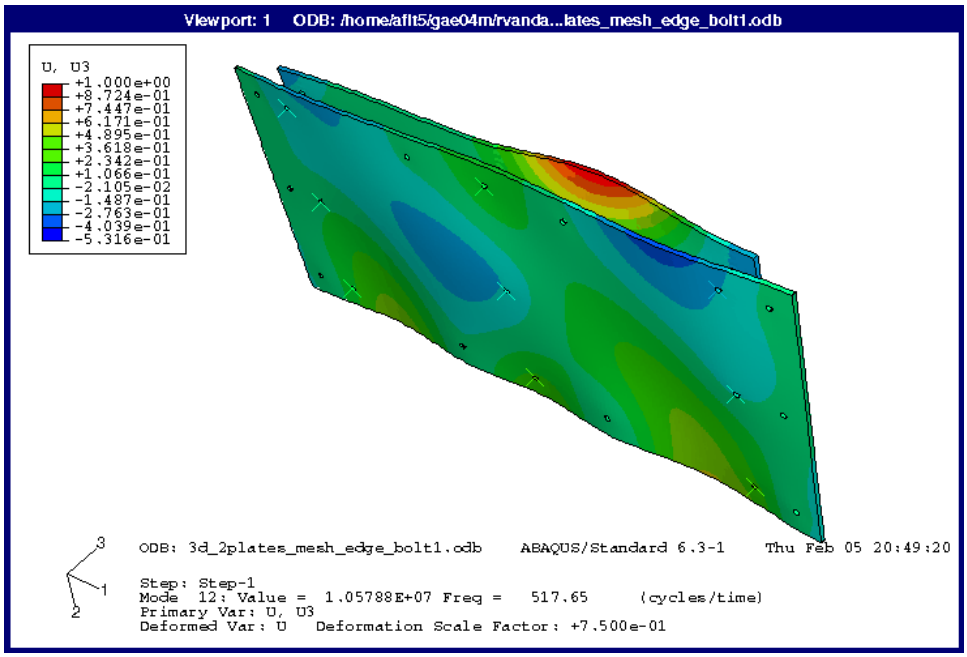

4th Correlated MAC Mode for Bolt 1 Removed. 512.50 Hz

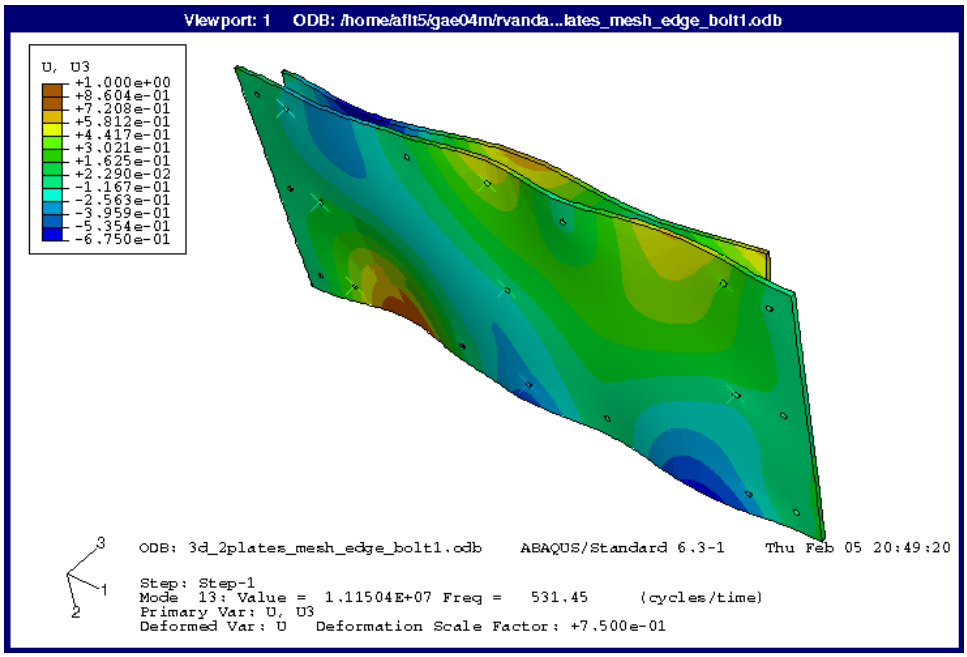

5th Correlated MAC Mode for Bolt 1 Removed. 536.72 Hz

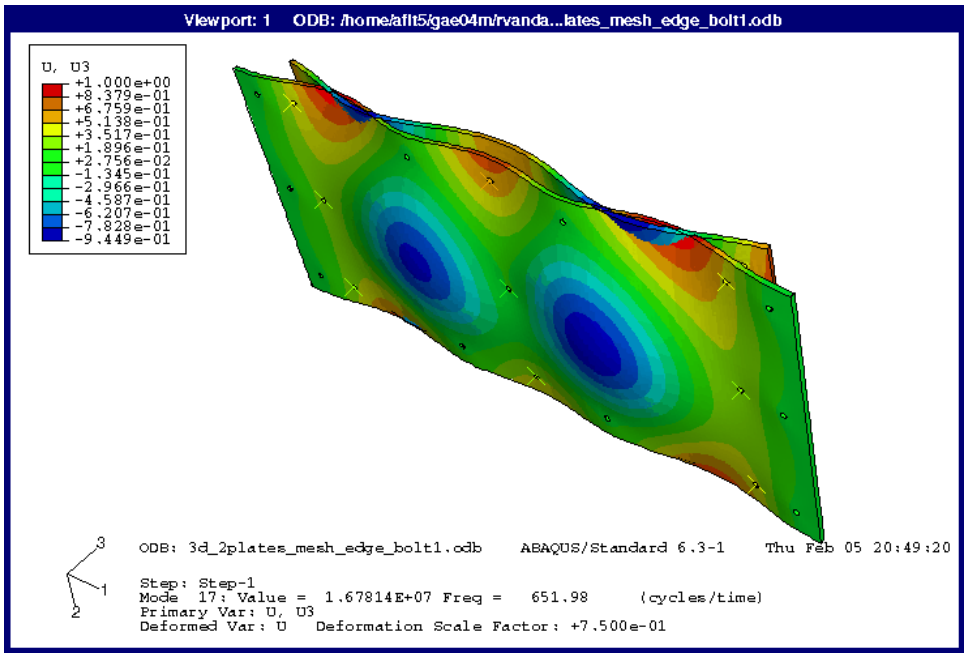

6th Correlated MAC Mode for Bolt 1 Removed. 646.88 Hz

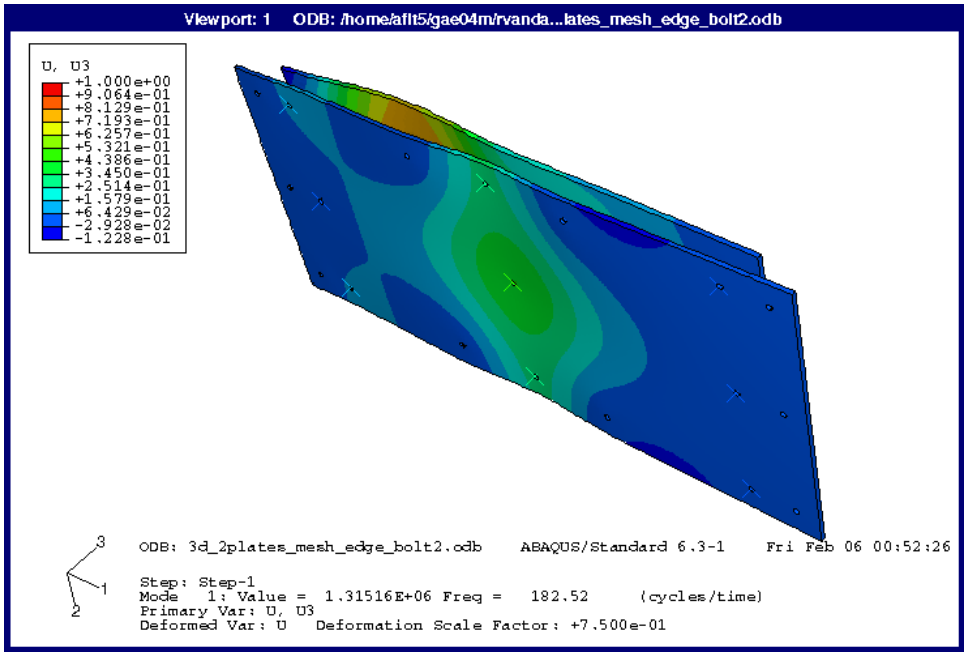

1st Correlated MAC Mode for Bolt 2 Removed. 185.16 Hz

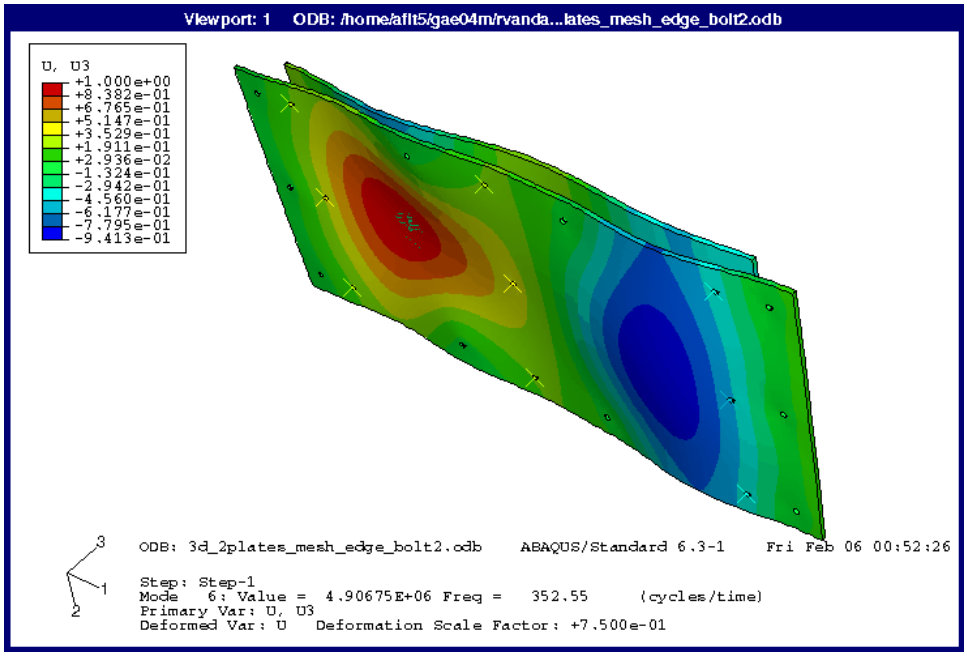

2nd Correlated MAC Mode for Bolt 2 Removed. 332.03 Hz

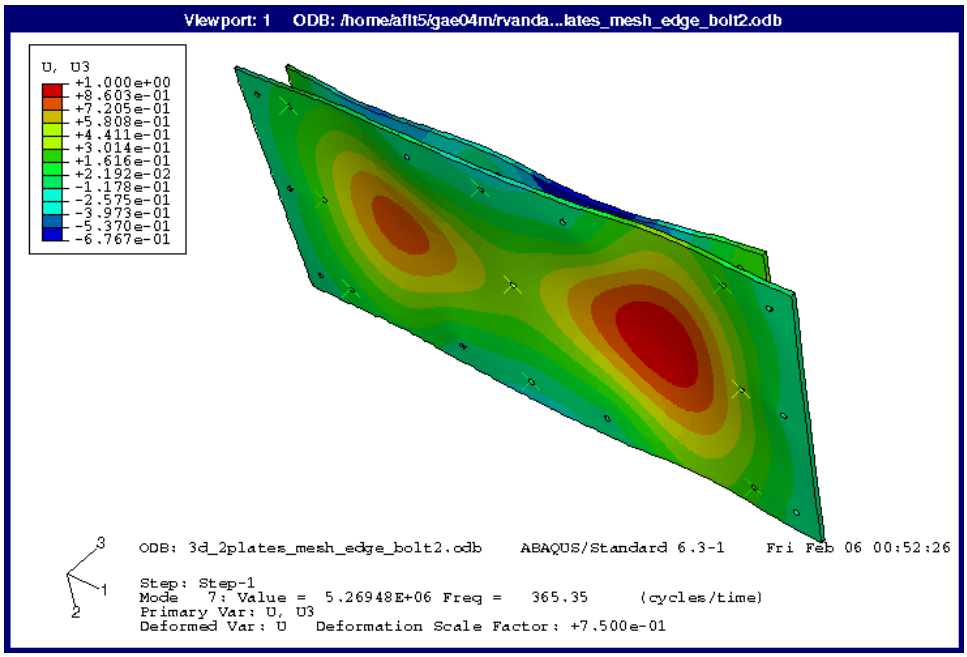

3rd Correlated MAC Mode for Bolt 2 Removed. 347.66 Hz

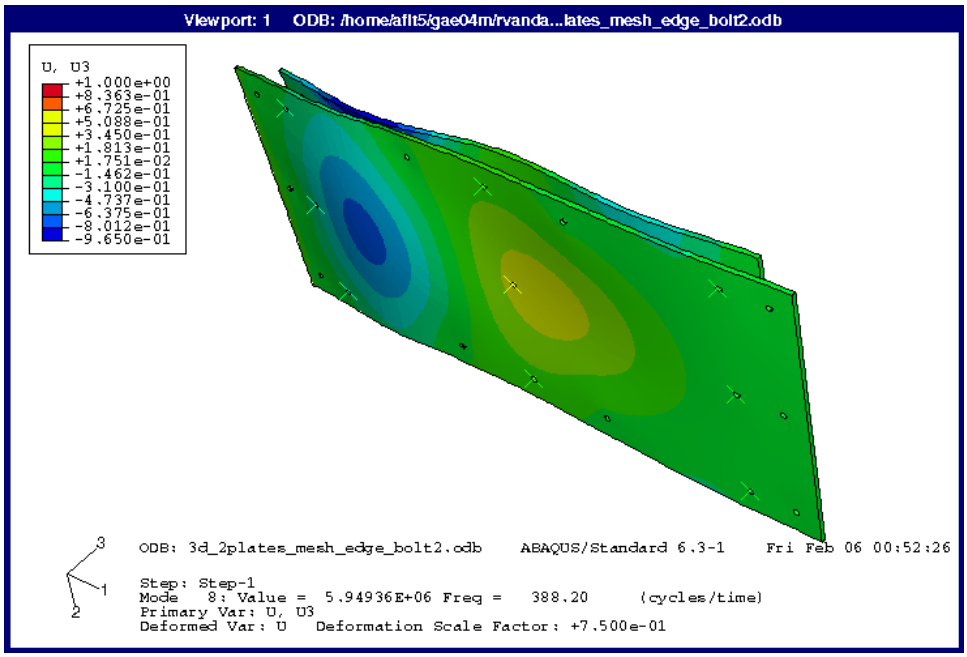

4th Correlated MAC Mode for Bolt 2 Removed. 402.34 Hz

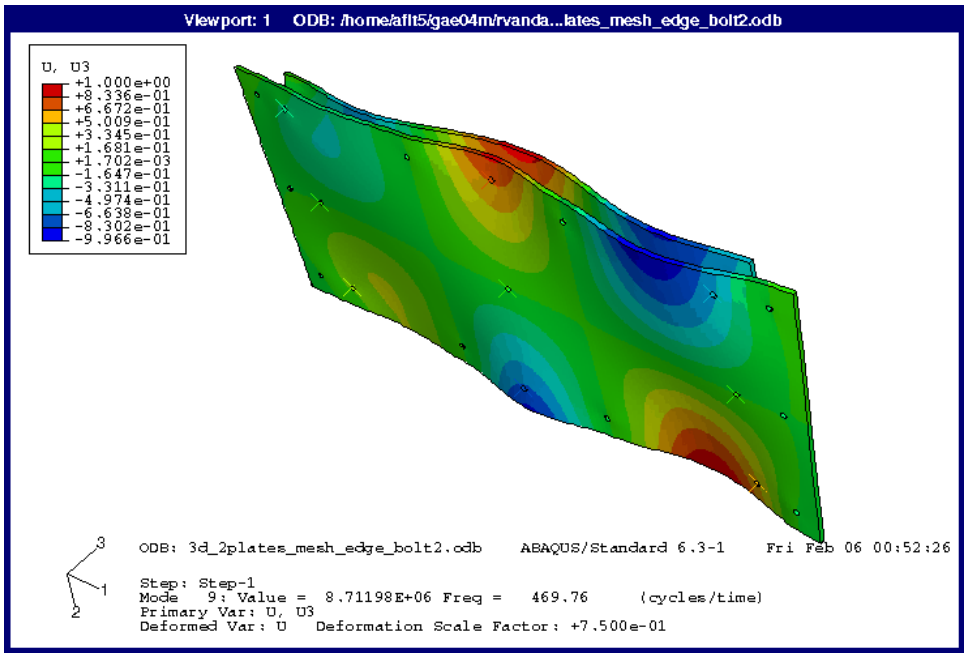

5th Correlated MAC Mode for Bolt 2 Removed. 457.03 Hz

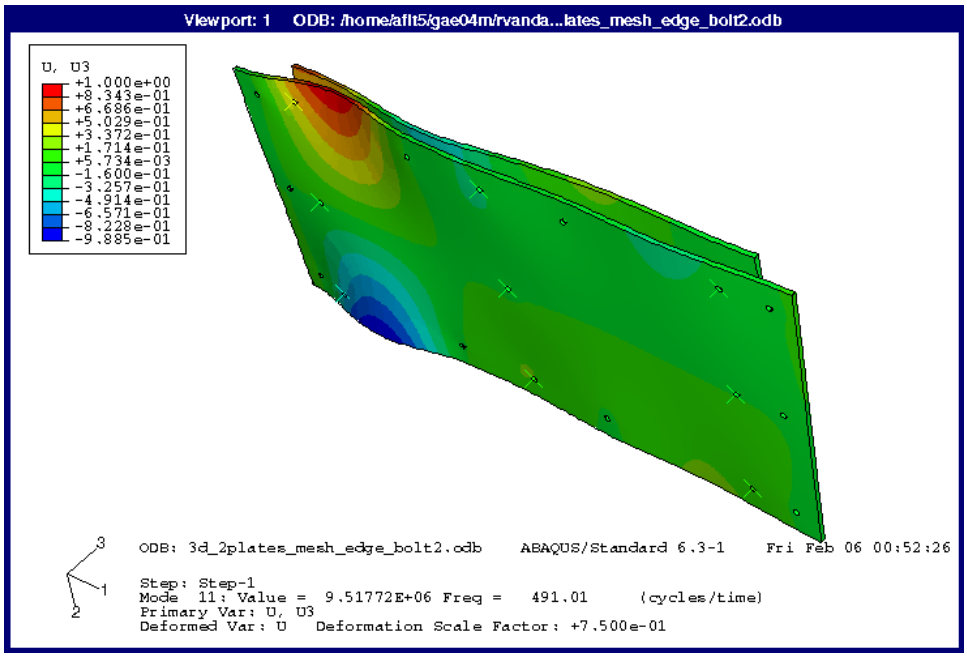

6th Correlated MAC Mode for Bolt 2 Removed. 483.59 Hz

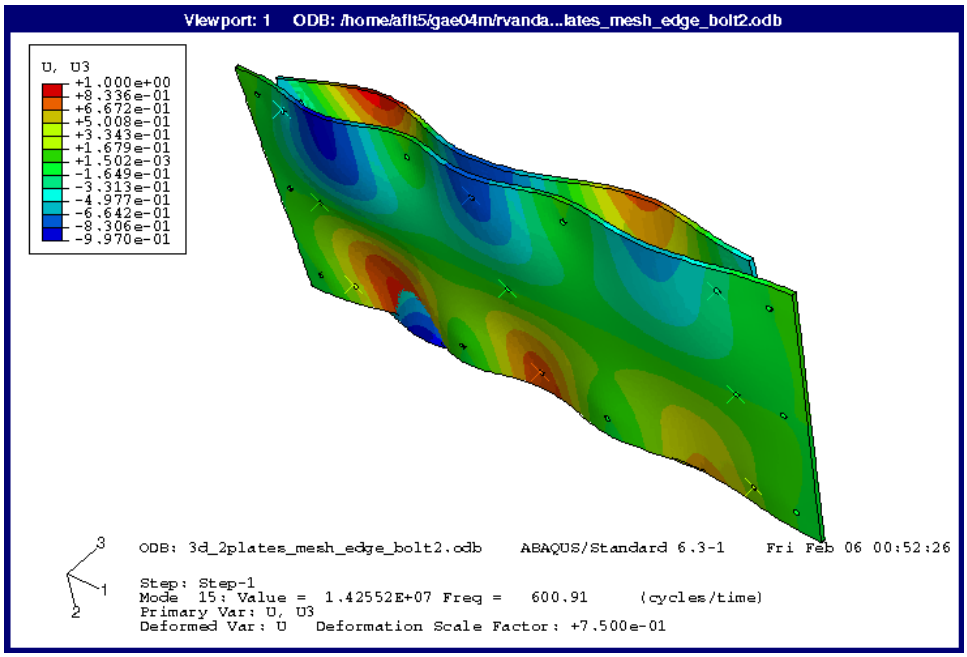

7th Correlated MAC Mode for Bolt 2 Removed. 596.88 Hz

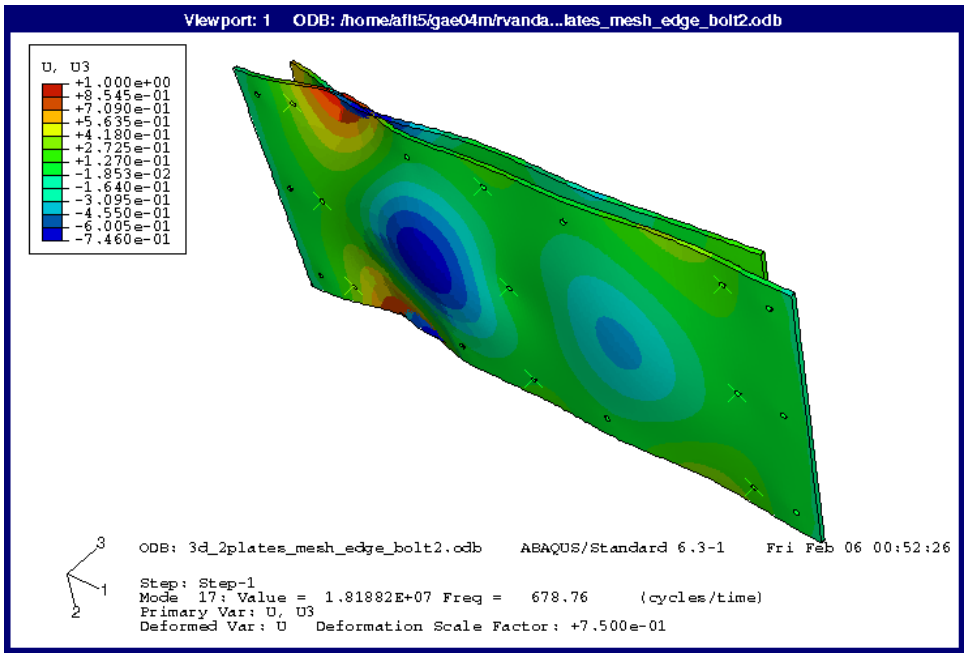

8th Correlated MAC Mode for Bolt 2 Removed. 686.72 Hz

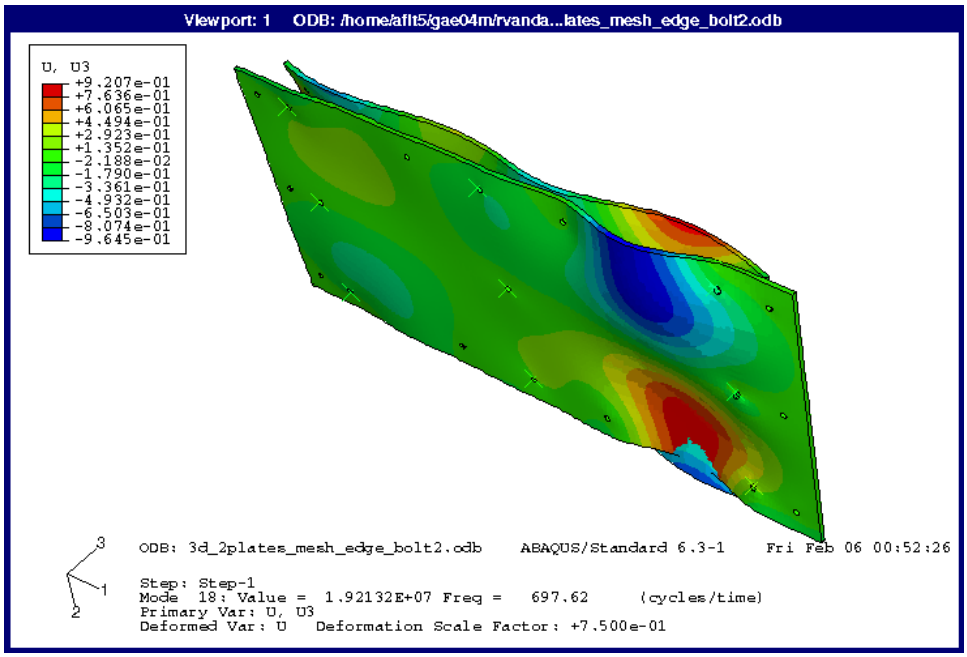

9th Correlated MAC Mode for Bolt 2 Removed. 709.38 Hz

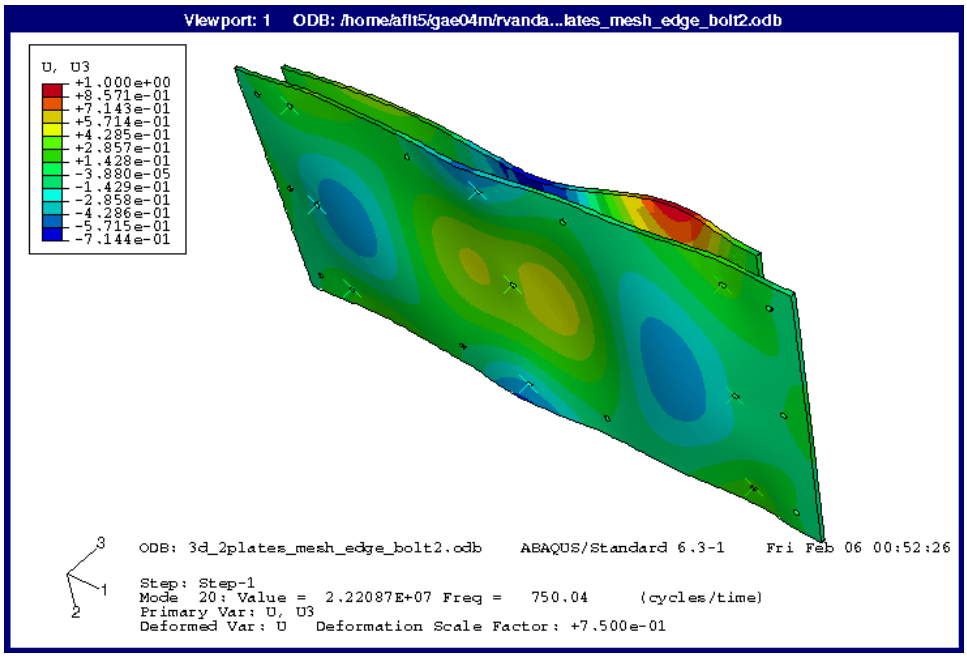

10th Correlated MAC Mode for Bolt 2 Removed. 735.16 Hz

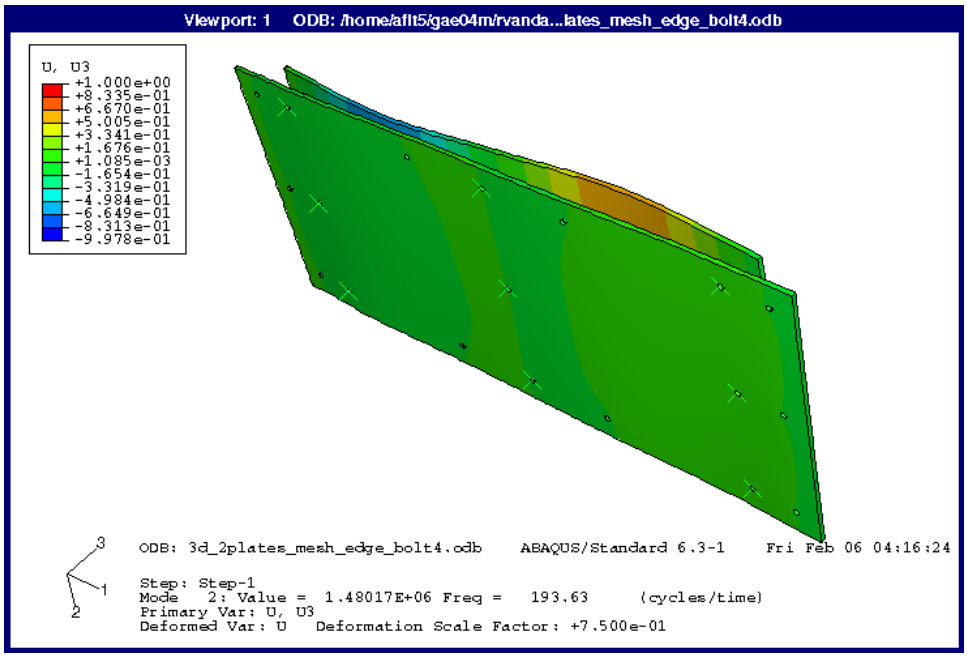

1st Correlated MAC Mode for Bolt 4 Removed. 214.06 Hz

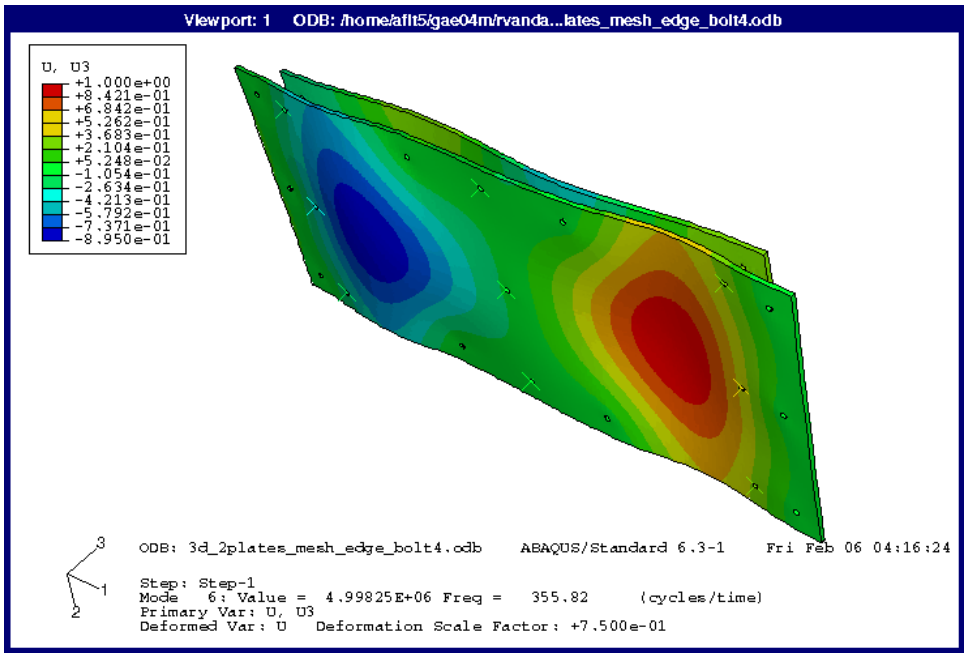

2nd Correlated MAC Mode for Bolt 4 Removed. 339.84 Hz

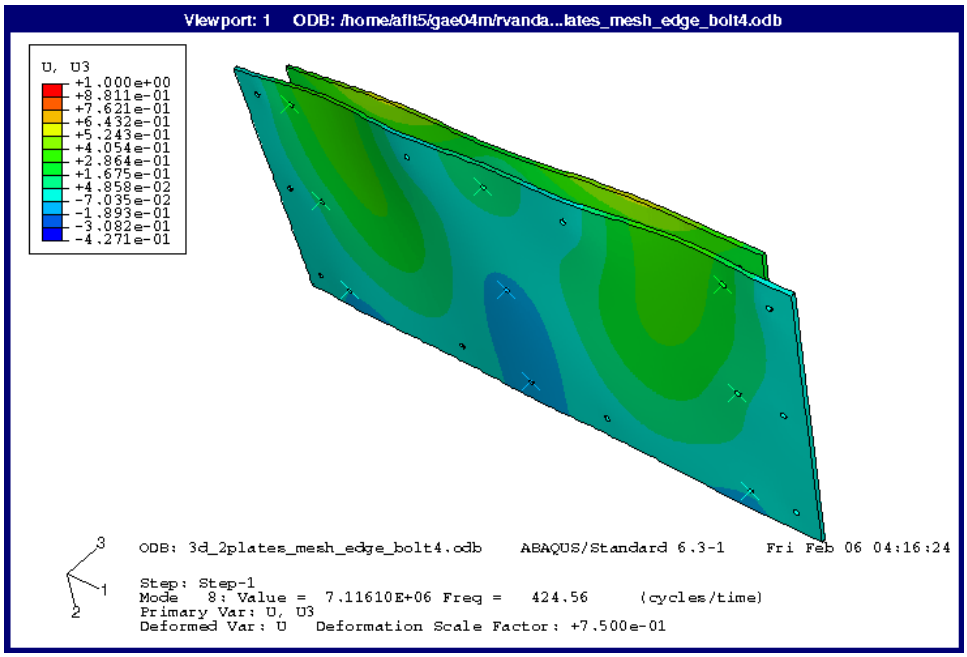

3rd Correlated MAC Mode for Bolt 4 Removed. 424.22 Hz

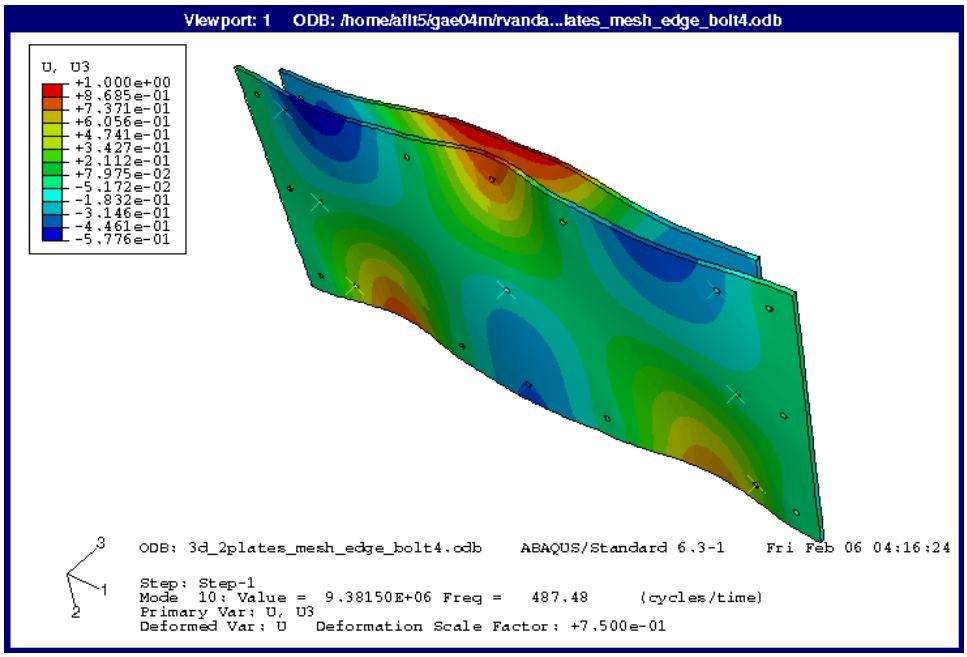

4th Correlated MAC Mode for Bolt 4 Removed. 476.56 Hz

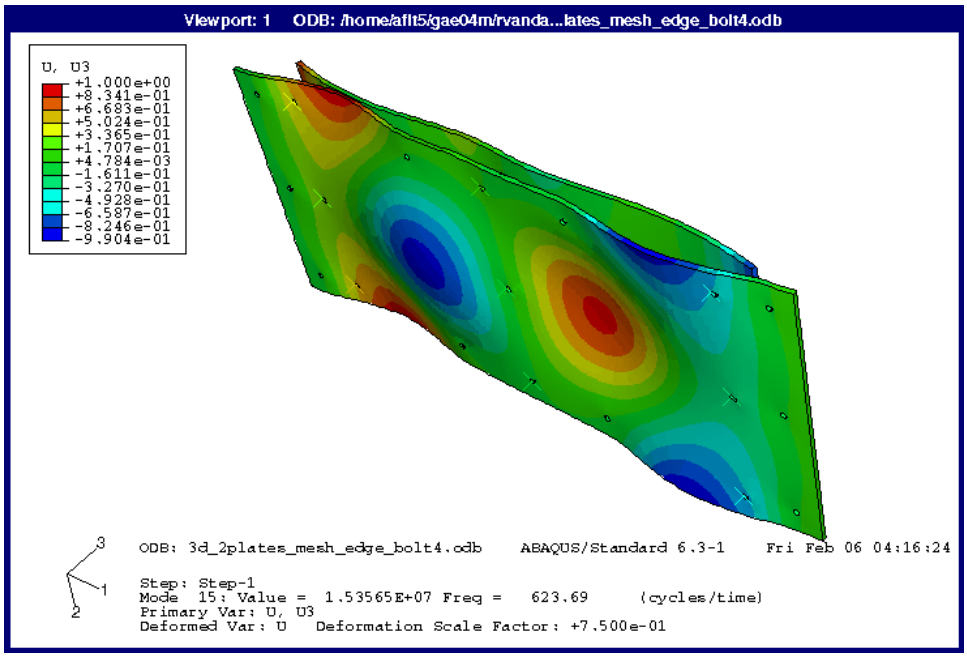

5th Correlated MAC Mode for Bolt 4 Removed. 685.16 Hz

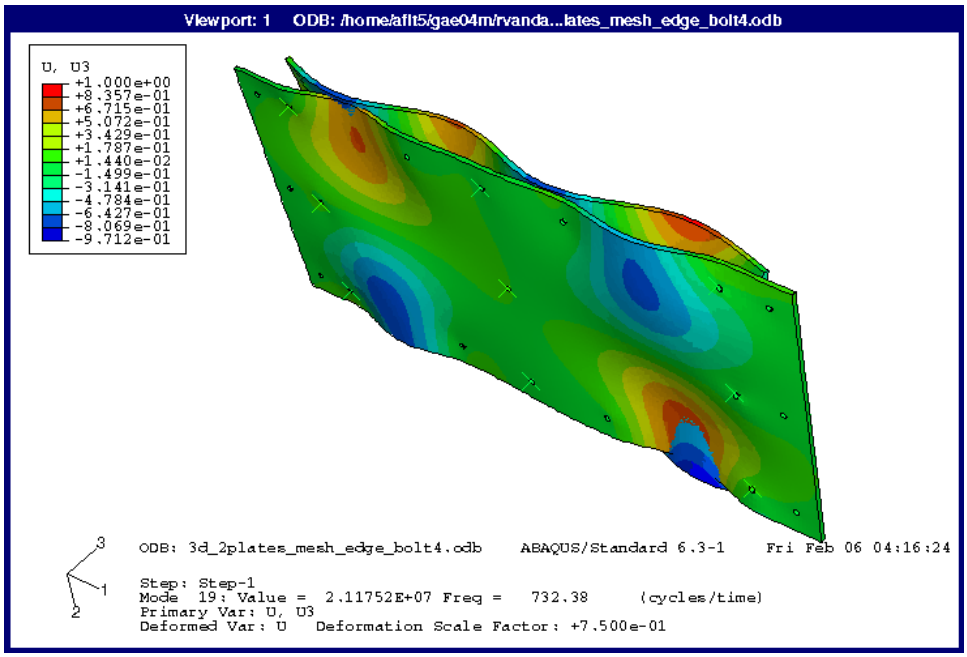

6th Correlated MAC Mode for Bolt 4 Removed. 732.03 Hz

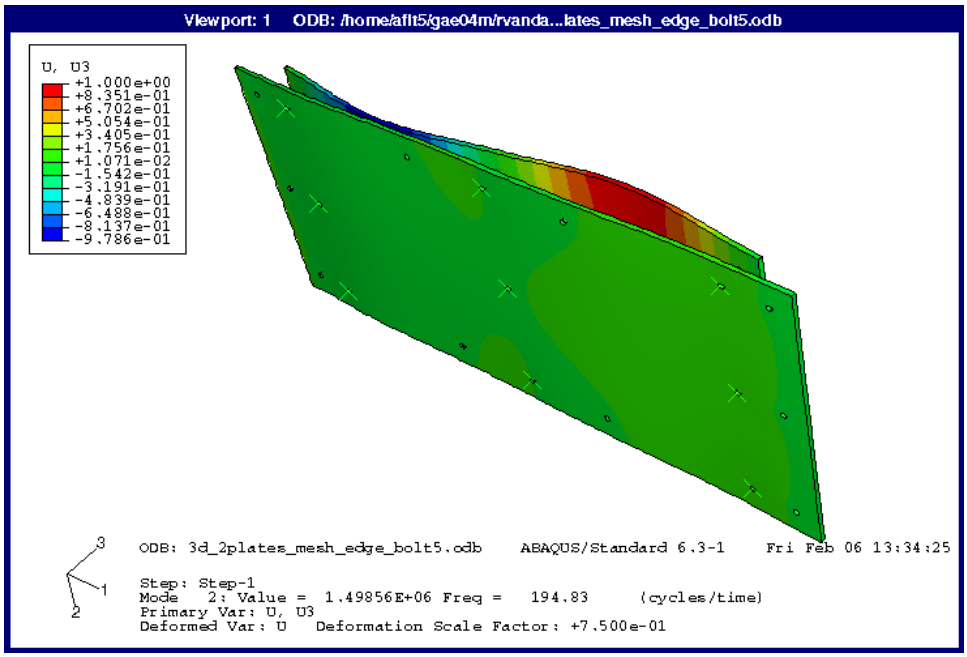

1st Correlated MAC Mode for Bolt 5 Removed. 217.19 Hz

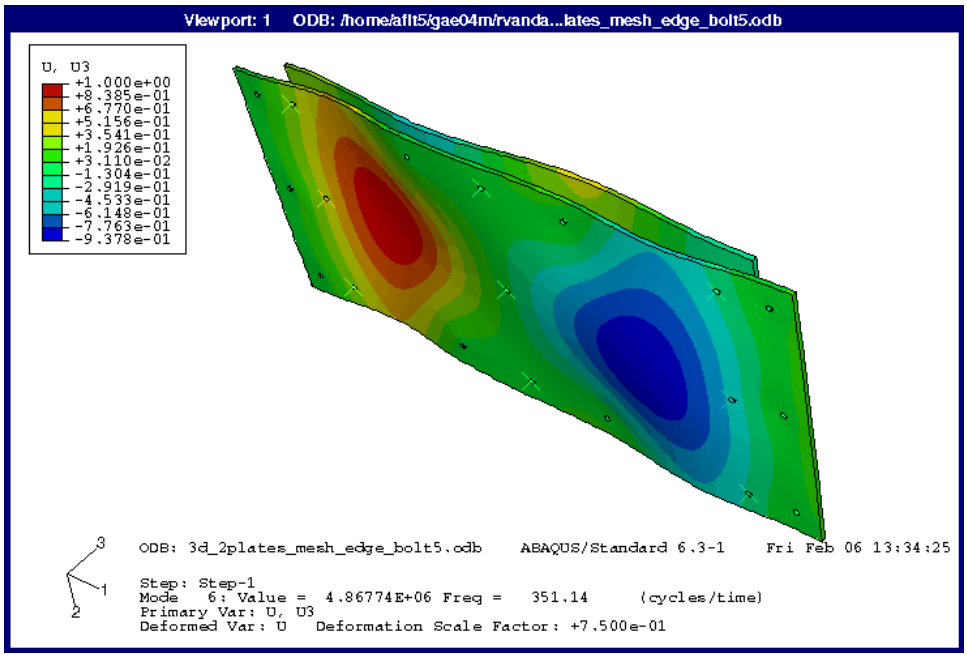

2nd Correlated MAC Mode for Bolt 5 Removed. 332.81 Hz

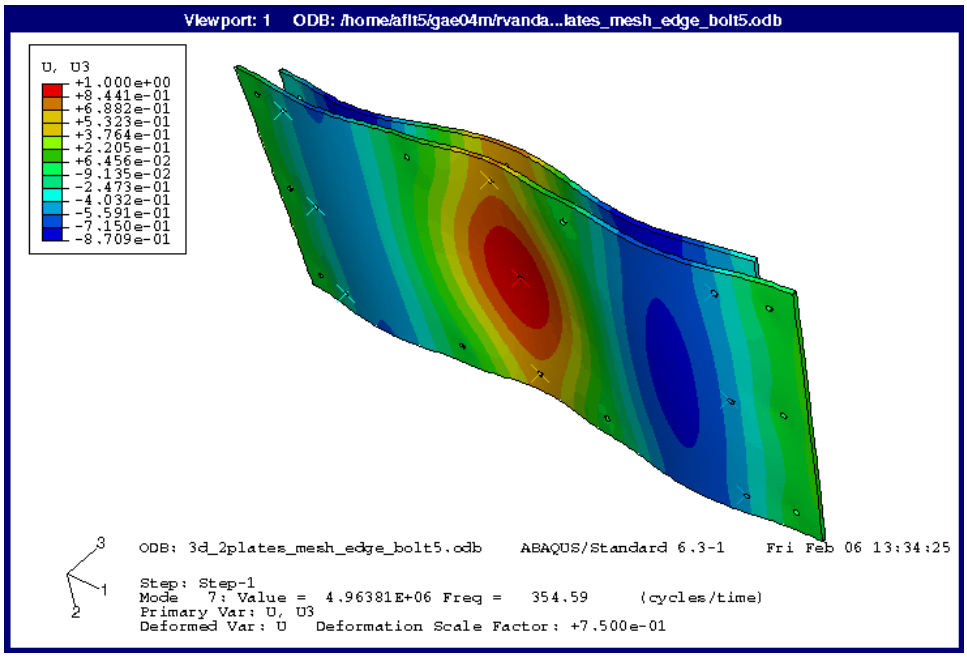

3rd Correlated MAC Mode for Bolt 5 Removed. 353.91Hz

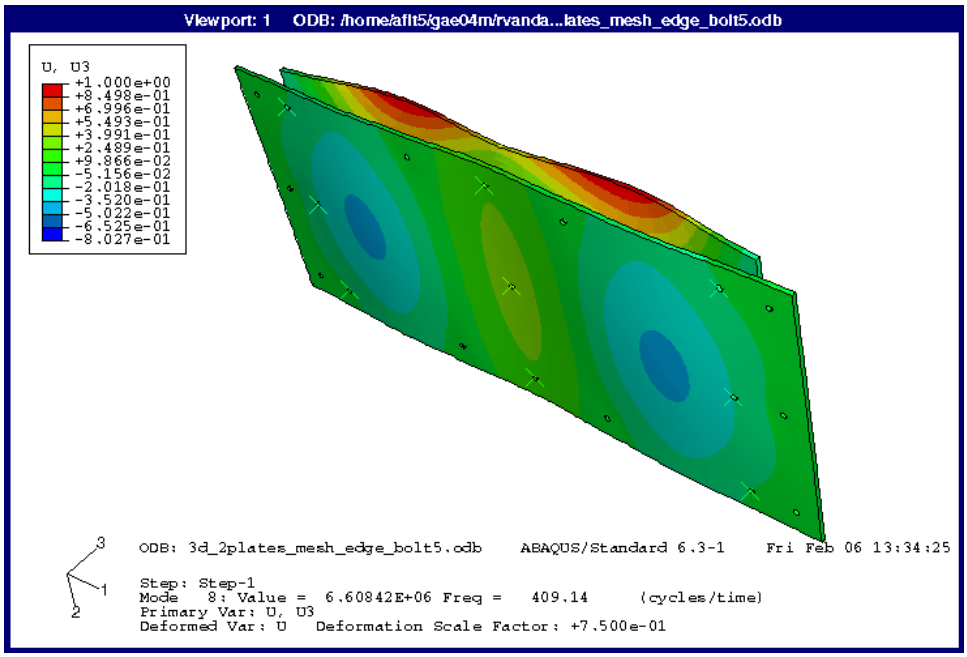

4th Correlated MAC Mode for Bolt 5 Removed. 432.81 Hz

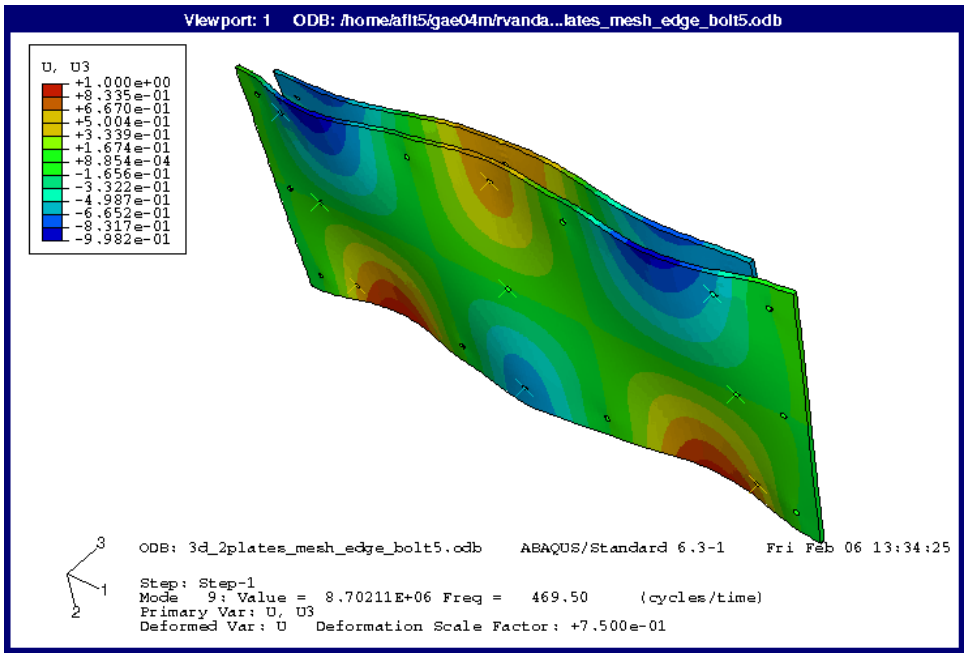

5th Correlated MAC Mode for Bolt 5 Removed. 456.25 Hz

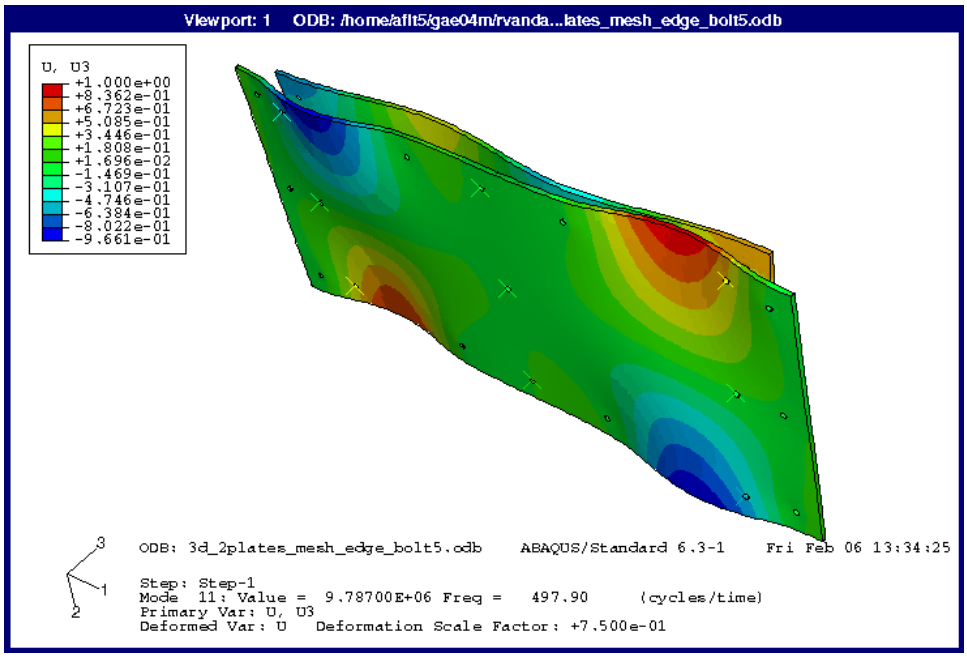

6th Correlated MAC Mode for Bolt 5 Removed. 485.16 Hz

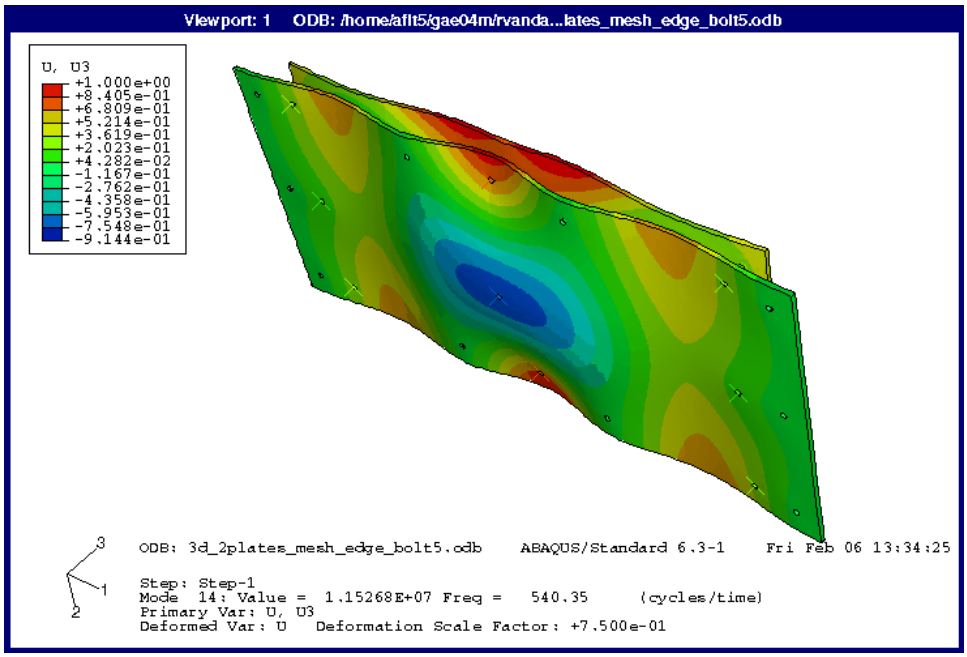

7th Correlated MAC Mode for Bolt 5 Removed. 549.22 Hz

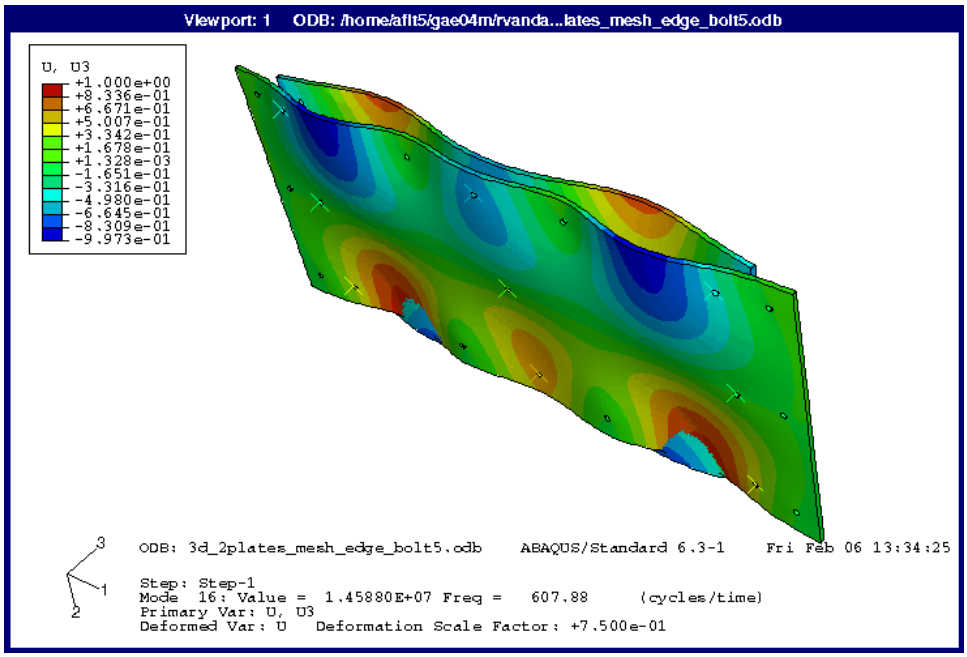

8th Correlated MAC Mode for Bolt 5 Removed. 600.78 Hz

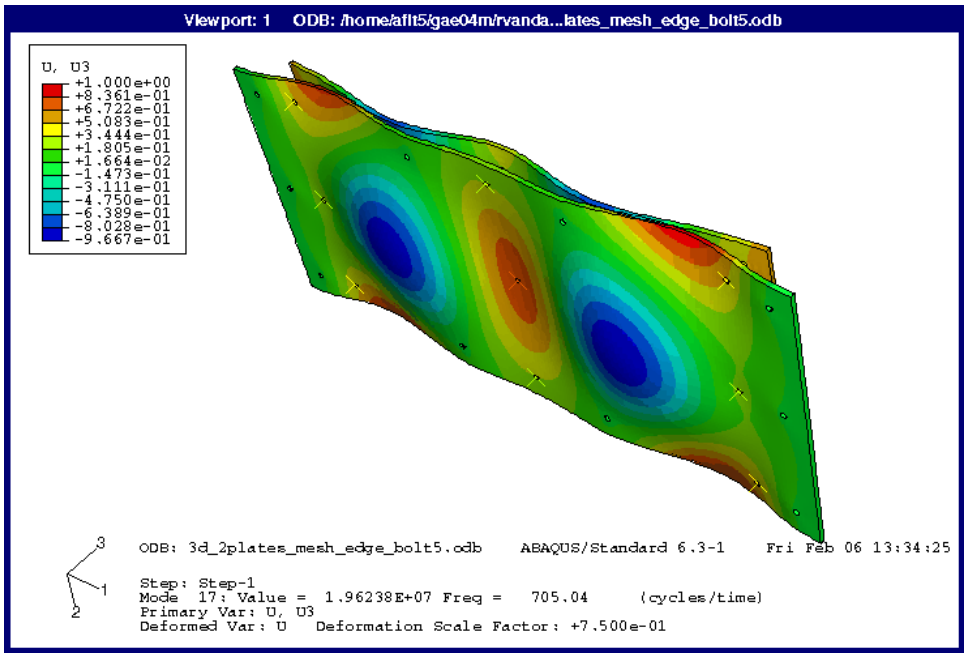

9th Correlated MAC Mode for Bolt 5 Removed. 676.56 Hz

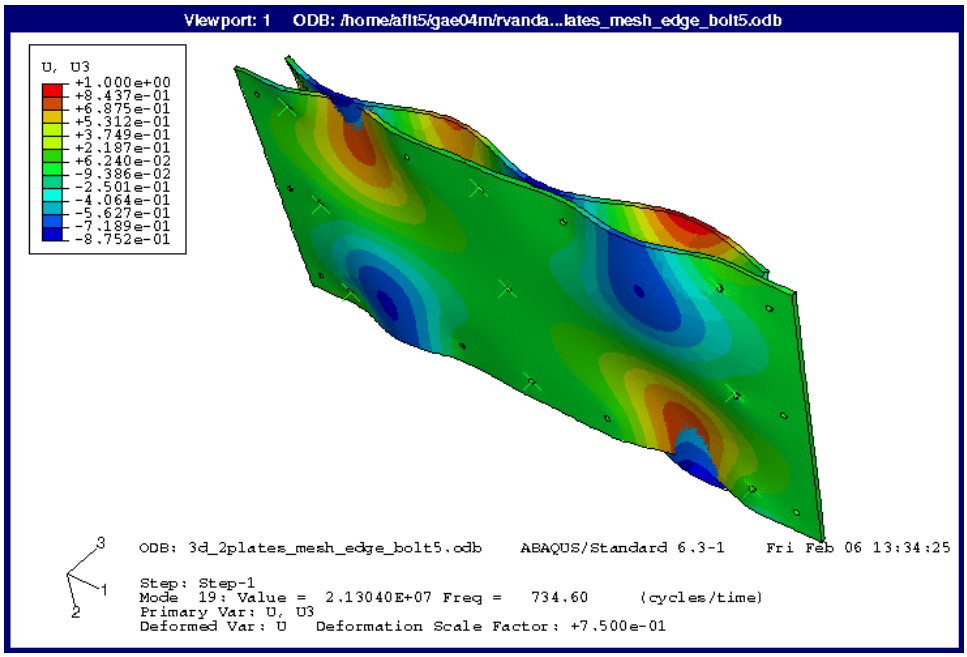

10th Correlated MAC Mode for Bolt 5 Removed. 1120.31 Hz

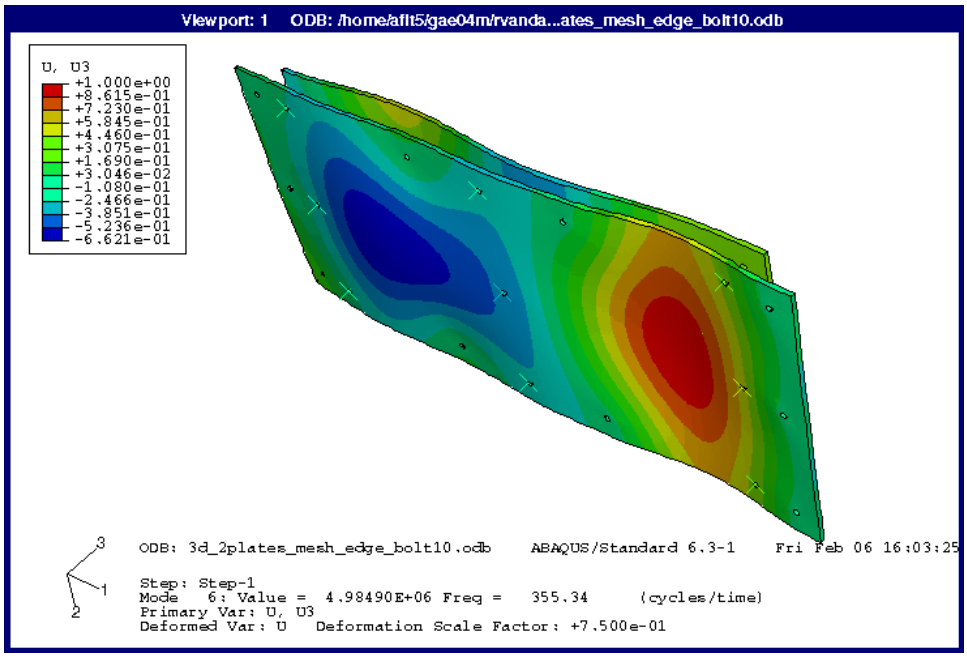

1st Correlated MAC Mode for Bolt 10 Removed. 341.41 Hz

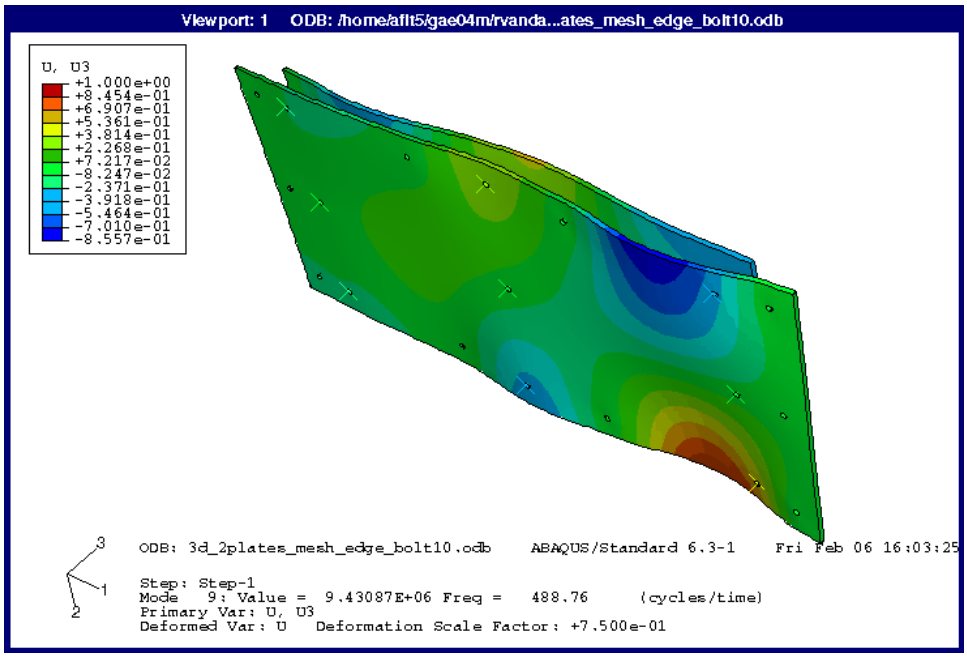

2nd Correlated MAC Mode for Bolt 10 Removed. 474.22 Hz

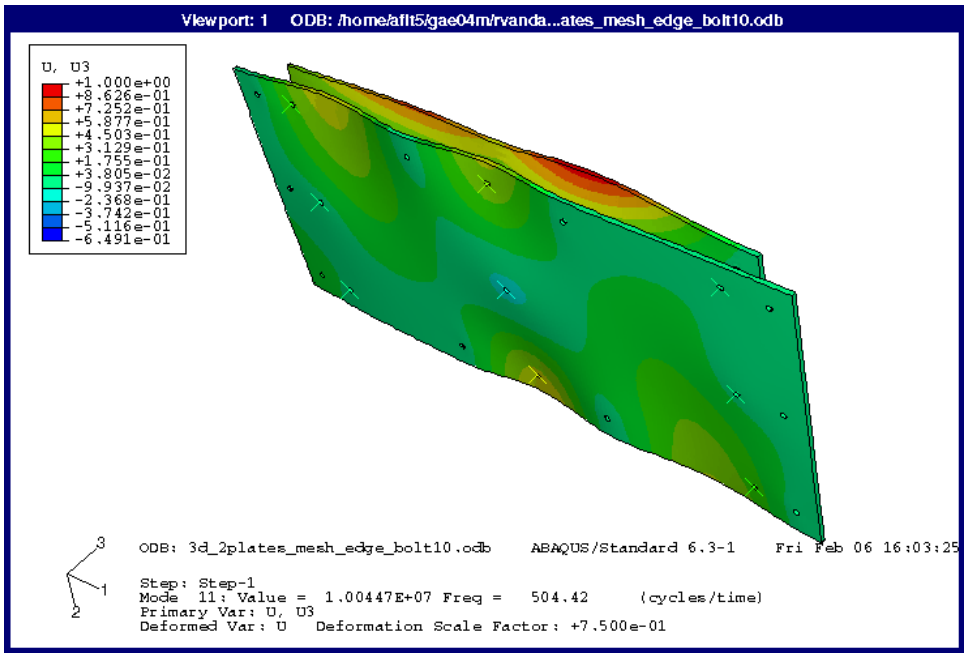

3rd Correlated MAC Mode for Bolt 10 Removed. 502.34 Hz

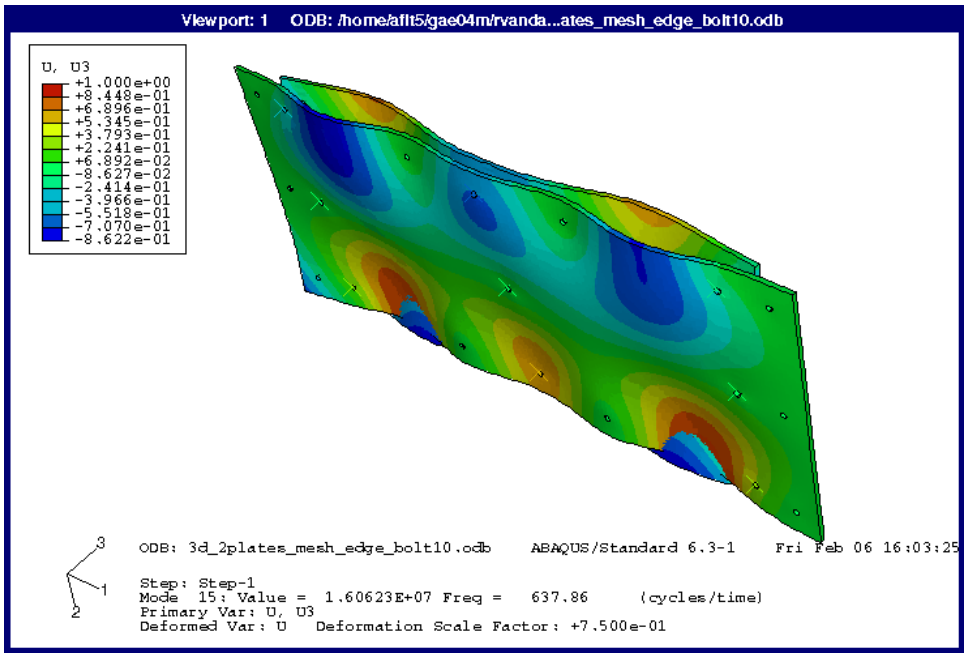

4th Correlated MAC Mode for Bolt 10 Removed. 620.31 Hz

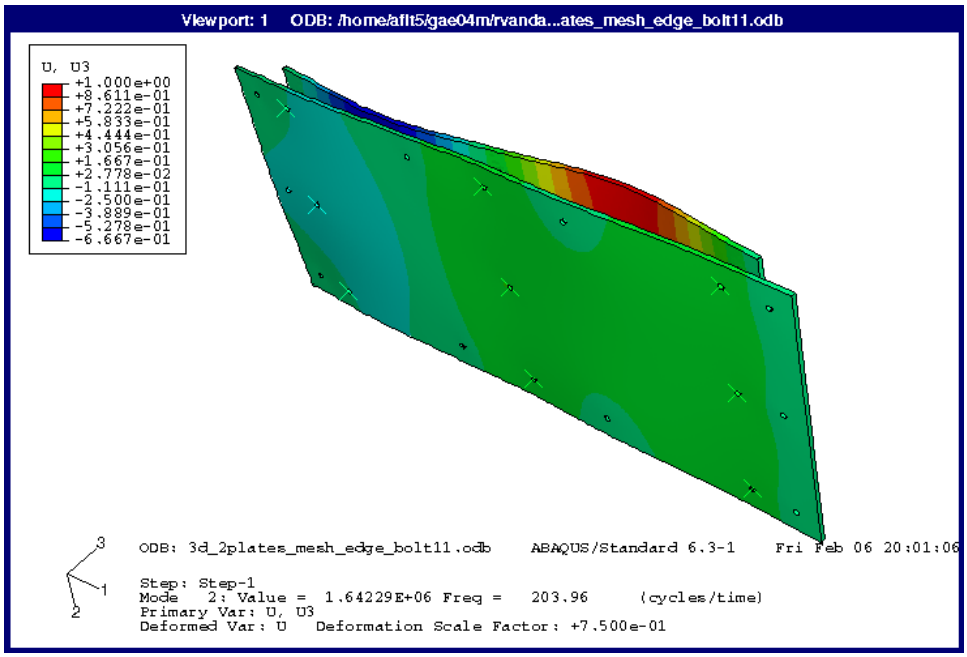

1st Correlated MAC Mode for Bolt 11 Removed. 230.47 Hz

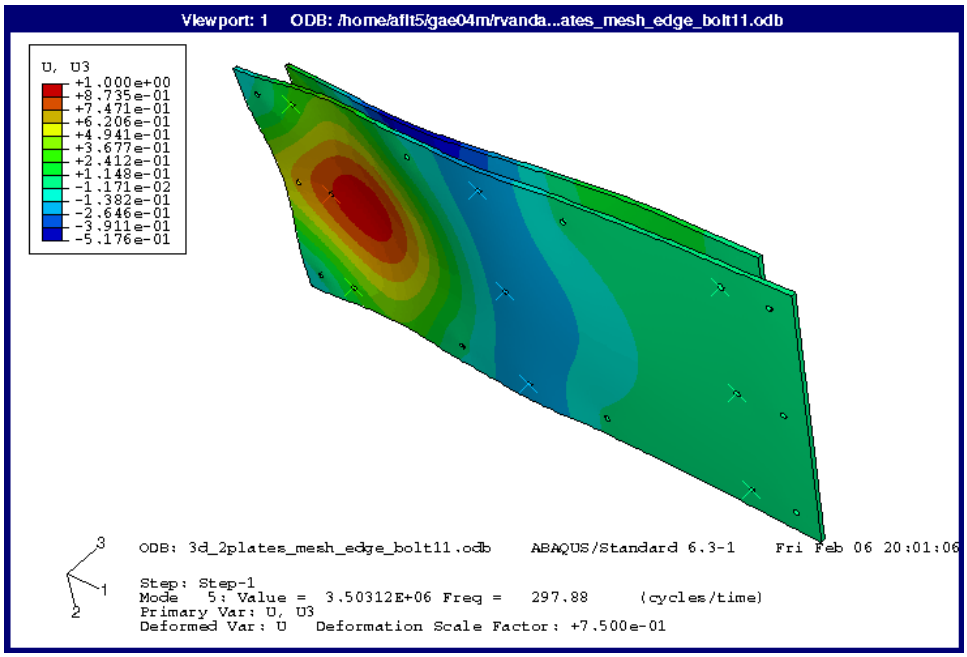

2nd Correlated MAC Mode for Bolt 11 Removed. 302.34 Hz

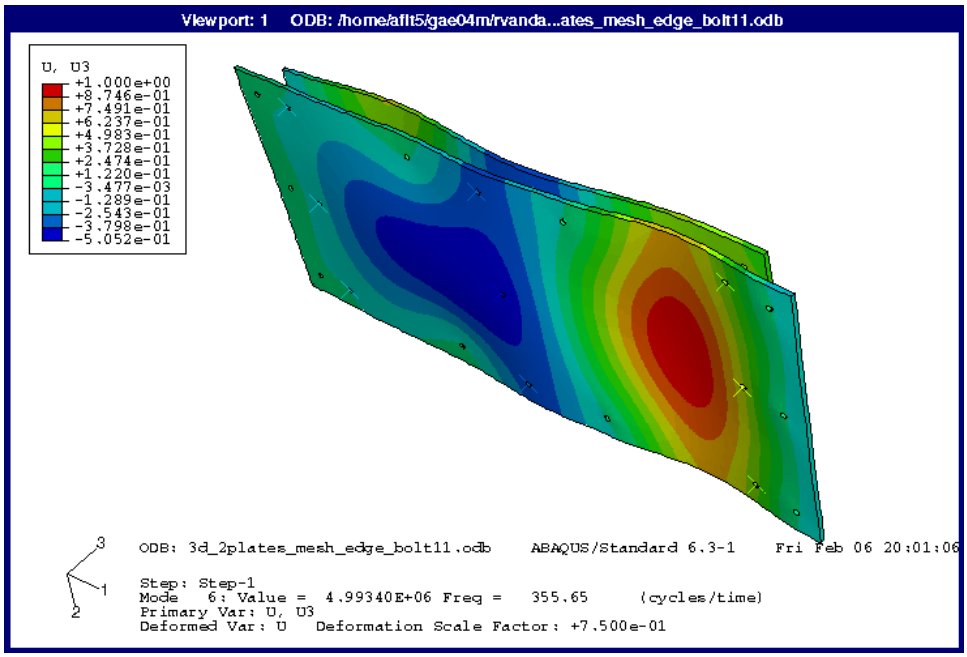

3rd Correlated MAC Mode for Bolt 11 Removed. 341.41 Hz

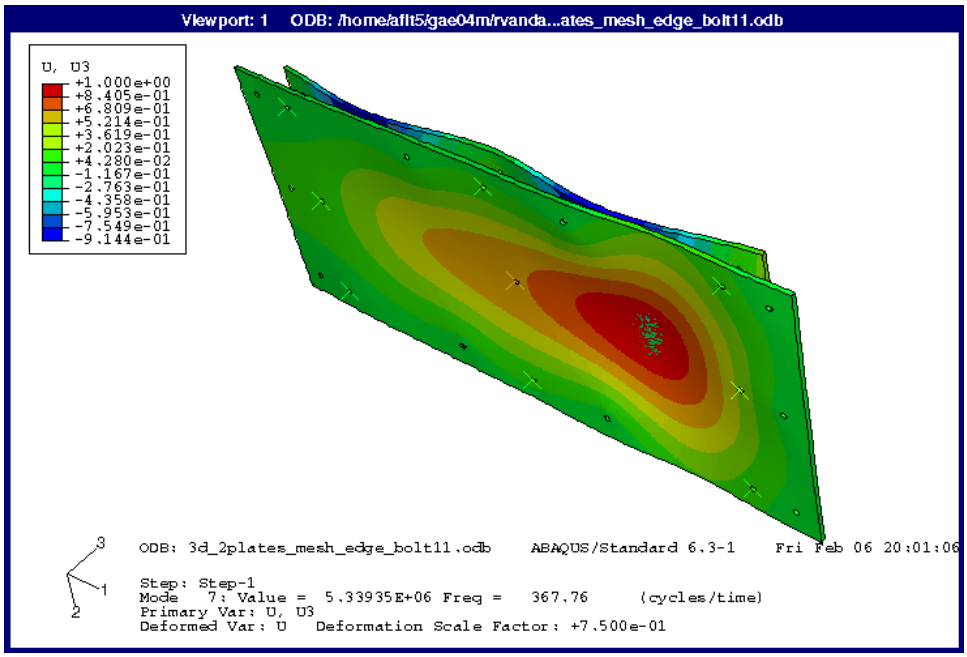

4th Correlated MAC Mode for Bolt 11 Removed. 358.59 Hz

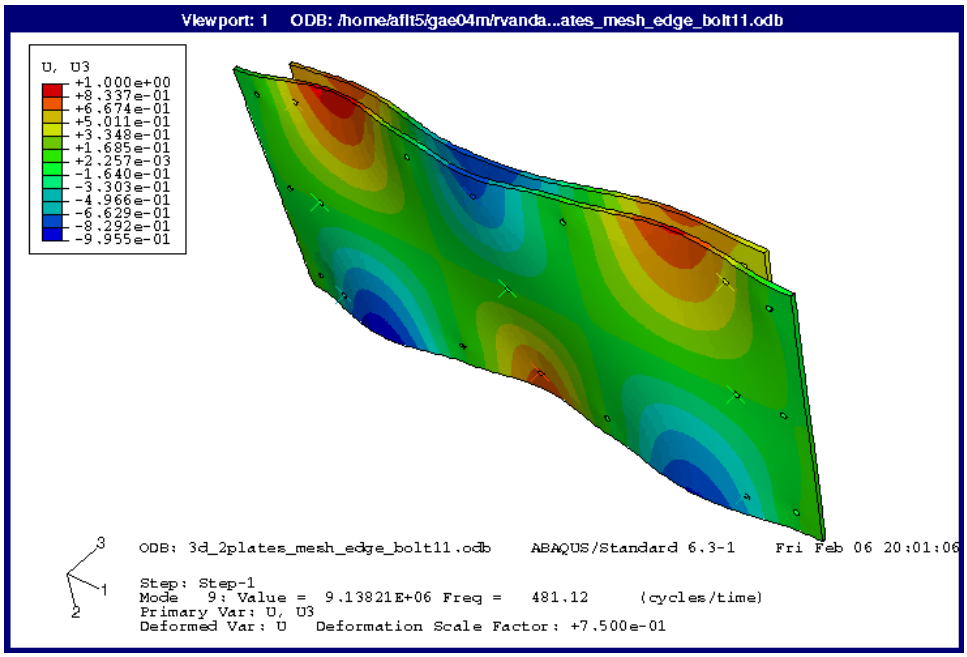

5th Correlated MAC Mode for Bolt 11 Removed. 470.31 Hz

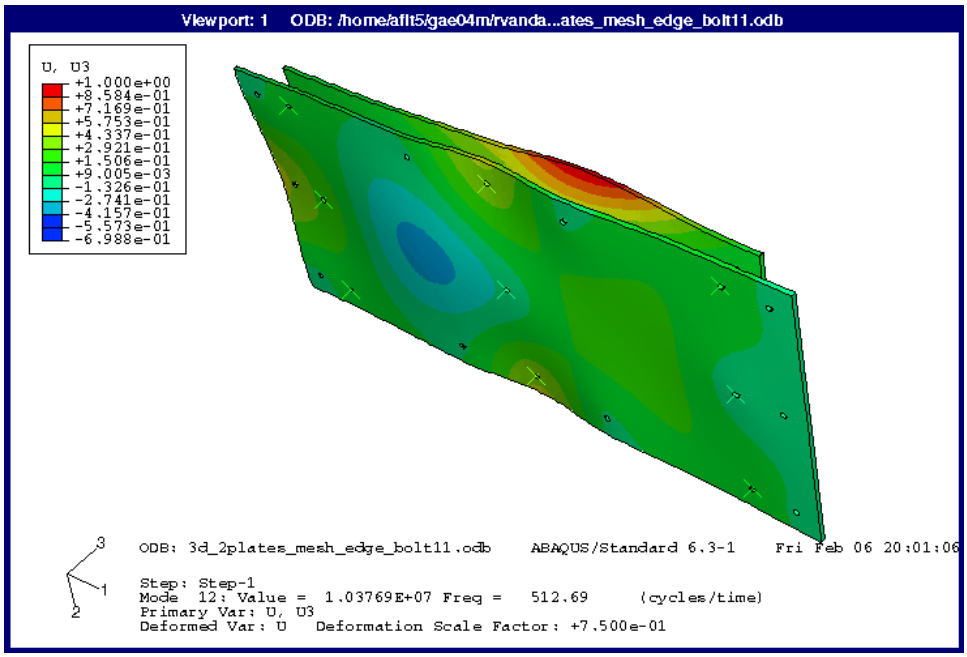

6th Correlated MAC Mode for Bolt 11 Removed. 510.94 Hz

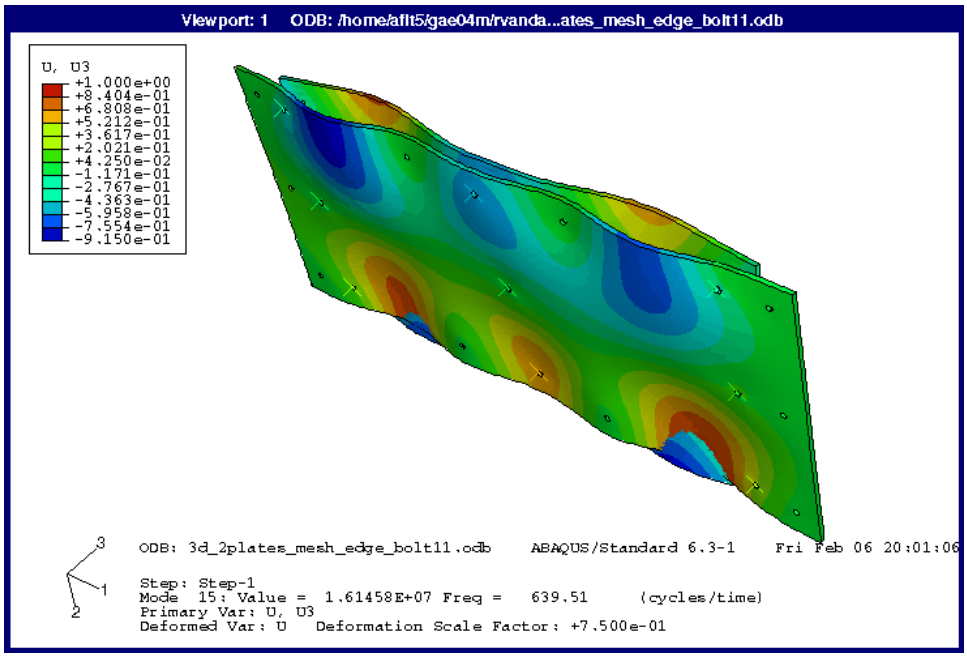

7th Correlated MAC Mode for Bolt 11 Removed. 612.50 Hz

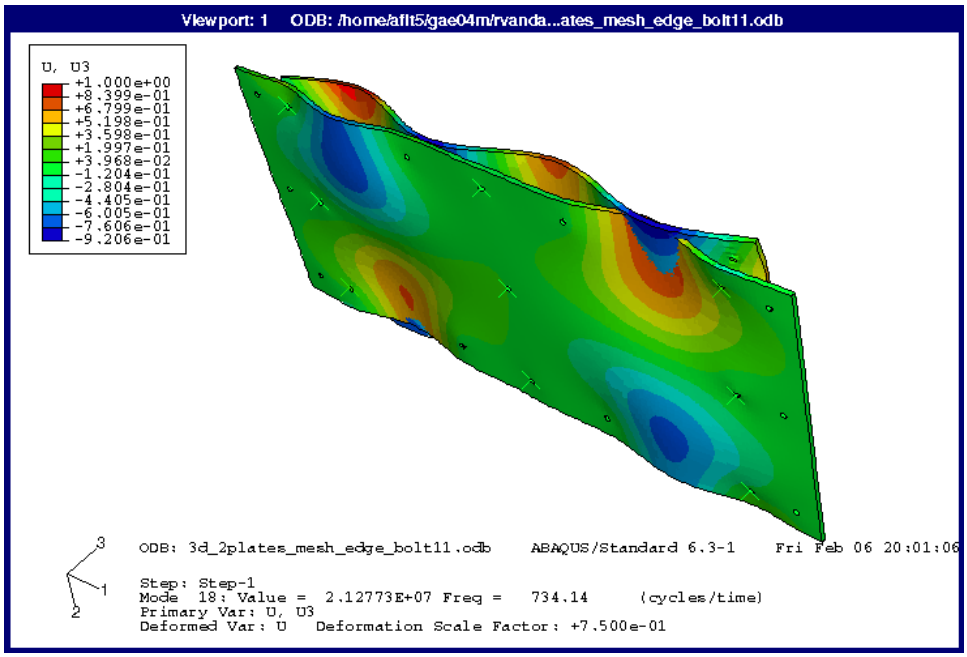

8th Correlated MAC Mode for Bolt 11 Removed. 725.78 Hz

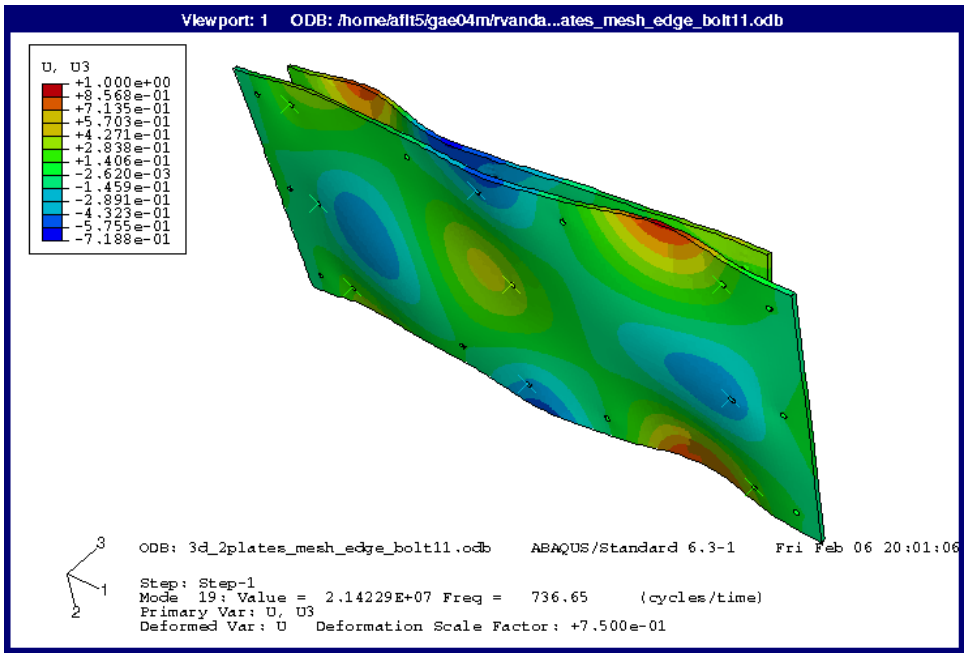

9th Correlated MAC Mode for Bolt 11 Removed. 744.53 Hz

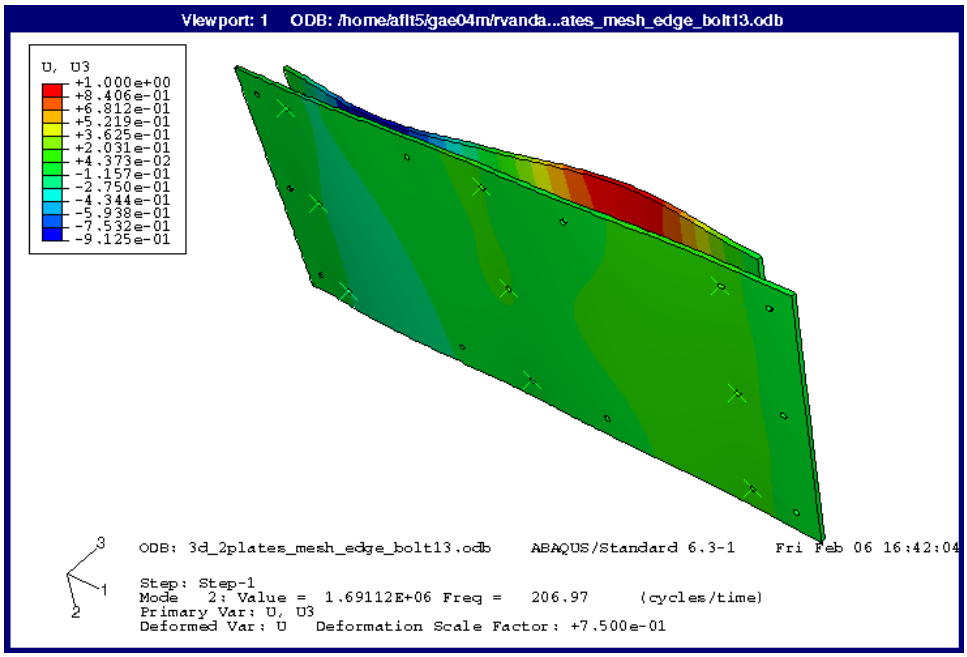

1st Correlated MAC Mode for Bolt 13 Removed. 234.38 Hz

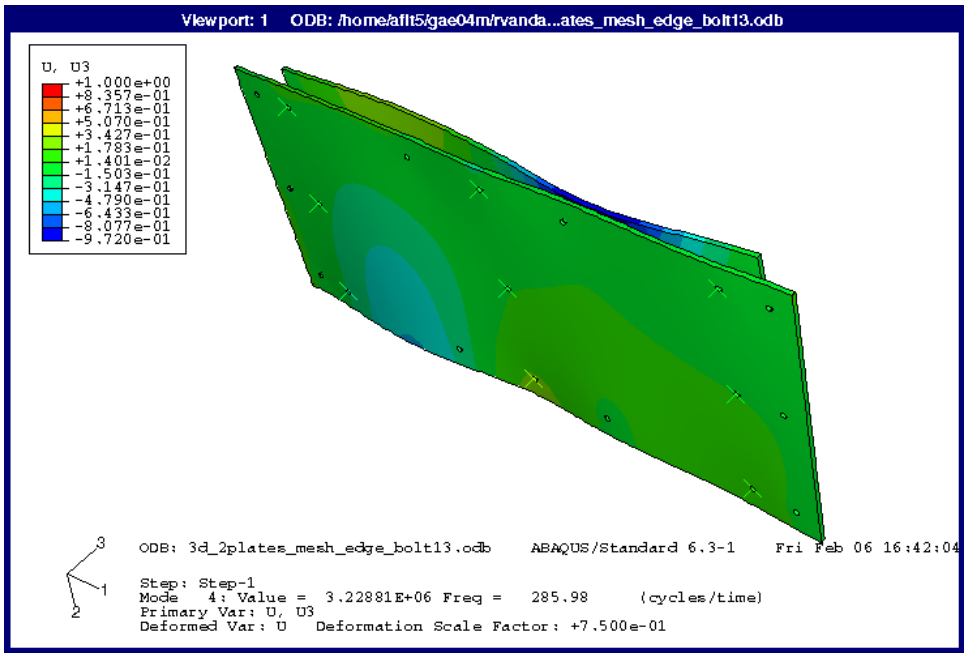

2nd Correlated MAC Mode for Bolt 13 Removed. 296.09 Hz

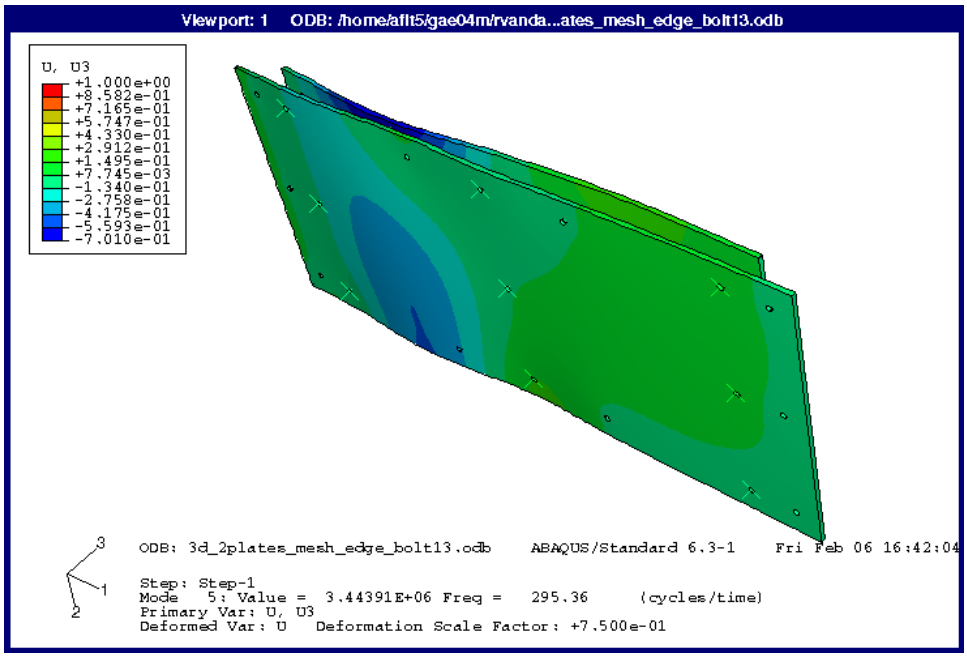

2nd Correlated MAC Mode for Bolt 13 Removed. 296.09Hz

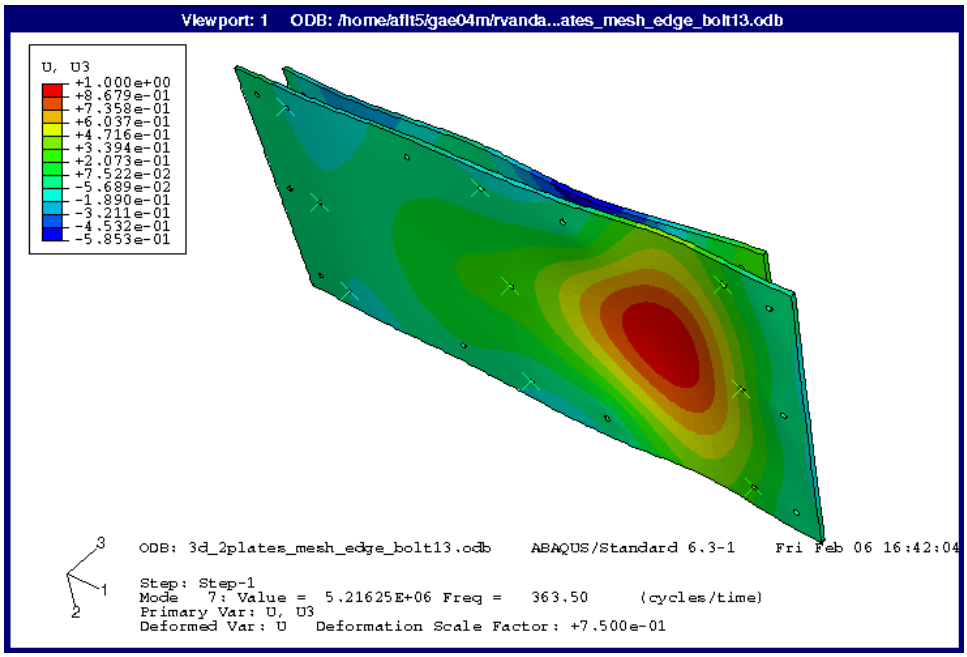

3rd Correlated MAC Mode for Bolt 13 Removed. 347.66 Hz

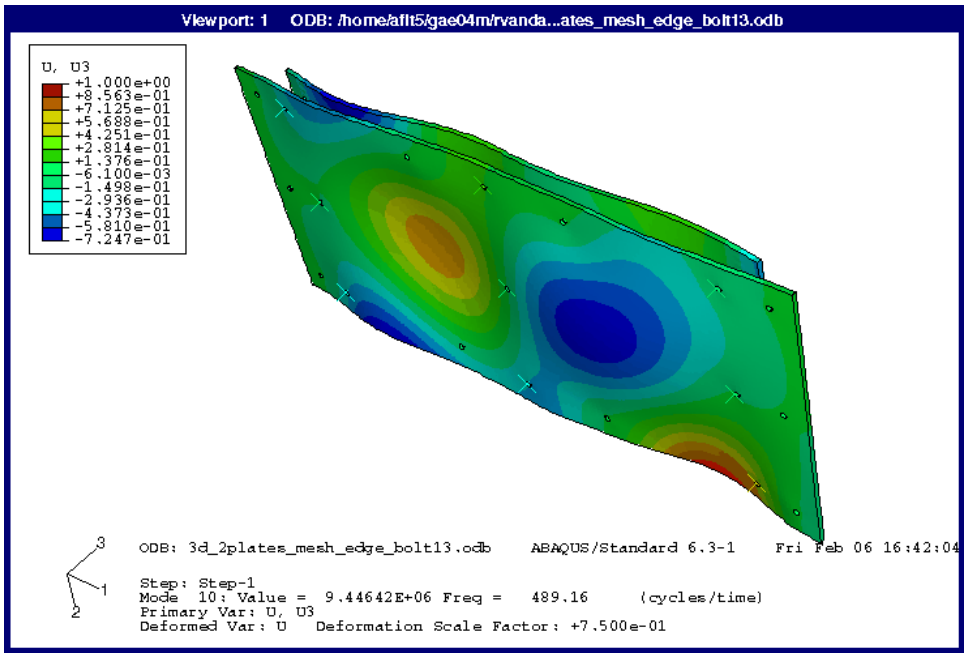

4th Correlated MAC Mode for Bolt 13 Removed. 472.66 Hz

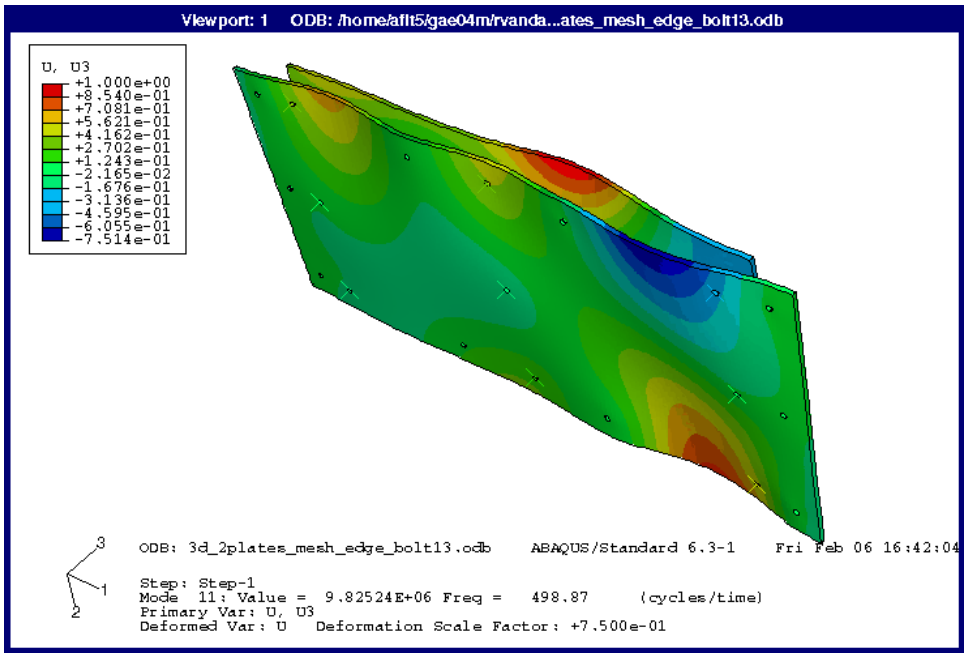

5th Correlated MAC Mode for Bolt 13 Removed. 492.19 Hz

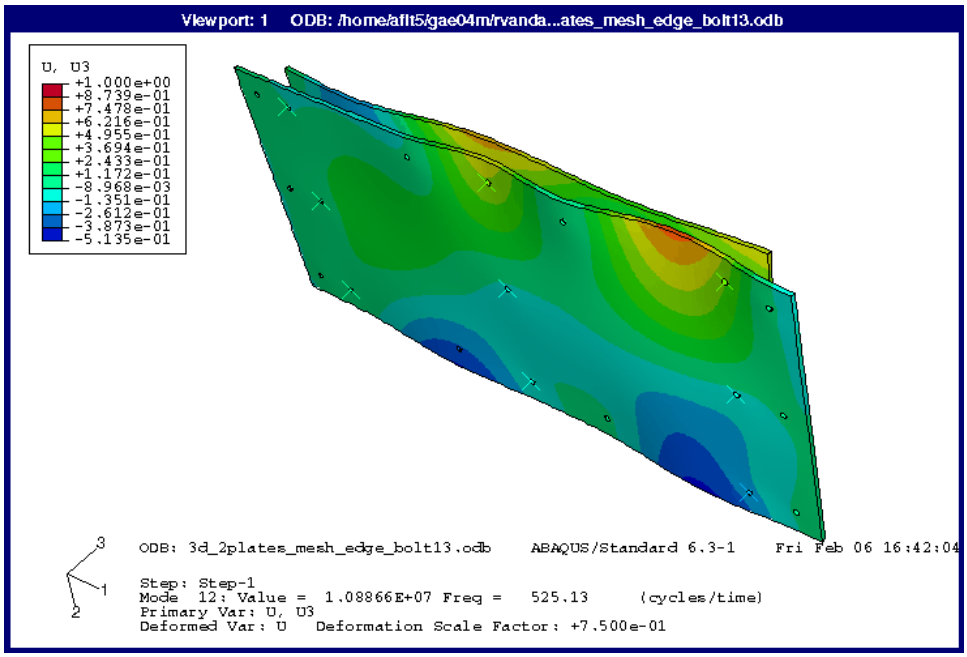

6th Correlated MAC Mode for Bolt 13 Removed. 519.53 Hz

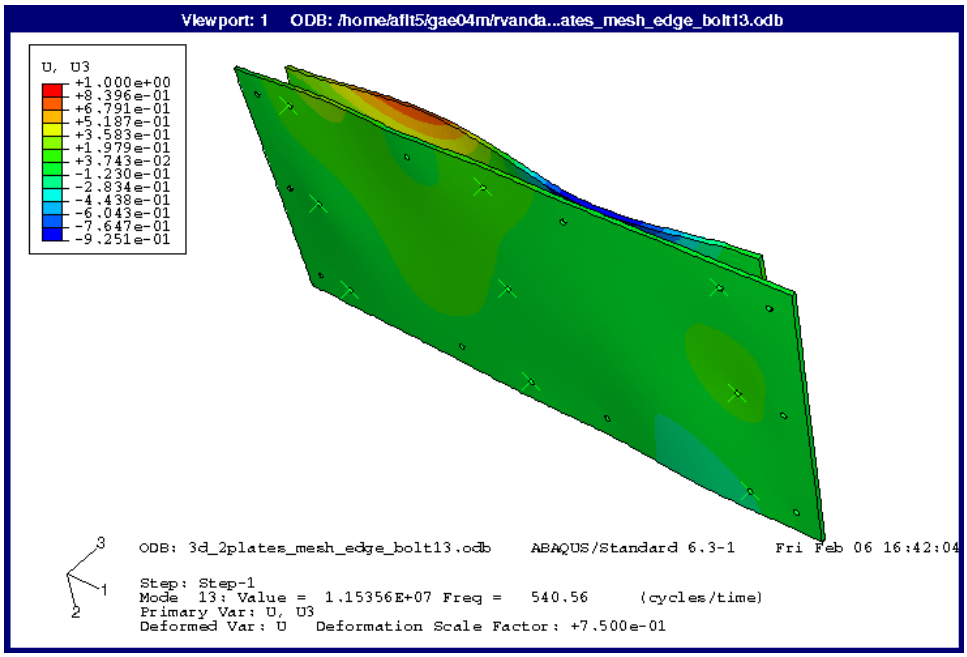

7th Correlated MAC Mode for Bolt 13 Removed. 544.53 Hz

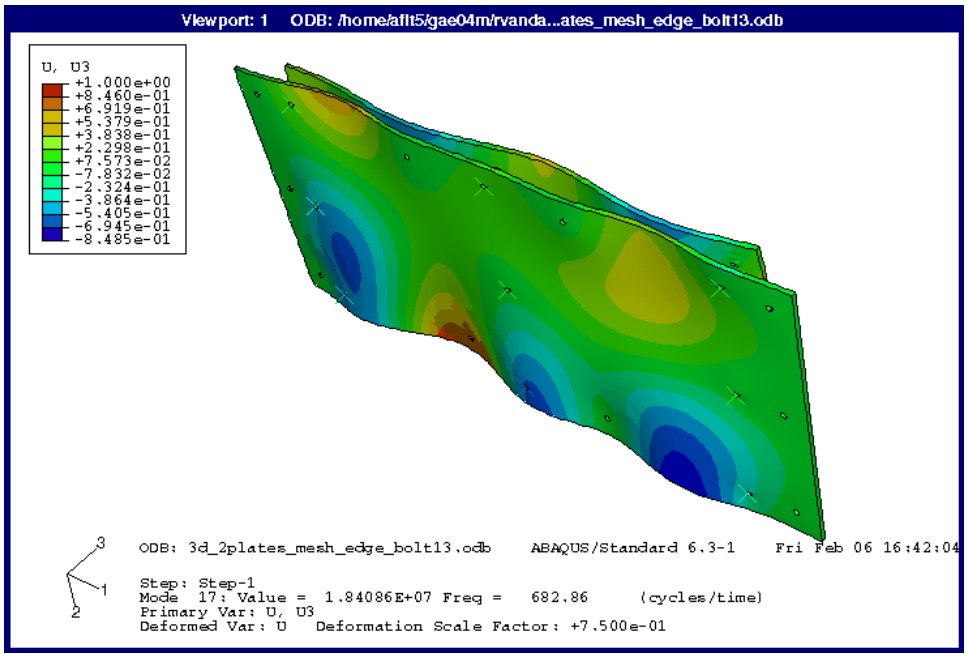

8th Correlated MAC Mode for Bolt 13 Removed. 667.19 Hz

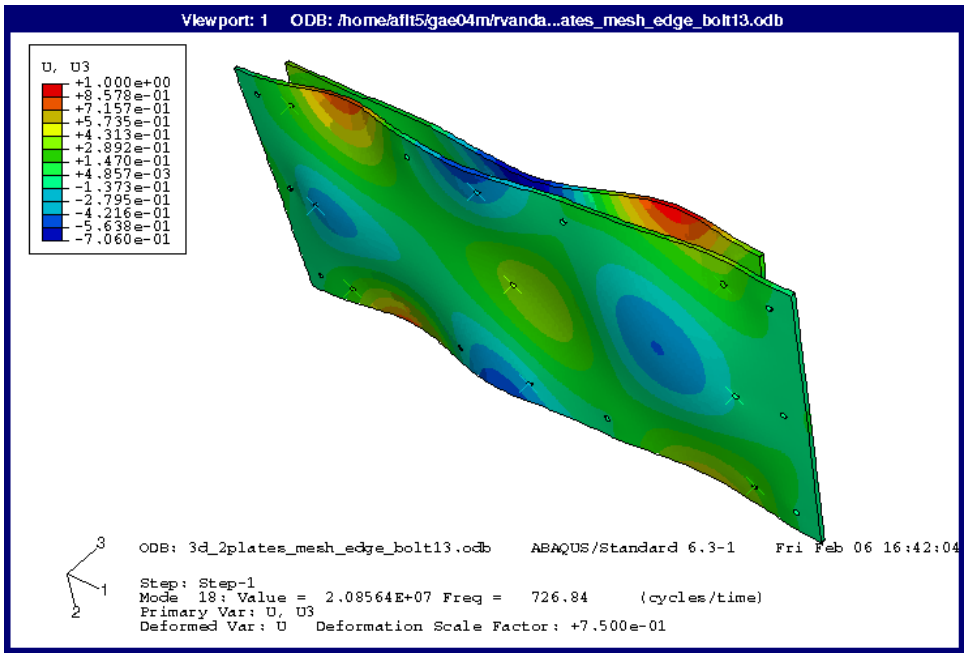

9th Correlated MAC Mode for Bolt 13 Removed. 729.69 Hz

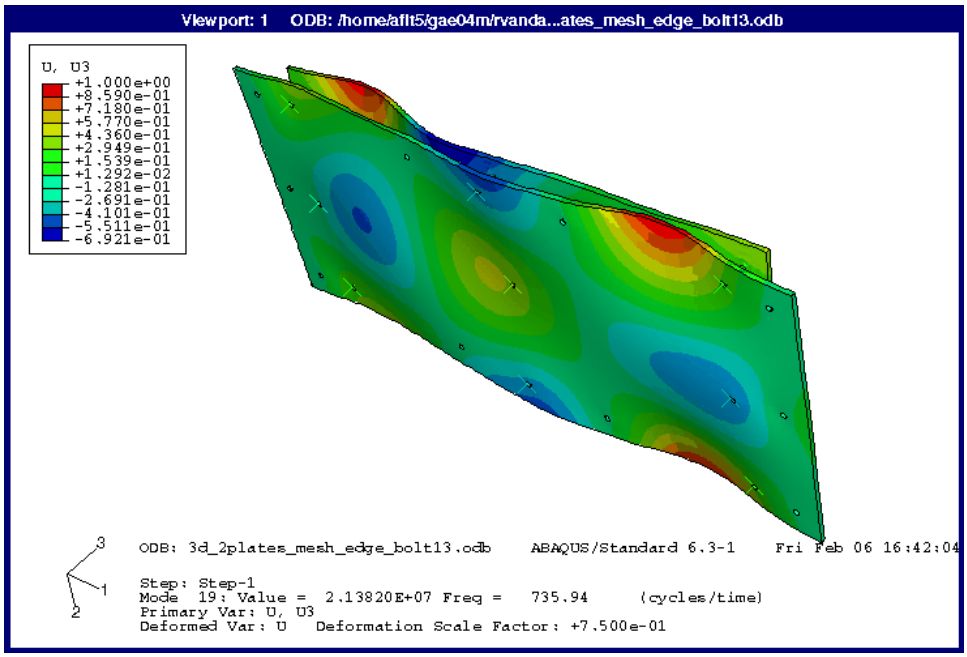

9th Correlated MAC Mode for Bolt 13 Removed. 729.69 Hz

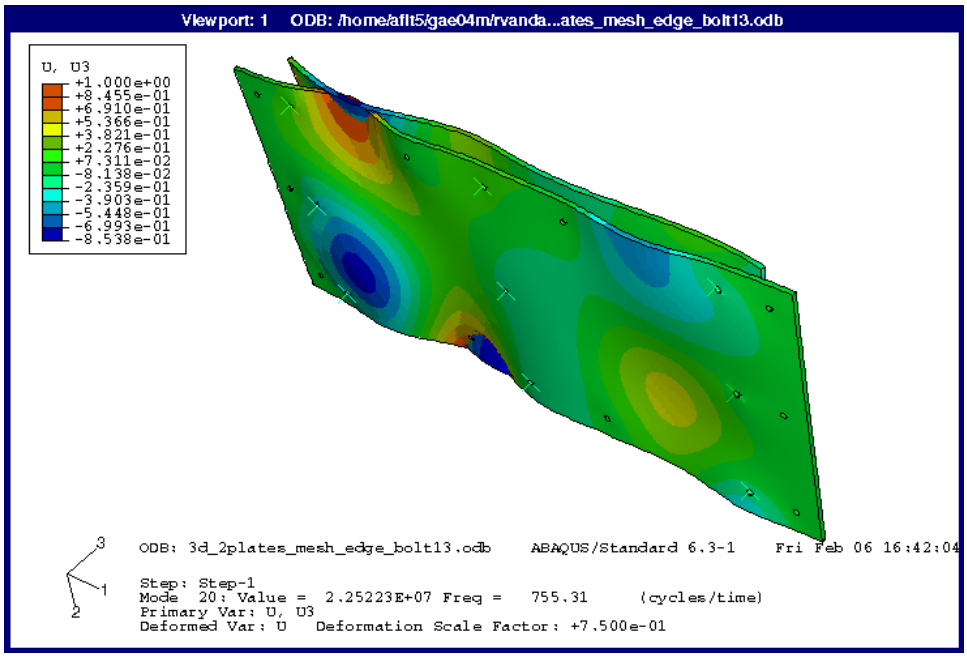

10th Correlated MAC Mode for Bolt 13 Removed. 757.81Hz

Bibliography

1. ABAQUS/Standard User's Manual. Version 6.3 (2002).

2. "Active Control Experts." http://www.acx.com, 2003

3. Allemang, Randall J., "The Modal Assurance Criterion (MAC): Twenty Years of Use and Abuse," *Proceedings of IMAC-XX: A Conference on Structural Dynamics*, Los Angeles, 397-405, 2002.

4. Avitable, Peter. "Experimental Modal Analysis: A Simple Non-Mathematical Presentation," *Sound and Vibration*, January 2001.

5. Bartkowicz, Theodore J, et al. "Autonomous Structural Health Monitoring System: A Demonstration," *AIAA* A96-26975 (1996).

6. Brillhart, Ralph, Deiters, Tom, Smith Ken, "Improved Model Correlation Through Test Preparation and Conduct," *Proceedings of IMAC XVI*. Santa Barbara, 464-469, (1998).

7. Cobb, Richard G. Class Notes, MECH 719, Vibration Damping and Control. School of Engineering and Management, Air Force Institute of Technology, Wright-Patterson AFB OH, Fall Quarter 2003.

8. Cobb, Richard G and B.S. Liebst. "Sensor Placement and Structural Damage Identification form Minimal Sensor Information," *AIAA Journal*, 35(2): 369-374 (February 1997).

9. Cook, Robert D. et al. *Concepts and Applications of Finite Element Analysis*, 4th ed., John Wiley & Sons, Inc., New York, 2002.

10. "Cranfield Aerospace Ltd." http://www.cranfieldaerospace.com, 2003.

11. Data Physics Corporation. *Making Measurements with SignalCalc 620*. Data Physics Corporations, San Jose CA, 2000.

12. Demarchi, D. and J.A. Pereira e V. Lopes, Jr., "Non-Destructive Evaluation Tool for Monitoring and Detection of Structural Damage by Using Neural Network." *Proceedings of IMAC XVIII: A conference on Structural Dynamics*. San Antonio TX, 2000.

13. Derisso, Mark. "AFRL/VA Health ManagementTechnical Program Overview." Presented to AFRL Health Management Technology Review. Wright-Patterson AFB OH. June 2003.

14. Derisso, Mark. "Structural Health Monitoring of Aerospace Vehicles Using Advanced Signal Analysis and Physics-Based Models." Presented to 132nd TMS Annual Meeting and Exhibition. San Diego CA. March 2003.

15. Dorfi, Hans R and Robert L. Wheeler and Gordon H. Griffiths. "Tire Vibration Transmission Part I: FEA Solution Correlation," *Proceedings of IMAC XVIII*. San Antonio, 1244-1250, (2000).

16. Dossing, Ole. "Going Beyond Modal Analysis or IMAC in a New Key," *Proceedings of IMAC XIII*. Nashville, xxiv-xxxii, (1995)

17. Ewins, D.J., *Modal Testing: Theory and Practice*. John Wiley, 1984

18. Friswell, M.I. and Mottershead, J.E., *Finite Element Model Updating in Structural Dynamics*, Kluwer Academic Publishers, Dordrecht, 1995

19. "Global Security." http://www.globalsecurity.org. 2003

20. Giurgiutiu, V., Bao, J., Zhao, W. "Piezoelectric-Wafer Active-Sensor Embedded Ultrasonics in Beams and Plates," *Experimental Mechanics*, 43(4): 428-449, (December 2003)

21. Giurgiutiu, V., Zagrai, A. N., Bao J., Redmond, J., Roach, D., Rackow, K. "Active Sensors for Health Monitoring of Aging Aerospace Structures," *International Journal of the Condition Monitoring and Diagnostic Engineering Management*, UK, 6(1): 3-21, (January 2003)

22. Giurgiutiu, V. "Embedded NDE with Piezoelectric Wafer Active Sensors in Aerospace Applications," *Journal of Materials (JOM) – Special Issue on NDE*, January 2003

23. Giurgiutiu, V., Zagrai, A. N., Bao, J. "Piezoelectric Wafer Embedded Active Sensors for Aging Aircraft Structural Health Monitoring," *Structural Health Monitoring – An International Journal*, 1(1): 41-61 (July 2002)

24. Hagemaier, Donald and Hoggard, Amos. "NDI Technology as it Relates to Aging Aricraft," *Materials Evaluation*, December 1993: 1360-1366.

25. Kim, Hyoung M. and Mohamed Kaouk. "Modal Analysis and Model Correlation of the MIR Space Station," *Proceedings of IMAC XVIII*. San Antonio, 1724-1730, (2000).

26. Lim, Tae W. et al. "Structural health monitoring using real-time modal parameter identification algorithm," *AIAA* A96-27071 06-39. (1996)

27. Mace, B.R. and Rosenberg, J. "The SEA of Two Coupled Plates: An Investigation into the Effects of Subsystem Irregularity," *Journal of Sound and Vibration*, 212(3): 395-415 (1998).

28. Meirovitch, Leonard, *Elements of Vibration Analysis*, 2d ed., McGraw-Hill Book Co., New York, 1986.

29. "Panametrics-NDT." http://www.panametrics-ndt.com. 2003

30. "PCB Piezotronics" http://www.pcb.com. 2003

31. Prosser, William H. and Michael R. Gorman and Donald H. Humes. "Acoustic Emission Signals in This Plated Produced by Impact Damage," *Journal of Acoustic Emission*, 17(1-2): 29-36 (June 1999)

32. Proulx, B. and Cheng, L., "Dynamic Analysis of Peizoceramic Actuation effects on Plate Vibrations," *Thin-Walled Structures*, 37: 147-162 (2000)

33. Schulz, Mark J and P. Frank Pai and Sunil K. Thyagarajan. "Structural Damage Diagnosis by Frequency Response Function Optimization," *AIAA* A96-27130. (1996)

34. Schweikhard, Keith A et al. "Flight Demonstration of X-33 Vehicle Health Management System Components on the F/A-18 Systems Research Aircraft," NASA/TM-2001-209037, (December 2001).

35. Stanbridge, A.B. and Ewins, D.J., "Modal Testing Using a Scanning Laser Doppler Vibrometer," *Mechanical Systems and Signal Processing*, 13(2): 255-270 (1998)

36. "Structural Technology Corporation." http://www.structuraltechnology.com, 2003.

37. "STScI Instrument Lab Opto-Mechanical." http://www.stosc.stsci.edu, 2004

38. Voracek, David F. and Marco Hurtado et al. "Ground and Flight Test Results of a PZT Health Monitoring System," *American Institute of Aeronautics and Astronautics, Inc.*, (1997).

39. Walter, Patrick L., "Accelerometer Selection for and Application to Modal Analysis," *Proceedings of the 17th IMAC*, Kissimmee, 566-572, 1999.

40. Wester, E. C. N. and B.R. Mace. "Statistical Energy Analysis of Two Edge-Coupled Rectangular Plates: Ensemble Averages," *Journal of Sound and Vibration*, 193(4): 793-822 (1996).

41. Yang, X.F., A.S.J. Swamidas and R. Seshadri. "Crack Identification in Vibrating Beams Using the Energy Method," *Journal of Sound and Vibration*, 244(2): 339-357 (2001).

Vita

Captain Robert M. Vandawaker graduated from Dryden High School in Dryden, Michigan. He entered undergraduate studies at Lawrence Technological University in Southfield, Michigan where he graduated with a Bachelor of Science degree in Mechanical Engineering in May 1999. He was commissioned through Officer Training School in November 1999.

His first assignment was at Kelly AFB as a mechanical engineer. He entered the Air Force Institute of Technology in August of 2002. Upon graduation he will be assigned to the Air Force Research Laboratory.

REPORT DOCUMENTATION PAGE

Form Approved
OMB No. 074-0188

1. REPORT DATE *(DD-MM-YYYY)*	2. REPORT TYPE	3. DATES COVERED *(From – To)*
12-03-2004	**Master's Thesis**	Jun 2003 – Mar 2004

4. TITLE AND SUBTITLE

EXPERIMENTAL AND COMPUTATIONAL ANALYSIS OF MODES IN A PARTIALLY CONSTRAINED PLATE

5a. CONTRACT NUMBER

5b. GRANT NUMBER

5c. PROGRAM ELEMENT NUMBER

6. AUTHOR(S)

Vandawaker, Robert M., Captain, USAF

5d. PROJECT NUMBER

5e. TASK NUMBER

5f. WORK UNIT NUMBER

7. PERFORMING ORGANIZATION NAMES(S) AND ADDRESS(S)

Air Force Institute of Technology
Graduate School of Engineering and Management (AFIT/EN)
2950 Hobson Way, Building 641
WPAFB OH 45433-7765

8. PERFORMING ORGANIZATION REPORT NUMBER

AFIT/GAE/ENY/04-M15

9. SPONSORING/MONITORING AGENCY NAME(S) AND ADDRESS(ES)

AFRL/VASA
Attn: Mr. Mark Derriso
2790 D Street
WPAFB OH 45433-7765
DSN: 674-6876
e-mail: mark.derriso@wpafb.af.mil

10. SPONSOR/MONITOR'S ACRONYM(S)

11. SPONSOR/MONITOR'S REPORT NUMBER(S)

12. DISTRIBUTION/AVAILABILITY STATEMENT

APPROVED FOR PUBLIC RELEASE; DISTRIBUTION UNLIMITED.

13. SUPPLEMENTARY NOTES

14. ABSTRACT

The field of structural health monitoring (SHM) attempts to reduce labor and cost by allowing technicians to monitor selected properties of an aircraft's structure to detect impending failure. This research examines methods to detect damage to a thermal protection system (TPS) tile using representative 2024-T3 aluminum plates. Plates are subjected to modal analysis in single and joined conditions in an attempt to provide the capability of sensing damage to a tile on the surface of a vehicle while the sensors remain on the superstructure of the airframe. Jointly, the development of a means to model the system using finite element techniques is explored. It is found that the finite element modeling technique produces correlating modal frequencies within a 7.19% worst case average when compared to the physical tests. This leads to the ability to compare mode shapes and frequencies to detect damage in a system.

15. SUBJECT TERMS

Structural Health Monitoring, SHM, Vibrations, Modal Analysis, Finite Element Analysis, Damage Detection

16. SECURITY CLASSIFICATION OF:			17. LIMITATION OF ABSTRACT	18. NUMBER OF PAGES	19a. NAME OF RESPONSIBLE PERSON
a. REPORT	b. ABSTRACT	c. THIS PAGE			Anthony N. Palazotto, PhD (ENY)
U	U	U	UU	171	19b. TELEPHONE NUMBER *(Include area code)* (937) 255-3636, ext 4599; e-mail: anthony.palazotto@afit.edu